PETROGRAPHIC AND STRATIGRAPHIC ANALYSIS OF THE BARNETT SHALE (MISSISSIPPIAN) IN HILL COUNTY, TEXAS: EVIDENCE FOR EUSTACY AND TECTONISM

By

RACHAEL MARIE MONROE

Bachelor of Science, 2007
The University of Texas at Dallas
Richardson, Texas

Submitted to the Graduate Faculty of the
College of Science and Engineering
Texas Christian University
In partial fulfillment of the requirements for the degree of

MASTER OF SCIENCE

May, 2009

ACKNOWLEDGEMENTS

I gratefully acknowledge the help and generosity of all individuals and organizations without whom I would not have been able to complete this project. I began this project with little knowledge of the Barnett Shale. In the past two years I have gained insight into the total petroleum system of the Fort Worth basin as well as the industry in which I will be making my career.

First I would like to thank EOG Resources and David Trice in particular for providing the core, digital log data, and funding for thin sections for this project. I would like to thank my former boss and mentor, Lindell Bridges for enlightening me with his insight and expertise in shale gas plays. I would also like to thank Jeff May for taking the time to look at my research and share his knowledge of turbidites and sequence stratigraphy. I would like to extend my gratitude to Dan Jarvie for his generosity in providing the geochemical data used in this project. I would also like to thank the TCU Energy Institute for providing the funding for well logs. I would like to acknowledge the entire TCU geology faculty for a wonderful graduate education. I have really enjoyed my graduate experience at TCU.

I would like to thank my parents for their unending support. Much of my gratitude also goes towards my husband, Justin, for providing the mental support necessary to maintain my sanity. Justin also helped in cutting geochemical and thin section samples. For that I am grateful. I would also like to dedicate this thesis to my Grandpa, Lee Blanton, and thank him for sparking my interest in the earth sciences ever since I was a little girl.

Most of all, I would like to thank Dr. John Breyer for his mentorship and guidance without which this study would not have been possible.

TABLE OF CONTENTS

LIST OF FIGURES

LIST OF TABLES

INTRODUCTION

High gamma-ray counts on well logs through the Barnett Shale (Mississippian) in the Fort Worth basin are caused by enrichment in uranium and may represent condensed sections. Condensed sections are the sedimentary record of maximum flooding events during cycles of relative change in sea level (Loutit et al., 1988). They play an important role in stratigraphic correlation, because condensed sections are deposited over wide areas and are well preserved in basinal settings. Fine-grained sediments rich in biogenic and chemogenic deposits represent deeper water settings, where deposition rates are slow and commonly bioturbation is high. The sediments usually have a high organic matter content and abundant glauconite and phosphate grains (Loutit et al., 1988; Creaney and Passey, 1993). Under reducing conditions, of the type that prevailed in the Fort Worth basin in the Mississippian, organic material and phosphate grains concentrated uranium in several intervals, possibly in response to changes in sea level. A siliceous siltstone enriched in glauconite and phosphate at the top of core from the EOG 2H Two-O-Five, Johnson County, Texas, has a high gamma-ray response (Bunting, 2007), and might be a condensed section. Other gamma-ray spikes in the core correlate to different lithologies. The purpose of this study is to establish a correlation if any between gamma-ray spikes and particular lithologies in the Barnett Shale. Well logs from the EOG Gordon SWD, Hill County, Texas, and EOG 2H Two-O-Five were correlated with descriptions of core and thin sections to determine if gamma-ray spikes on well logs can reliably be interpreted as condensed sections.

Sequence Stratigraphy

The Barnett Shale in north-central Texas was deposited in 400-700 feet (120-210 m) of water in a foreland basin during the Mississippian, over a period of some 25 million years (Loucks and Ruppel, 2007). A prolonged second-order highstand of global sea level began in the Middle Devonian (Eifelian) and persisted through the Mississippian (Ross and Ross, 1988). Deposition of the Barnett Shale took place during the latter part of this highstand, from 345-320 million years ago (Osagean to Chesterian) (Loucks and Ruppel, 2007). At least ten third-order cycles of change in global sea level took place during this interval (Ross and Ross, 1988).

Third-order cycles of relative change in sea level produce the depositional sequences of seismic and sequence stratigraphy (Vail et al., 1977; Vail and Wornardt, 1991). Sequence stratigraphy utilizes physical surfaces for subdividing the fill of a sedimentary basin into units for stratigraphic analysis. It is a form of allostratigraphy as redefined by Walker (1992). Depositional sequences are bound by unconformities and their correlative conformities (Mitchum and Vail, 1977). Unconformities are significant gaps in time in the stratigraphic record that may be caused by periods of erosion or nondeposition (Krumbein and Sloss, 1951). Sequence-bounding unconformities form as a result of forced regressions caused by eustacy, tectonism or a combination of both (Posamentier and Allen, 1997). At some point seaward of the coastline, the sequence-bounding unconformity dies out and passes basinward into its correlative conformity. Sedimentation is continuous across this surface and no hiatus occurs.

In basinal settings, where sedimentation is continuous and resedimentation events are rare, the correlative conformity will be in a continuous sequence of pelagic and hemipelagic

sediments. Such a surface would be difficult to recognize by lithologic criteria in outcrop and core. It might be marked by a change in the rate of sediment accumulation, but measuring this change would be beyond the limits of resolution of paleontologic data. No physical basis for a distinct log signature would exist. Surfaces other than correlative conformities must be used to subdivide thick shale sequences that accumulated in deep-water basins. Depositional sequences contain widespread surfaces within them that can be identified by physical criteria and used to subdivide a given stratigraphic interval into smaller units for analysis (Van Wagoner et al., 1990; Walker, 1992; Posamentier and Allen, 1997). These include the transgressive surface at the base of the transgressive systems tract (TST), tidal and wave ravinement surfaces within the TST, and the maximum flooding surface at the top of the TST. In areas where sedimentation rate is low, the TST may be extremely thin and the sequence boundary, transgressive surface and maximum flooding surface can coalesce into a single major erosional or non-depositional surface (Wignal, 1994).

Condensed sections associated with maximum flooding surfaces are deposited widely across the shelf and far into the basin. They accumulate during the late transgressive and early highstand systems tract (HST), persisting until prograding sediments reach the area (Schutter, 1998). They separate the TST from the overlying HST (Figure 1) (Loutit et al., 1988). Condensed sections are widespread, typically low-energy deposits resulting from relatively constant, low sedimentation rates (<1cm/1,000 yrs). They provide a clear correlation between deep-water sediments and deposits higher on the slope and shelf. Recognition of this type of sedimentation in a continental margin setting provides a surface to subdivide the strata. Deposition of a condensed section ceases when the long-term rate of increase in accommodation space is balanced with sediment supply and the next HST is

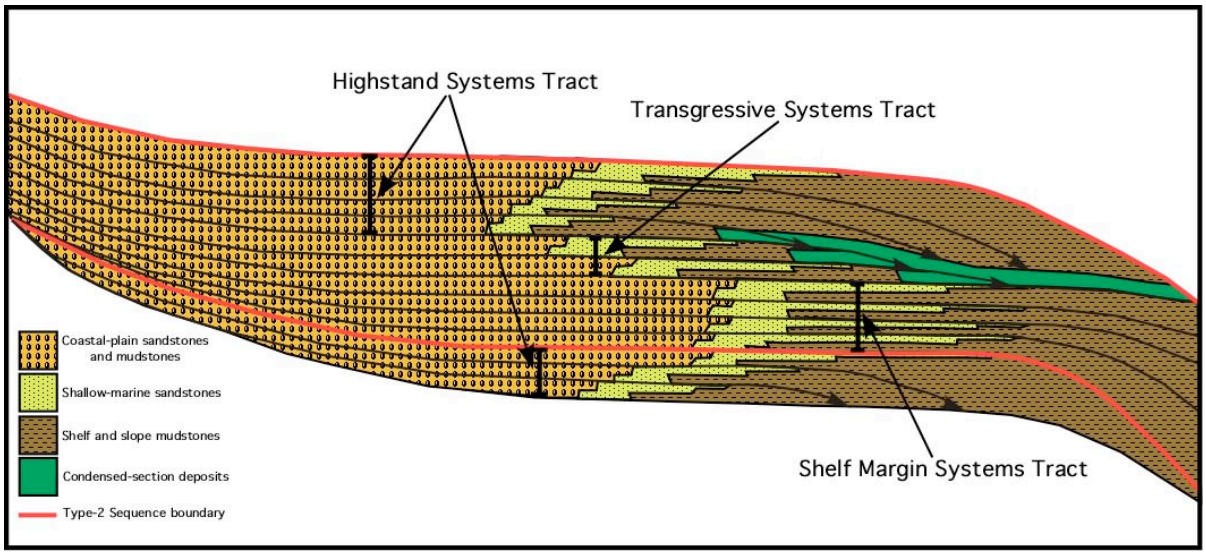

Figure 1. Sequence stratigraphic framework of a condensed section on a continental margin. After Van Wagoner et al. (1988).

deposited. The condensed section, which is the boundary between the TST and the HST, represents the downlap surface and can be recognized in seismic sections, outcrop, well logs and core. Because eustatic sea level rise is global, these surfaces can be traced regionally. However, sea level changes can also be affected by tectonics, so that occurrences of condensed sections can be confined to a single sedimentary basin. In the Fort Worth basin, changes in relative sea level reflect either increased subsidence or increased sedimentation associated with evolution of the Ouachita fold-thrust belt.

Condensed Sections

Condensed sections are thin marine stratigraphic units representing significant amounts of time. Rates of sedimentation are low because sediment is trapped higher on paleoslope in estuaries and bays. They are most extensive at the time of maximum transgression (Loutit et al., 1988). The lateral extent of condensed sections can range from tens to hundreds of kilometers (Schutter, 1998).

The sediments are typically fine grained and lack silt and coarse terrigenous debris. They often consist of skeletal remains of pelagic organisms and may concentrate age-diagnostic microfossils, which make them useful chronostratigraphic and biostratigraphic surfaces (Loutit et al., 1988). Diverse fossils are concentrated within the condensed section unless limited by low-oxygen conditions (Schutter, 1998). Other components of condensed sections include chemogenic sediments, such as phosphate, glauconite, and siderite, as well as unusual concentrations of platinum group elements such as iridium. Condensed sections commonly concentrate and preserve organic matter (Creaney and Passey, 1993).

Burrowing may be extensive depending on oxygen levels in the water column (Loutit et al., 1988). If the water column is oxygenated, bioturbation will be conspicuous and include the *Nerites* and *Zoophycos* ichnofacies assemblages in basinal settings (Schutter, 1998). Specific features of condensed sections are discussed below.

Organic Matter Content

The maximum total organic carbon (TOC) in a vertical marine sequence likely correlates with the maximum flooding surface (Bohacs, 1990; Creaney and Passey, 1993). This organic matter is of marine origin and tends to be more oil prone, producing type II kerogen. Low oxygen conditions at the sediment/water interface, the rate of degradation of organic matter, and sedimentation rate are the principal controls on organic matter accumulation (Wignall, 1994; Creaney and Passey, 1993). Basinal sediments are generally high in TOC when accommodation is high and clastic influx is low. During the formation of the maximum flooding surface, organic matter accumulates until the rate of clastic supply increases and the organic matter is diluted. Organic material deposited in a basinal setting is mainly the result of the rainout of plankton from the water column.

Organic matter accumulation is dependent on the amount of oxygen in the water column. If organic matter is deposited in oxidizing conditions, it will be consumed by bacteria and benthic organisms. Therefore, deposition in anoxic and/or dysoxic environments is required to preserve significant amounts of organic material. In areas of low dissolved oxygen, anaerobic bacteria degrade organic matter slightly, but do not remove it completely. Plankton and anaerobic bacteria constitute the bulk of organic matter in marine oil-prone source rocks (Creaney and Passey, 1993).

Pyrite

Pyrite is an authigenic mineral commonly found in deep, anoxic basins. At low sedimentation rates and/or low sulfate-reduction rates, pyrite forms by direct reaction of Fe^{2+} with H_2S. All reactive iron reacts to form pyrite and, in anoxic conditions, nearly all pyrite is preserved. In oxic conditions, pyrite is re-oxidized and is never preserved (Wignal, 1994).

The presence of framboidal pyrite indicates intense activity of sulfate-reducing bacteria resulting from the abundance of organic matter during sedimentation (Herbin et al., 1993). The presence and size of pyrite framboids relates to the chemistry of the water column and the level of dissolved oxygen. Very fine pyrite framboids (1-18μm) are associated with a euxinic (anoxic and sulfidic) water column (Loucks and Ruppel, 2007). Pyrite framboids are characteristic of very early diagenesis and form in the water column, settle to the bottom and cease to grow (Herbin et al., 1993; Loucks and Ruppel, 2007). Diffuse pyritic shale laminae, not associated with erosional surfaces, are enriched in diagenetic pyrite and organic matter, suggesting low sedimentation rates. Pyrite occurs in two different forms in the Barnett Shale, fine-grained (<10μm) framboids and euhedral crystals (Loucks and Ruppel, 2007). Shales with stratiform pyrite as well as *Tasmanites* cysts, which are generally filled with euhedral pyrite, indicate periods of non-deposition or very slow sedimentation (Schieber, 1998).

Phosphate

Marine phosphates are precipitated as francolite, a carbonate fluorapatite, containing up to 5-6 wt% CO_2, and are enriched in U, Sr, and Y (Odin and Letolle, 1980; Hoffman et al., 1998). Upwelling, which leads to an overall decrease in ocean temperatures, often results in the deposition of authigenic phosphate (Odin and Letolle, 1980). The nature of the initial

framework is calcitic, but other minerals are also common. Biological phosphate is the result of accumulation of bones, teeth or coprolites on the sea floor.

The concentration of phosphate is favored chemically and mechanically by a reduction in sedimentation rates, causing the influx of organic matter to greatly exceed clastic deposition (Odin and Letolle, 1980; Hoffman et al., 1998). Modern phosphates are closely linked to areas of high productivity and are favored by oxygen-depleted, mildly alkaline conditions (Hoffman et al., 1998). Phosphate hardgrounds and nodules are also common in deep water settings. Calcium phosphate in its early stages often becomes cemented as hardgrounds (Loucks and Ruppel, 2007).

Glauconite

Glauconite is an authigenic mineral formed in open marine settings. It originates as a green smectitic mineral, typically the potassium-rich end member mineral of the group (Odin and Letolle, 1980; Hesselbo and Huggett, 2001). Its most notable feature is the iron content, which is commonly more than 15% (Odin and Letolle, 1980).

Glauconitization occurs in areas removed from active sedimentation, and typically in areas of relatively warm temperatures (7-15°C). In continental and tropical areas, larger amounts of iron are liberated and carried to the sea (Odin and Letolle, 1980). Glauconite does not form at the surface of the ocean, but rather inside the sediment framework, in cracks, holes and pores. Authigenesis requires the exchange of ions between sea water and the pores inside the sediment. A semi-confined micro-environment is required to allow concentration of ions such as Fe, Si, and Al for the growth of glauconite. The framework acts as an ion-pump, catching ions from the sea (Odin and Letolle, 1980).

Concentrations of glauconite can occur at the base of a TST, where sedimentation rates are low. Sediment starvation makes authigenic minerals more obvious. However, glauconite is not a necessary occurrence under these conditions (Odin and Letolle, 1980; Hesselbo and Huggett, 2001).

Signature on Well logs

Electric logs are useful in recognizing condensed sections. Gamma-ray logs are especially useful as they detect radioactive elements, such as uranium, thorium and potassium. Uranium is related to deposition of organic matter and phosphate. Potassium is contained in glauconite. Organic matter, phosphate and glauconite are often concentrated in condensed sections (Loutit et al., 1988). Elevated uranium contents indicate reducing depositional environments, whereas K and Th are indicators of clay mineralogies (Doveton and Merriam, 2004).

Condensed sections can be recognized in core as calcitic hardgrounds and on well logs as a low gamma-ray and high density response (Loutit et al., 1988). On well logs, condensed sections can be recognized as the most shale-rich point between the TST and the HST (Macquaker et al., 1998). In some cases, a high resistivity spike may occur at the maximum flooding surface due to a concentration of calcareous fossils (Vail and Wornardt, 1991).

Correlations of condensed sections can be difficult in the Barnett Shale. However, Slatt et al. (2008) and Singh et al. (2008) have identified several fining- and coarsening-upward parasequences within the Barnett Shale using gamma-ray logs and core analysis. According to Slatt et al. (2008) and Singh et al. (2008), these parasequences are about 30 feet

(9 m) thick, laterally continuous and mappable. High gamma-ray counts can be correlated for long distances (Doveton and Merriam, 2004). Correlating logs using high gamma-ray counts should provide a means of subdividing the Barnett Shale for a more detailed stratigraphic analysis.

Geologic Setting

Geology of the Fort Worth Basin

The Fort Worth basin was formed in the Mississippian as a result of a continent/continent collision during the Ouachita orogeny (Figure 2) (Loucks and Ruppel, 2007). Laurussia (North American plate) was being subducted beneath Gondwana (South American plate) during this period. As Gondwana approached the craton of Laurussia, overthrusting began, causing a downwarping of the North American craton and forming a deep foreland basin.

During the Siluro-Devonian, the Laurentian craton was exposed (Figure 3). Shallow water Ordovician carbonates such as the Ellenburger and Viola Formations were eroding. Meanwhile, Ordovician deep-water deposits of the Ouachita facies, composed of shales, sandstone turbidites, and novaculites, were incorporated in an accretionary wedge. During the Late Mississippian and Early Pennsylvanian, the accretionary wedge was folded and thrust against the craton, creating a deep foreland basin to the west (Figure 4). Erosion of this fold-thrust belt created thick Mississippian and Pennsylvanian flysch deposits. The strata grade eastward from shallow-water limestones to shales and sandstones supplied from the growing subduction complex to the east (Walper, 1982). Mississippian Chappel reefs formed along the western margin of the basin, and the Barnett Shale was deposited in the newly

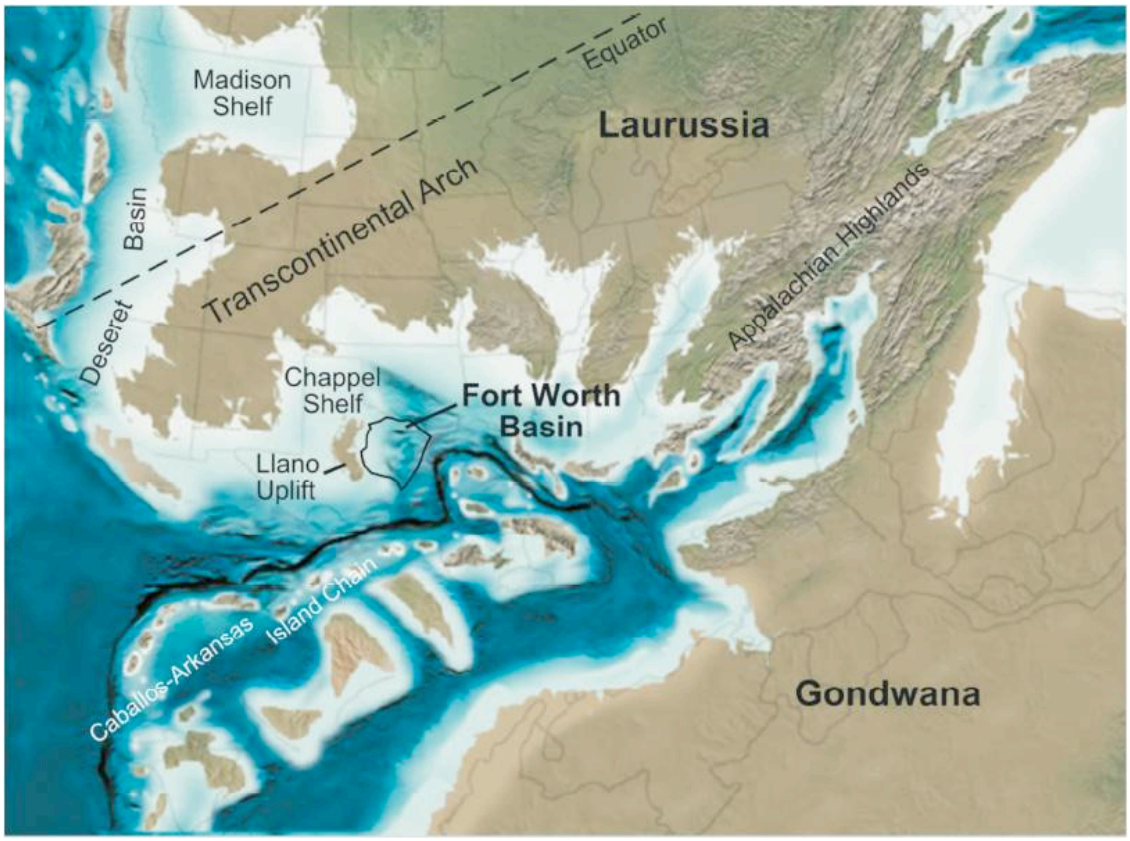

Figure 2. Paleogeography during the Mississippian. The location of the Fort Worth Basin is outlined in black. From Loucks and Ruppel (2007).

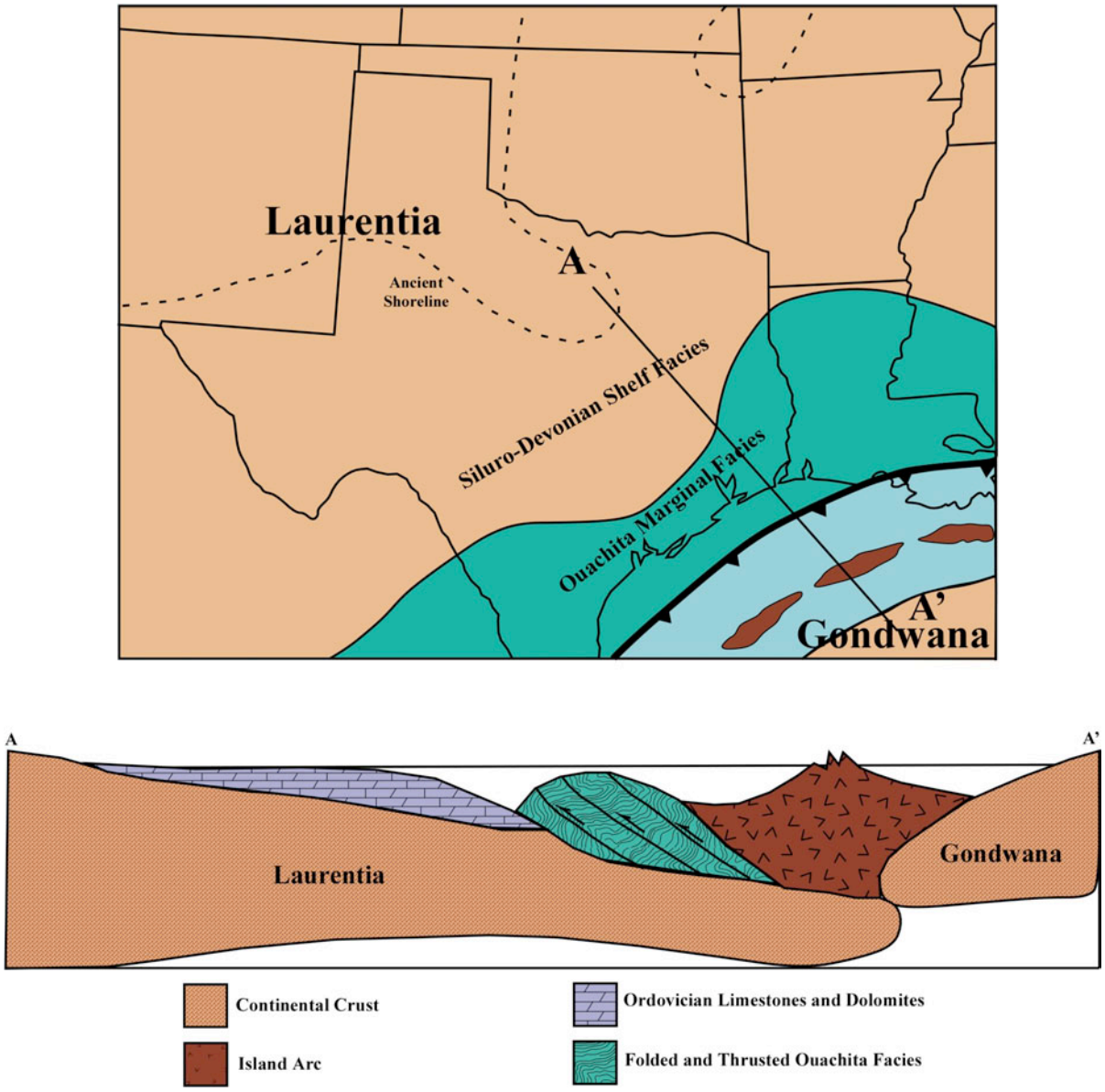

Figure 3. Paleogeography and generalized cross section of the mid-continent during the Siluro-Devonian. Modified from Walper (1982).

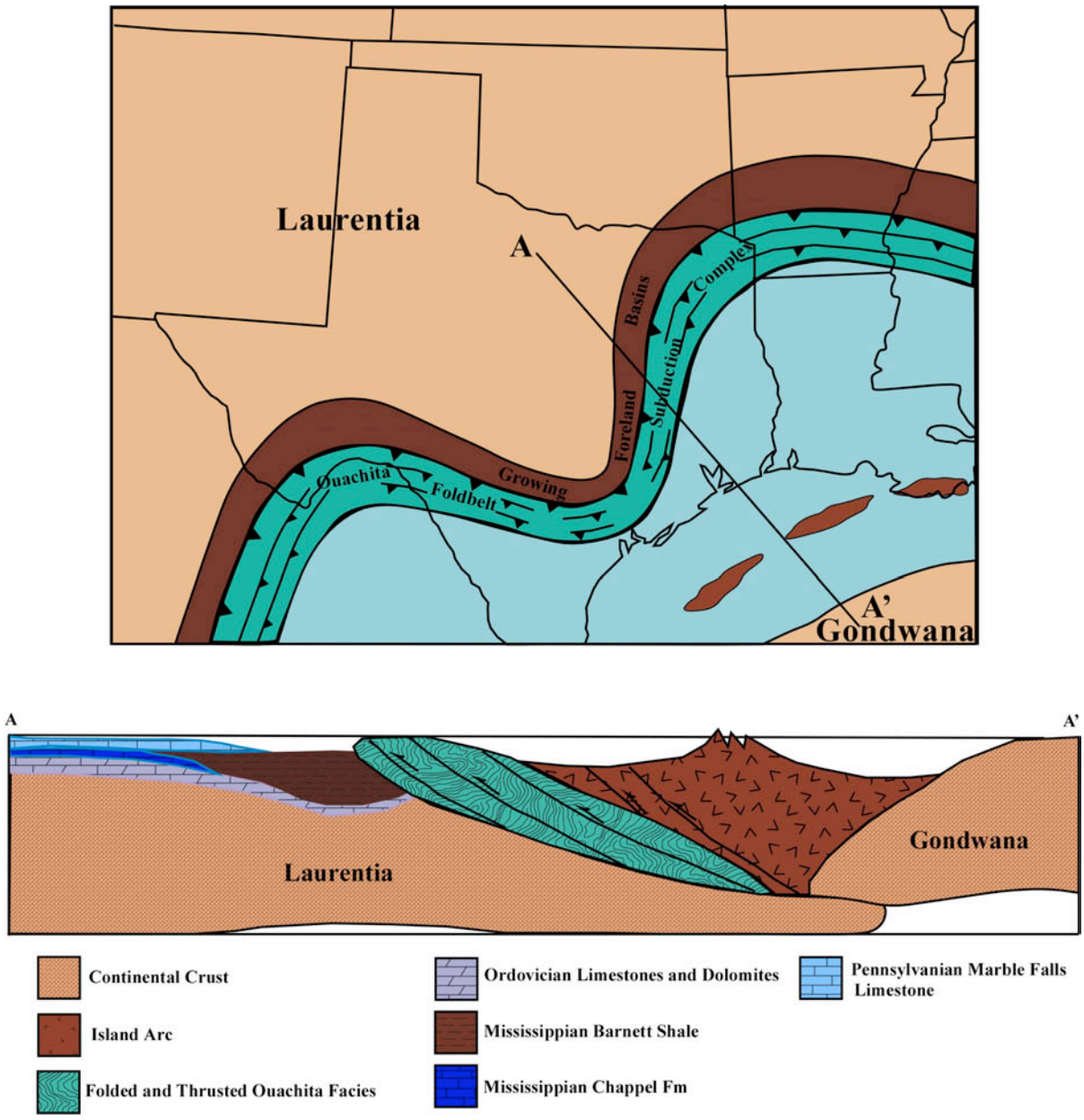

Figure 4. Paleogeography and generalized cross section of the mid-continent during the Late Mississippian-Early Pennsylvanian. Modified from Walper (1982).

formed, deep, anoxic basin. During the Early Pennsylvanian, the Marble Falls carbonate platform developed along the western margin of the basin. As the Ouachita fold-thrust belt advanced, the carbonate platform drowned and migrated westward (Walper, 1982; Erlich and Coleman, 2005). Sedimentation became more complex along the eastern margin of the Fort Worth basin during the Middle Pennsylvanian (Figure 5). Sediments eroded from the exposed Marble Falls carbonates intermingled with shales and sandstones shed from the Ouachita fold-thrust belt, which became a major source of sediment at this time. The Smithwick Shale, a spiculitic, organic-rich shale, is the basinal equivalent of the Upper Marble Falls Formation (Erlich and Coleman, 2005). The zone of interfingering between the Smithwick and the Marble Falls marched westward as the Ouachita fold-thrust belt advanced. As plate convergence ceased, subsidence decreased within the Fort Worth basin during the Late Atokan and Early Strawn (Walper, 1982). Strawn fluvial/deltaic sediments prograded across the foreland basin.

The stratigraphic section of the Fort Worth basin is shown in Figure 6. The Fort Worth basin is delimited on the west by the Bend arch, on the south by the Llano uplift, on the north by the Red River and Muenster arches, and on the east by the Ouachita overthrust. The deepest part of the Fort Worth basin is located on the eastern side along the Ouachita fold-thrust belt. The basin shallows to the west (Figure 7).

Depositional Environment of the Barnett Shale.

The Barnett was deposited in deep water in the Fort Worth basin during the Chesterian (Loucks and Ruppel, 2007). The oceanic waters in the long and narrow basin were restricted from the open ocean, which caused the Barnett Shale to be deposited in

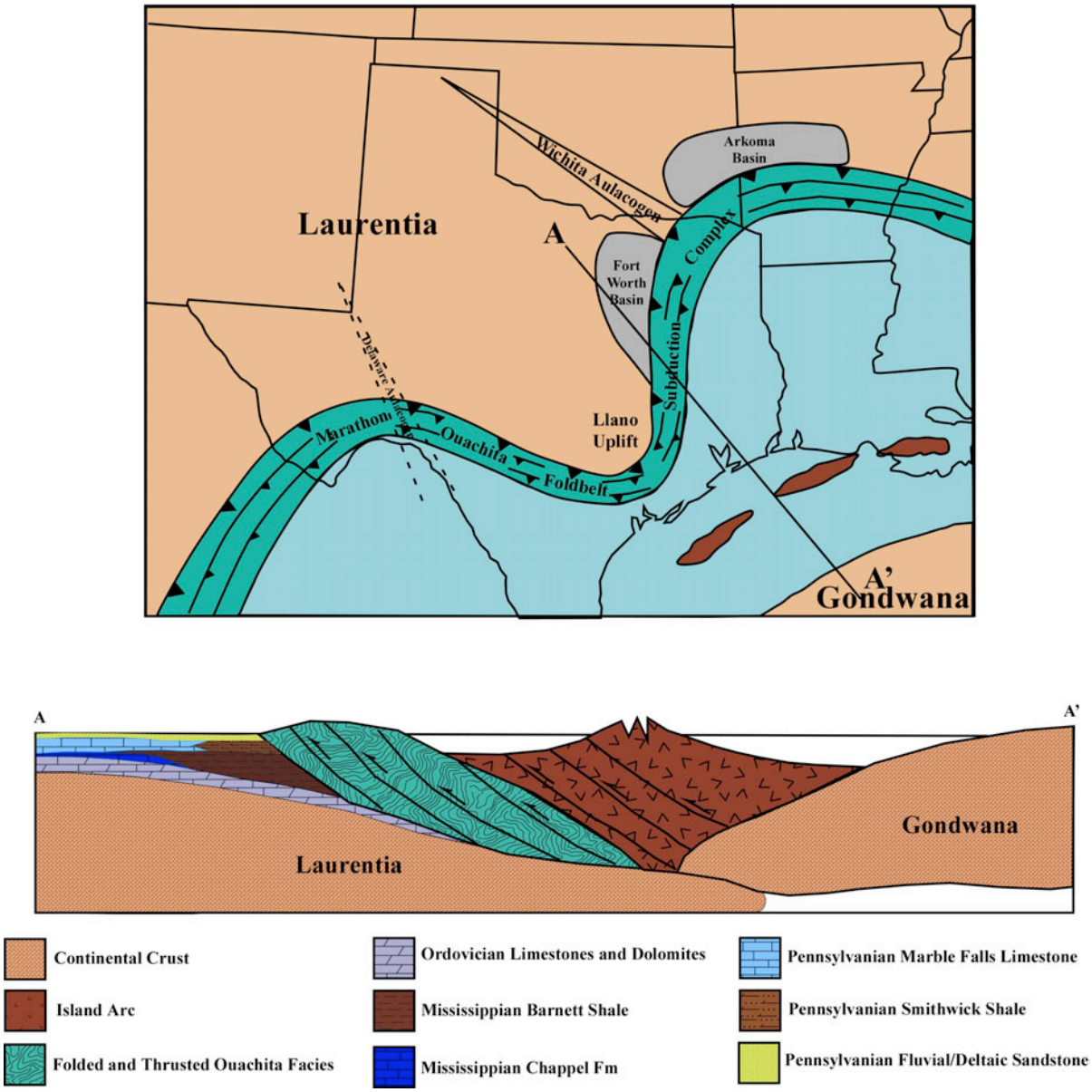

Figure 5. Paleogeography and generalized cross section of the mid-continent during the Middle Pennsylvanian. Modified from Walper (1982).

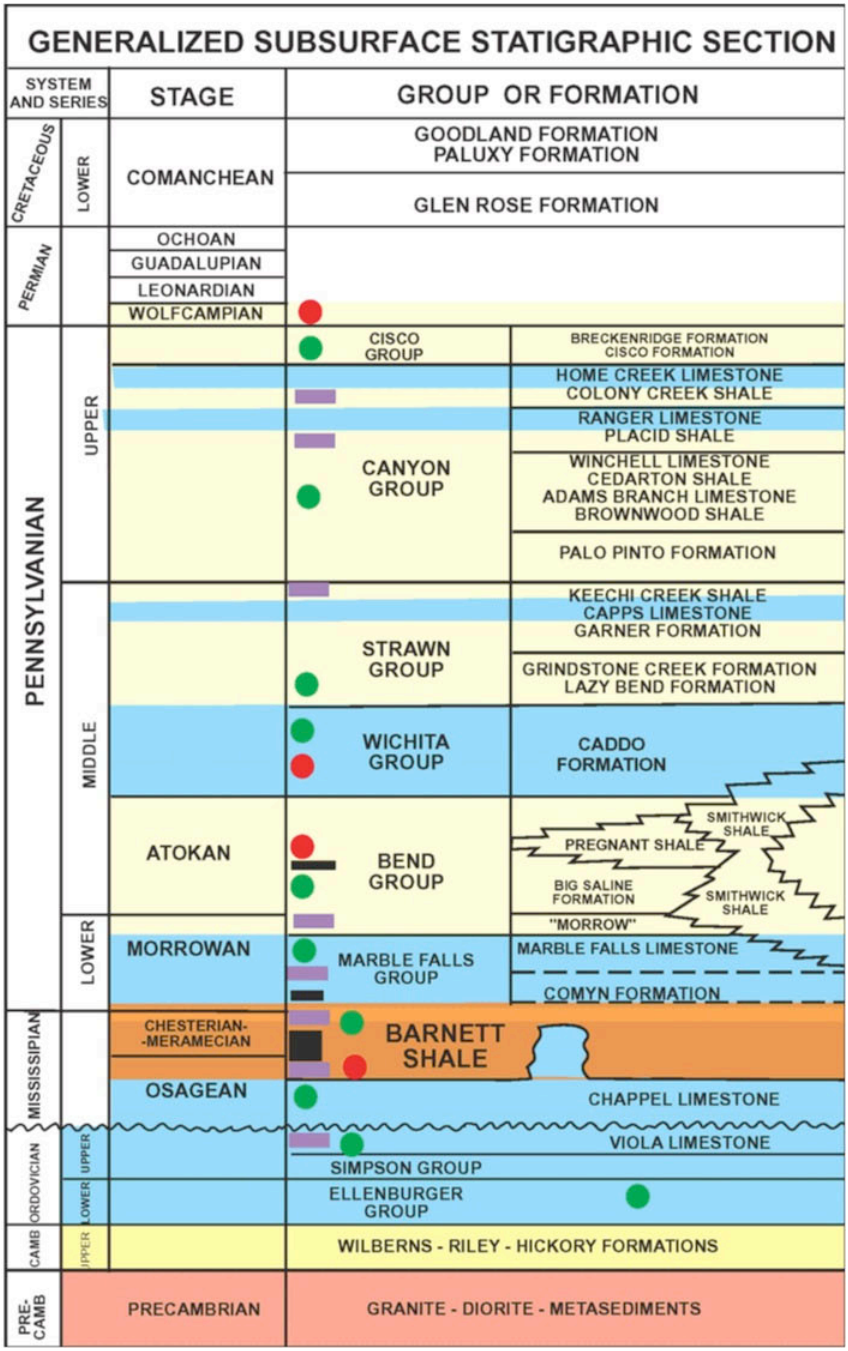

Figure 6. Generalized stratigraphic section of the Fort Worth Basin. Blue shows limestone and yellow shows clastics. Black rectangles show source rocks. Purple rectangles show seals. Green dots indicate oil reservoirs. Red dots indicate gas reservoirs. Modified from Pollastro (2007).

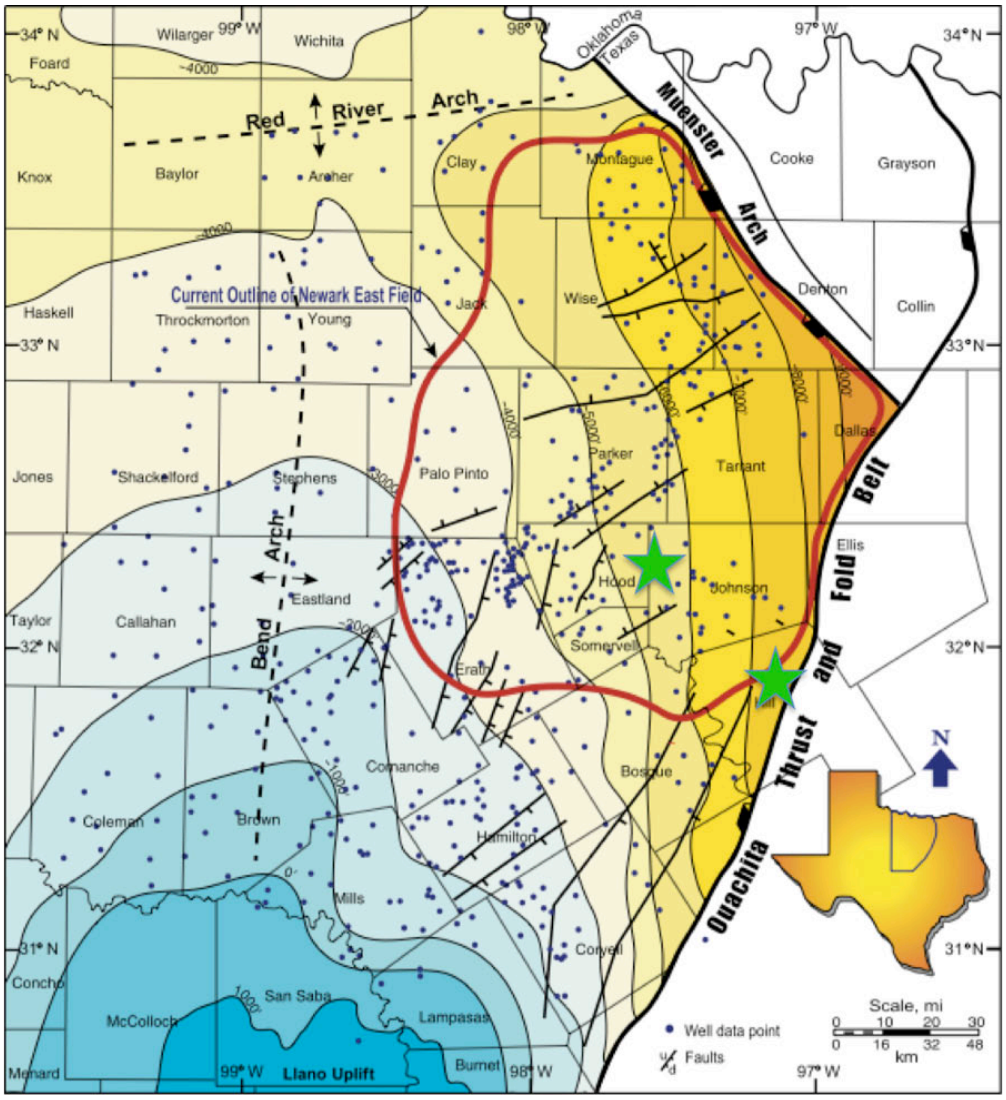

Figure 7. Regional geology and general structure on the base of the Barnett Shale. The orange area is the deepest part of the basin while the blue area is the shallowest. The contour interval is 1,000 ft. Newark East field is outlined in red. The locations of the core used in the study are marked by green stars. From Zhao et al. (2007).

anoxic conditions. The Barnett Shale was deposited over a 25 M. period, which means that sedimentation rate was approximately 14 μm/yr.

Loucks and Ruppel (2007) provide a depositional model for the Barnett Shale (Figure 8). The bottom waters were anaerobic or dysaerobic, which was a key factor in preserving organic matter. Because of anoxia, consumers of organic material were not able to thrive. Sedimentation was primarily a result of suspension settling and density currents from the adjacent shelf. Thin, planar laminae of fine-grained material marked by the absence of larger skeletal remains are evidence of suspension settling (Figure 8). The organic matter was derived from the water column and from further up on the shelf. It was deposited from hemipelagic mud plumes and as skeletal debris from planktonic organisms. Upwelling of bottom waters presumably promoted blooms of radiolaria and the development of phosphate grains on the slope. Phosphatic hardgrounds are found in the Barnett and represent depositional hiatuses (Loucks and Ruppel, 2007). These hardgrounds could represent condensed sections within the Barnett Shale.

Bioturbation is rarely observed in the Barnett Shale in the Fort Worth basin. The absence of bioturbation in the proposed condensed sections can be explained by the anoxic conditions that prevailed during the Mississippian. Rare burrows in the Barnett likely represent doomed pioneers, which were transported from the shelf margin into the deep anoxic basin by turbidity currents. The organisms burrowed into the substrate and quickly died.

Several global sea level changes occurred during the Mississippian (Ross and Ross, 1988), leading to the formation of maximum flooding surfaces and condensed sections (Figure 9). However, tectonics can also cause changes in relative sea level. The Fort Worth

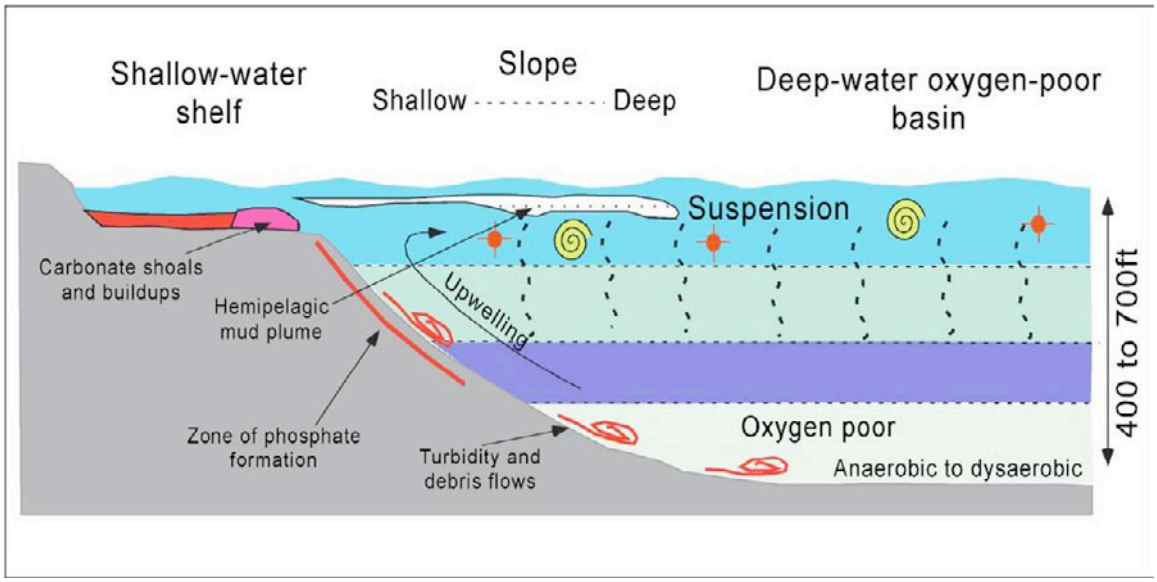

Figure 8. Environment of deposition of the Barnett Shale. The accumulation of organic matter was mostly due to suspension deposition from hemipelagic mud plumes and biota settling out of the water column. After Loucks and Ruppel (2007).

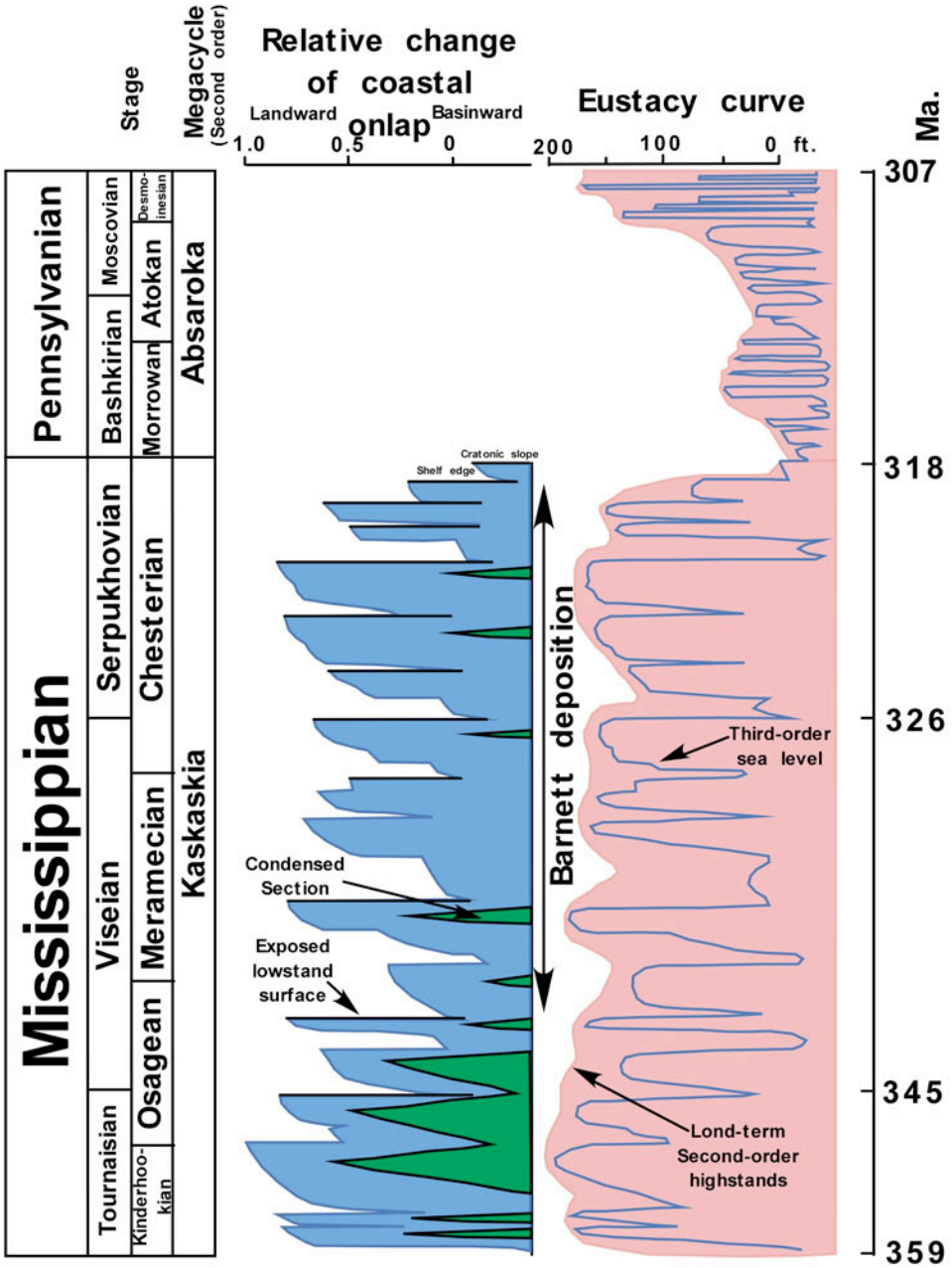

Figure 9. Global sea level curve during the Mississippian and Early Pennsylvanian. From Loucks and Ruppel (2007) and Ross and Ross (1987).

basin was an area of active tectonism during the Mississippian. This tectonism could have caused large changes in accommodation space. During highstands of relative sea level, the deepest part of the basin was starved of detrital sediment. Authigenic minerals such as glauconite and phosphate formed and the sediments were enriched in uranium concentrated in organic matter (Loucks and Ruppel, 2007).

METHODOLOGY

Bunting (2007) analyzed thin sections taken from core from the EOG 2H Two-O-Five. Facies A was described as a finely laminated, siliceous siltstone rich in glauconite and phosphate grains (Figure 10). Facies A also had abundant skeletal remains of pelagic organisms, especially sponge spicules (Figure 11). The well log for EOG 2H Two-O-Five shows that Facies A makes up the top 17 feet of core. The well log response in this interval shows high gamma-ray counts, corresponding to an enrichment of uranium (Figure 12). Facies A can be interpreted as a condensed section in the Barnett Shale. Core description and log analysis were performed on the EOG Gordon SWD core to compare the occurrences of condensed sections to the EOG 2H Two-O-Five. The goal is to determine whether high gamma-ray readings correspond directly to lithologies described and interpreted as condensed sections. Another goal was to construct a model for the depositional environment for the Barnett in Hill County, where the stratigraphy of the Barnett Shale is different from other published core studies in the Fort Worth basin.

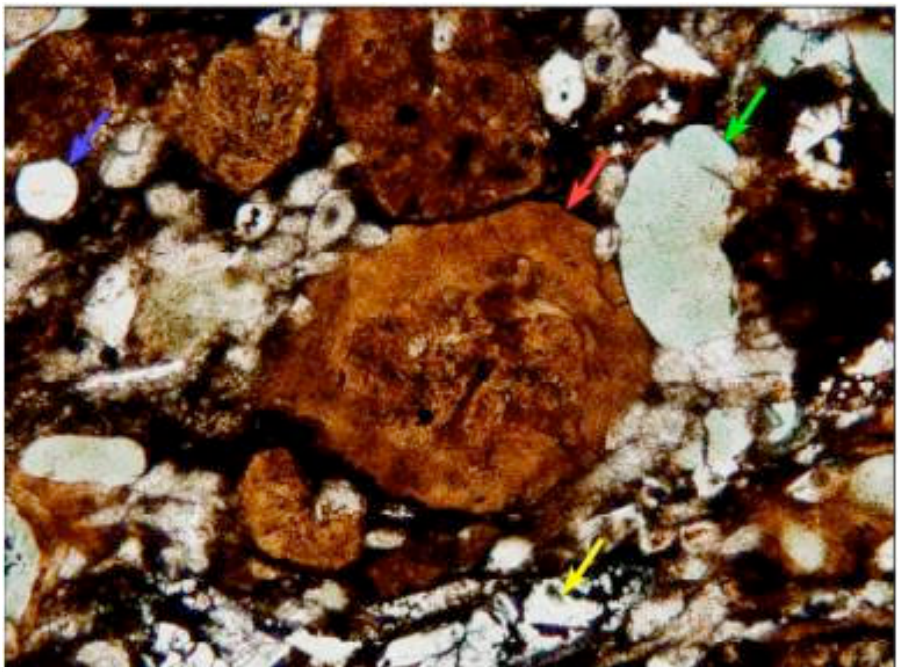

Figure 10. Photomicrograph of Facies A from Bunting (2007), showing phosphate grain (red arrow), glauconite grain (green arrow), sponge spicule (blue arrow), and cherty bioclast (yellow arrow). Plane Light. Field of view 1mm across.

Figure 11. Photomicrograph of Facies A, showing distinct lamination. The majority of white grains are sponge spicules. Plane light. Field of view 8mm across. From Bunting (2007).

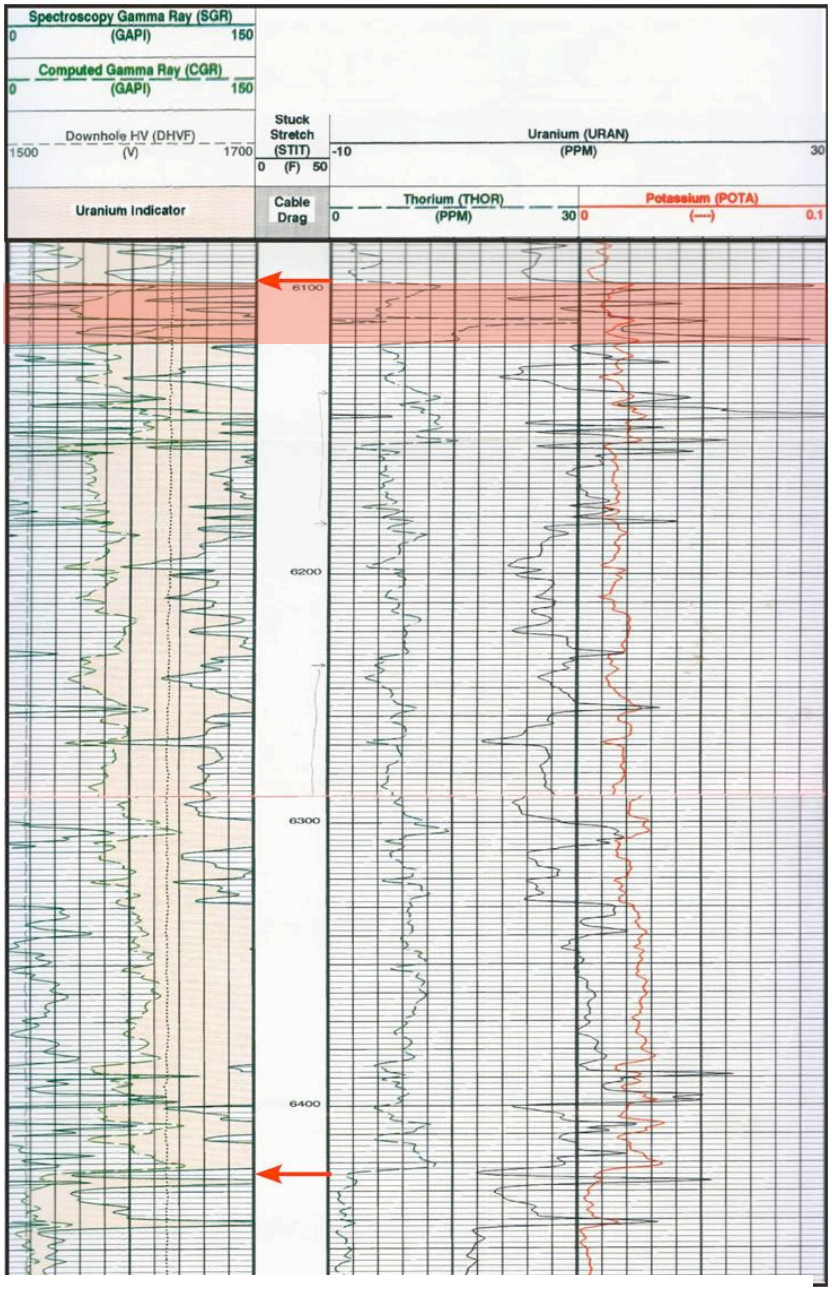

Figure 12. Well log from the EOG 2H Two-O-Five, Johnson County, Texas, showing the amounts of uranium, thorium and potassium plotted against gamma-ray response. Facies A of Bunting (2007) is highlighted in red. Red arrows indicate top and bottom of cored interval.

Core Description

EOG Resources provided core from the Gordon SWD, Hill County, Texas for this study. The cored interval (272 ft) extends from depths of 8,361 to 8,648 ft. The intervals from 8,534 to 8,541 ft and 8,602 to 8,610 ft were not recovered. A macroscopic and microscopic examination of the core was performed.

Macroscopic core description was aided by a binocular microscope. Color, grain size, sedimentary structures, fractures and composition were noted in a detailed core description (Appendix 1). Color was described using a Munsell soil color chart.

The microscopic core description was done with a standard petrographic microscope and a macroscope. One hundred and twenty-nine thin sections were made from typical lithologies identified using the macroscopic core description. Qualitative petrographic analyses of the thin sections were carried out, noting the ratios of clay to silt, abundance of calcite, quartz and other grains, fossil content, and sedimentary structures. Sections of normal thickness (30 microns) were used as well as thinner sections (about 25 microns) in certain clay-rich zones.

A sample from every foot of core was subjected to Rock-Eval pyrolysis. TOC data is important in determining the relationship between organic matter and condensed sections. It can also be used to establish a sequence stratigraphic framework for the Barnett Shale.

Well Log Analysis

Logs from 171 wells from Johnson and parts of Hill, Hood, Somervell and Bosque counties, Texas, were used to identify and map smaller units within the Barnett. Digital logs containing gamma-ray, resistivity, and density data were used to correlate from well to well.

A detailed cross section was constructed from the central part of the basin to the eastern edge. The cross section extends from the EOG 2H Two-O-Five to the EOG Gordon SWD and shows in detail the change in the stratigraphy. The gamma-ray and density logs show a strong correlation with calcite concretions as well as dolomitic facies in the Barnett Shale. These logs were used to tie the EOG Gordon SWD well log to the core.

RESULTS

Stratigraphy of the EOG Gordon SWD

The EOG Gordon SWD is divided into three separate packages based on gamma-ray response (Figure 13). The lower unit, which is identified as the Barnett, sits above the Viola Limestone and below the middle unit. The Barnett section in this well has a very high gamma-ray signature. The base of the Barnett is defined as a change from low gamma-ray to high gamma-ray response. The top of the Barnett is defined as a very high gamma-ray marker. The age of the rocks above the Barnett and its lithostratigraphic equivalent are unknown; therefore, “middle unit” and “upper unit” are used. The middle unit sits between the Barnett and the upper unit. The middle unit has a gamma-ray signature that is relatively high, but is lower than that in the Barnett. The base of the middle unit is defined by a very high gamma-ray marker, and its top is defined as the base of the low gamma-ray marker, which represents the start of the upper unit which has a low gamma-ray signature throughout. The top of the upper unit was not cored, but based on well-log analyses, is marked by a regional flooding surface.

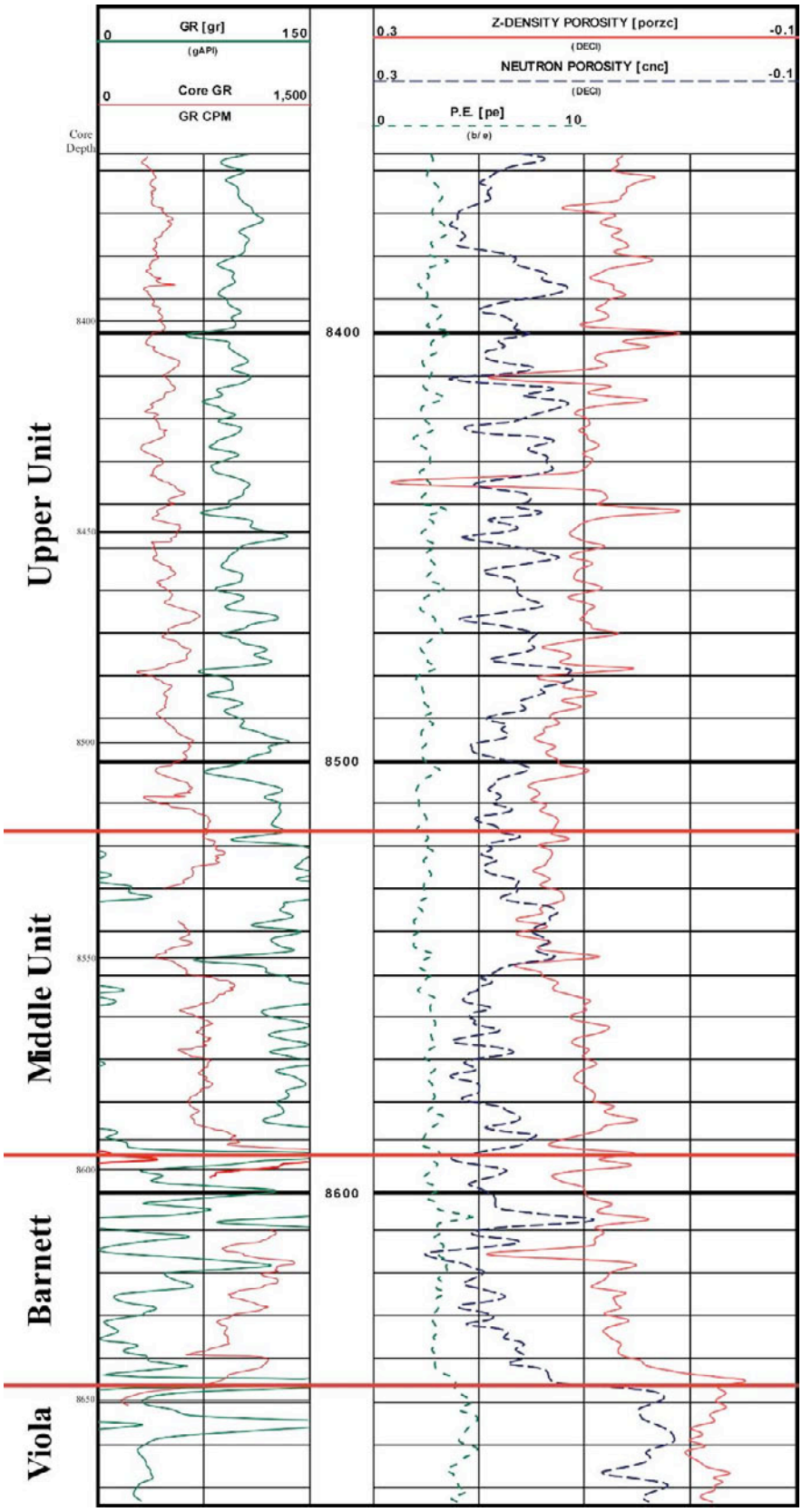

Figure 13. Stratigraphy of EOG Gordon SWD

Core Description

Five major facies containing eight subfacies are present in the core (Table 1). The stratigraphic distribution of each facies in the core varies with depth (Figure 14) and also relates to the well log response (Figure 15). Each facies is described below.

Facies A

Facies A is a dark mudstone or claystone. Subfacies A_1 is a grayish-black to black mudstone or claystone with faint planar fabric to relatively massive internal structure (Figure 16). Calcite- and pyrite-filled fractures are common, as are open fractures. A few small shell fragments replaced by chalcedony and pyrite can be seen in thin section. The clay matrix is rich in organic material and contains mostly small (.03mm) and a few larger (.07mm) sponge spicules, which were originally made of opal A and are now replaced by chalcedony, calcite, dolomite, and pyrite (Figures 17-19). Pelagic fossils found in Facies A_1 include compacted agglutinated forams containing microcrystalline quartz grains (Figure 20, 21). Other microfossils include *Tasmanites* (algal cysts) and radiolaria, both of which are replaced by calcite (Figures 22-24). The well log response for subfacies A_1 generally shows a higher gamma-ray response (about 95 API units) than the other subfacies (Figure 15).

Facies A_2 is a grayish-black to black dolomitic mudstone or claystone. This subfacies is lighter in color than subfacies A_1 (Figure 25) and is relatively massive with little or no internal lamination. In thin section, dolomite can be seen as small, irregular patches scattered throughout the clay matrix. Dolomite rhombs are not conspicuous (Figures 26, 27). The organic shale matrix was altered to dolomite during diagenesis. Sponge spicules are also present and are often replaced by dolomite. The gamma-ray response for this subfacies is

Facies	Description
A	**Dark mudstone or claystone**
A_1	Organic rich. Contains hemipelagic fauna: sponge spicules, radiolaria, forams
A_2	Dolomitic mudstone to claystone. Matrix is altered to dolomite
A_3	Contains pyrite and phosphate nodules in clay matrix
B	**Siltstone**
B_1	Continuous, planar laminae. Abundant sponge spicules
B_2	Discontinuous, wavy, non-parallel laminae. Abundant sponge spicules
B_3	Massive. Silt-sized detrital quartz in clay matrix
C	**Phosphatic Facies**
C_1	Phosphatic streaks. Thin layers of phosphate in clay matrix
C_2	Phosphatic sand. Sand-sized grains of phosphate in clay matrix
D	**Compacted shell layers**
E	**Calcite concretions**

Table 1. Facies observed in core.

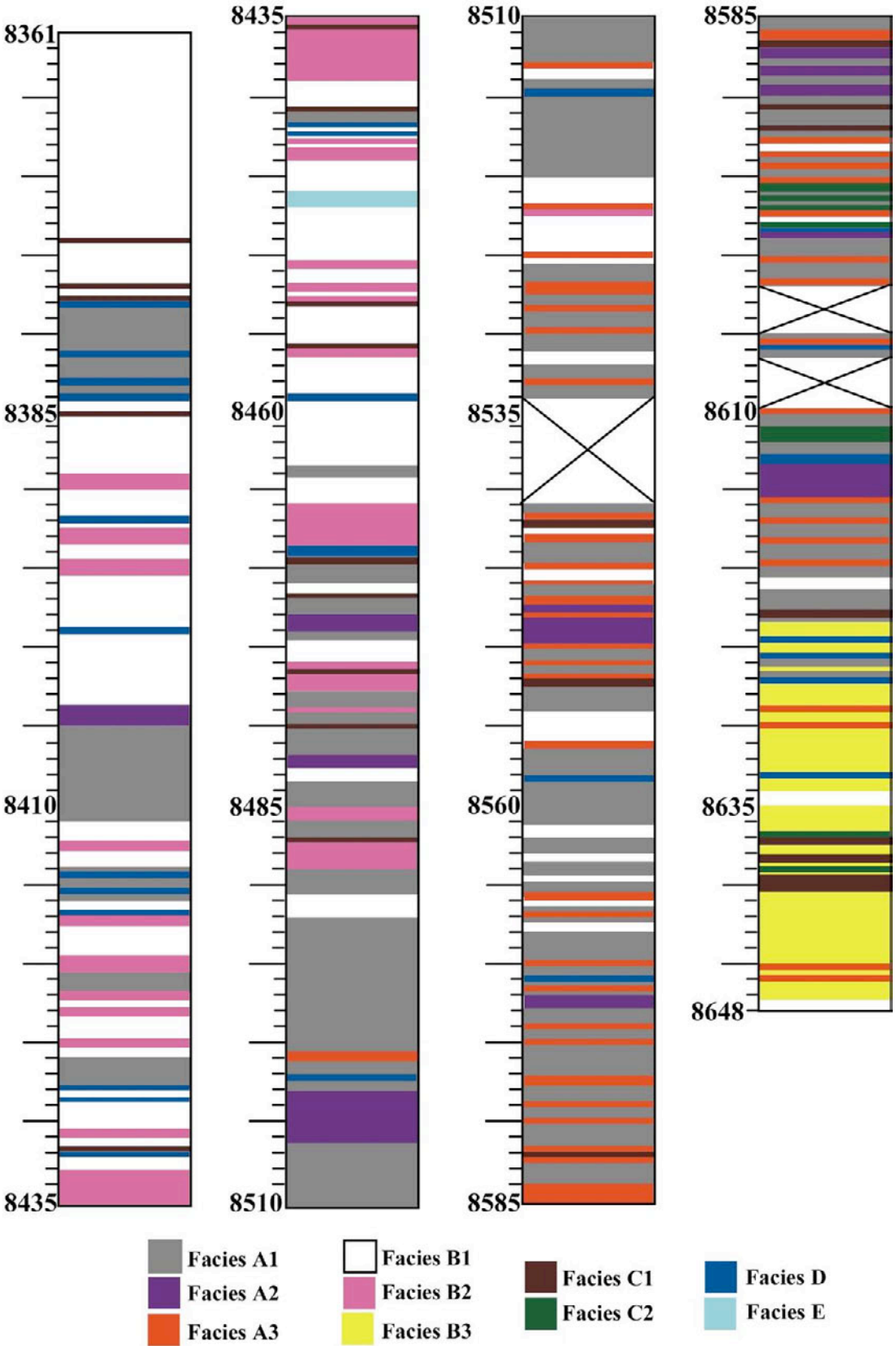

Figure 14. Distribution of facies with depth.

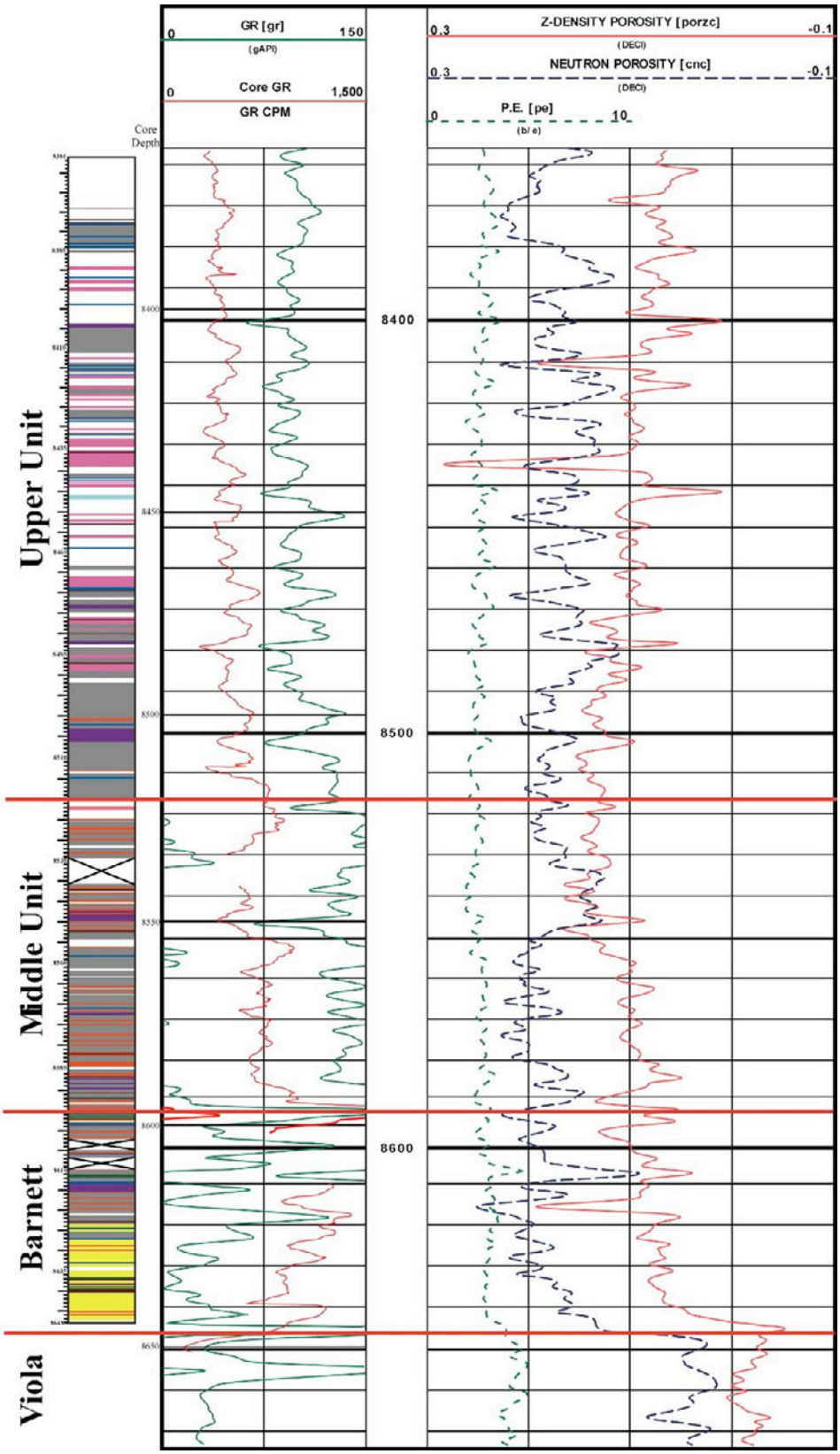

Figure 15. Well log of EOG Gordon SWD compared to distribution of facies in core.

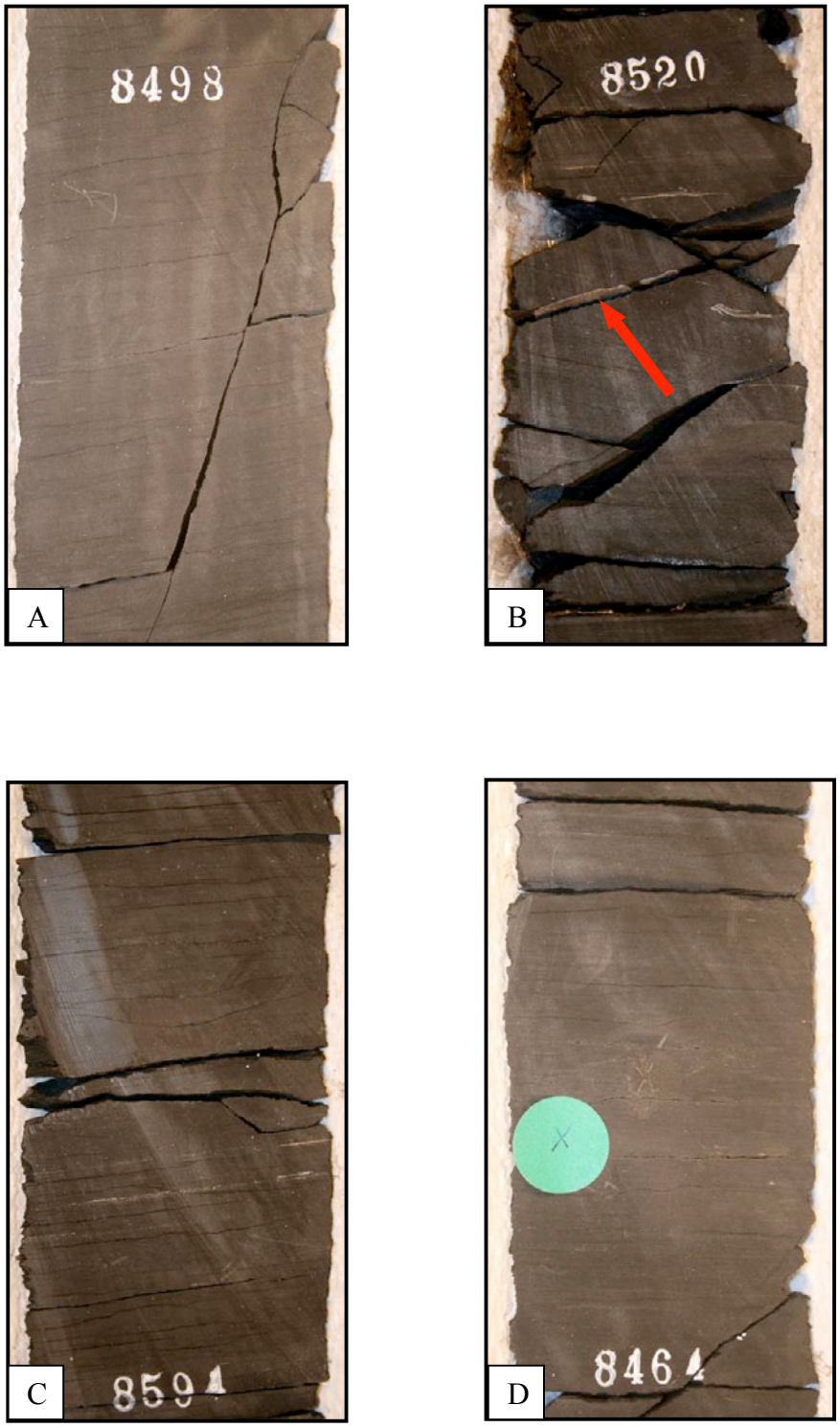

Figure 16. Core photos of subfacies A_1. Red arrow points to healed fracture. In this and following photographs, green and blue circles indicate locations where thin sections were made. Core is 6cm wide.

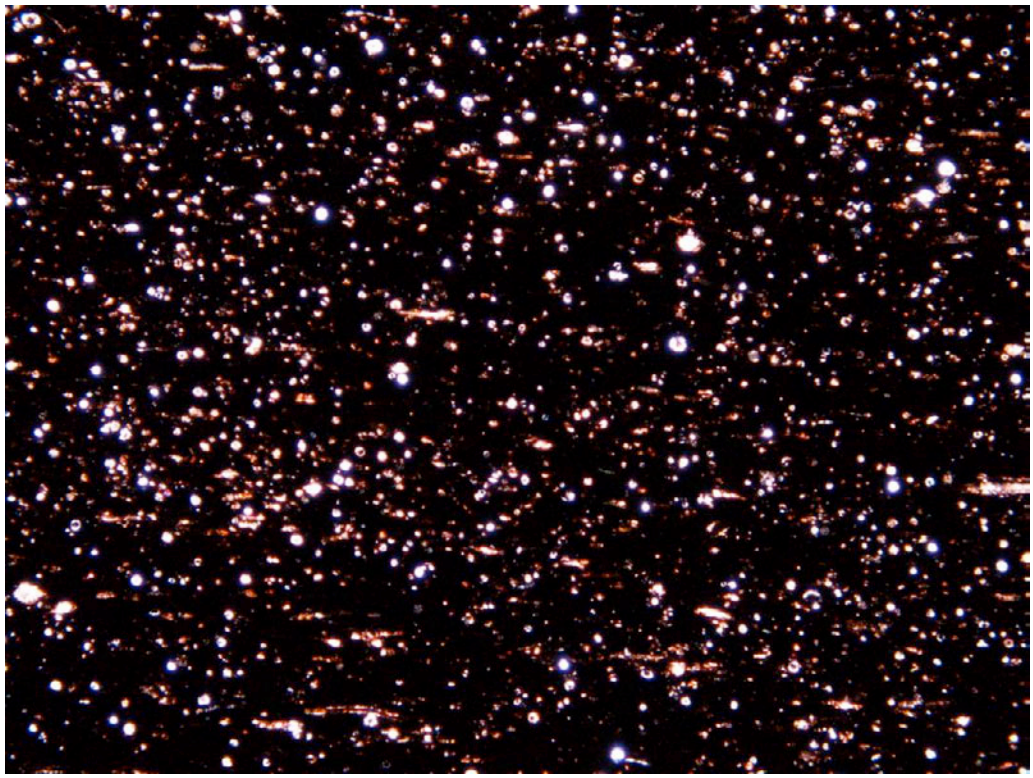

Figure 17. Photomicrograph of subfacies A_1. Most of the silt-sized grains are sponge spicules. Cross-polarized light. Field of view is 2.2mm across. 8479.8 ft.

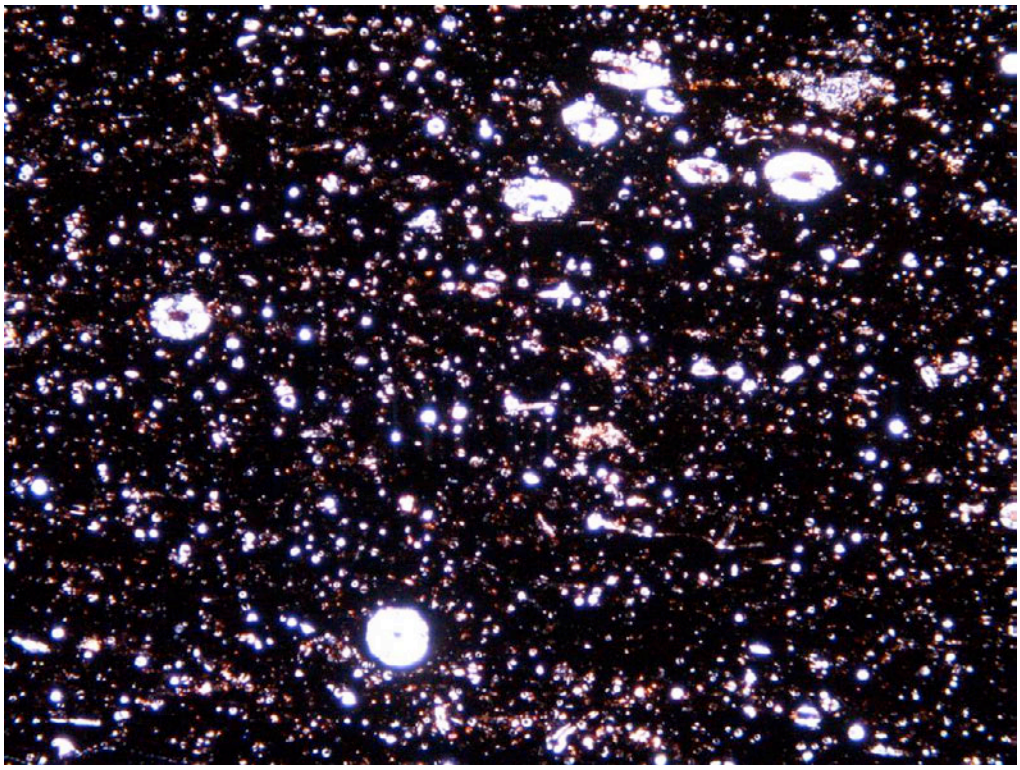

Figure 18. Photomicrograph of subfacies A_1. Note the larger sponge spicules. Cross-polarized light. Field of view is 2.2mm across. 8526.6 ft.

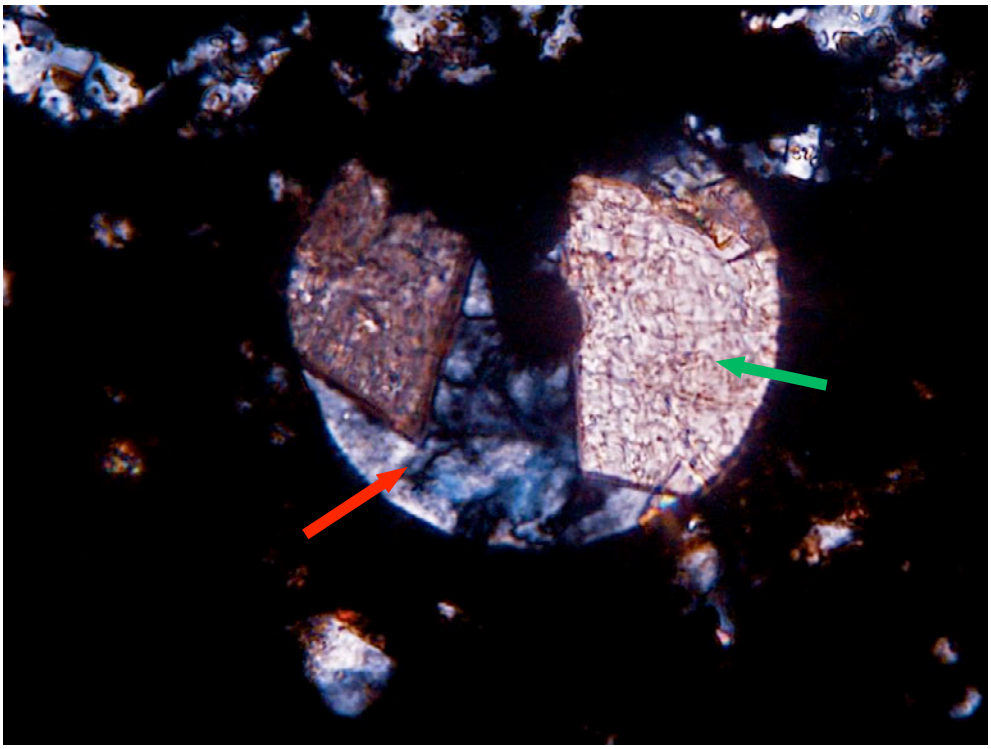

Figure 19. Photomicrograph of a sponge spicule being replaced by dolomite rhombs in subfacies A_1. Red arrow points to chalcedony and green arrow points to dolomite. Cross-polarized light. Field of view is 0.3mm across. 8533.5 ft.

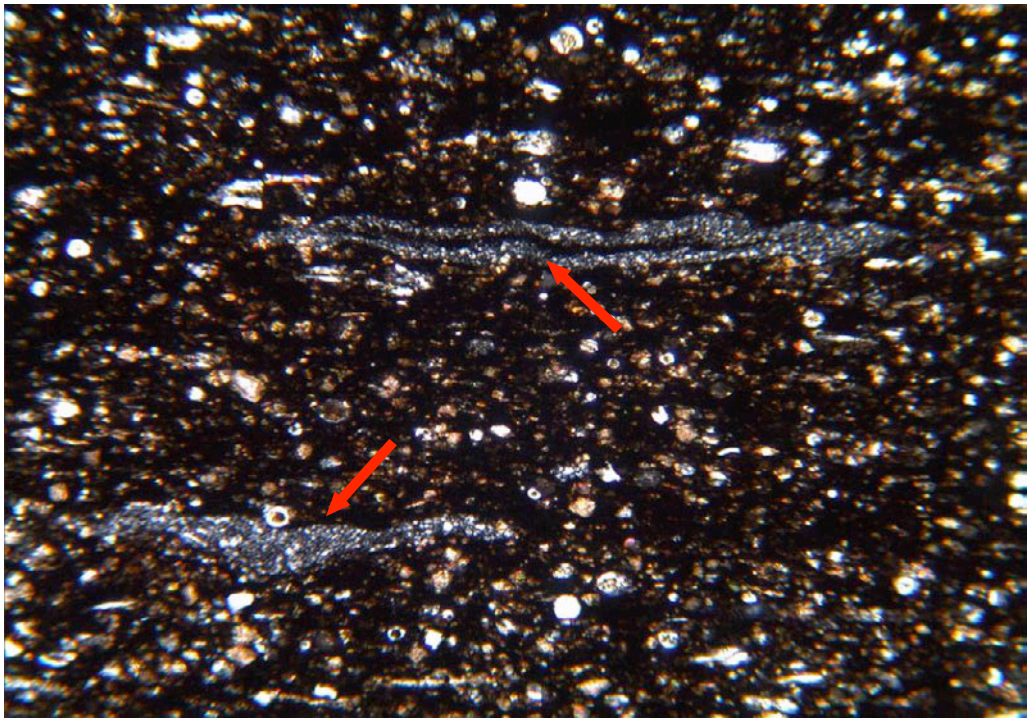

Figure 20. Photomicrograph of subfacies A_1 showing compacted agglutinated forams (red arrows) comprised of microcrystalline quartz. Cross-polarized light. Field of view is 1mm across. 8406 ft.

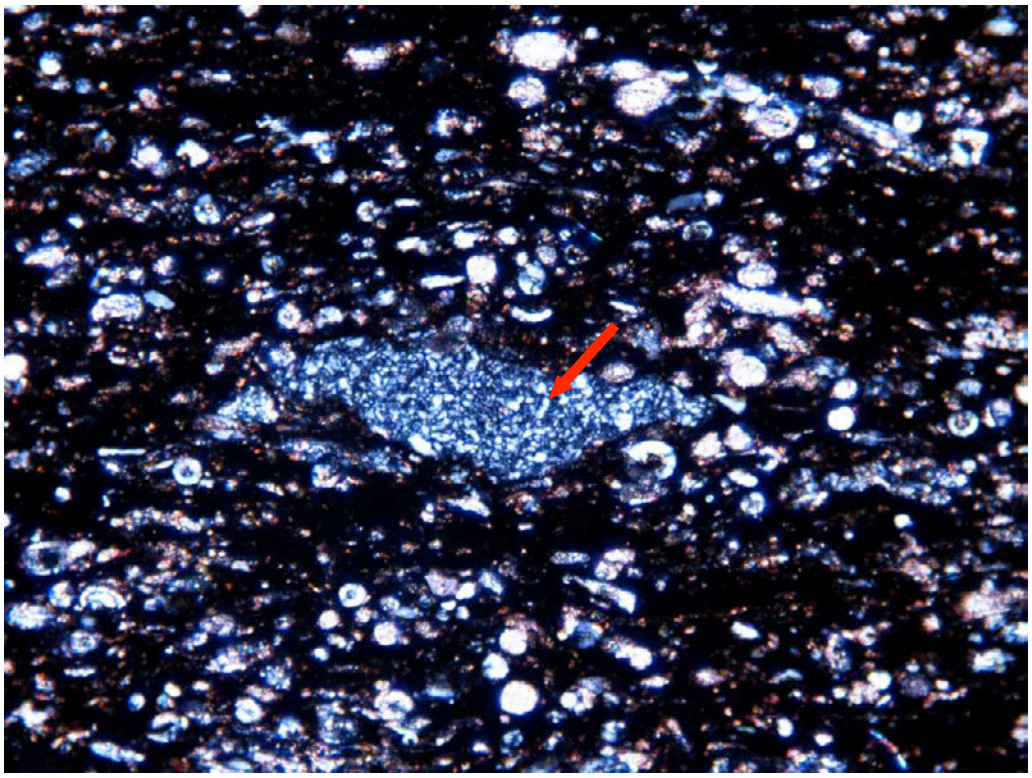

Figure 21. Photomicrograph of subfacies A_1 showing agglutinated foram (red arrow). Cross-polarized light. Field of view is 0.9mm across. 8368.3ft.

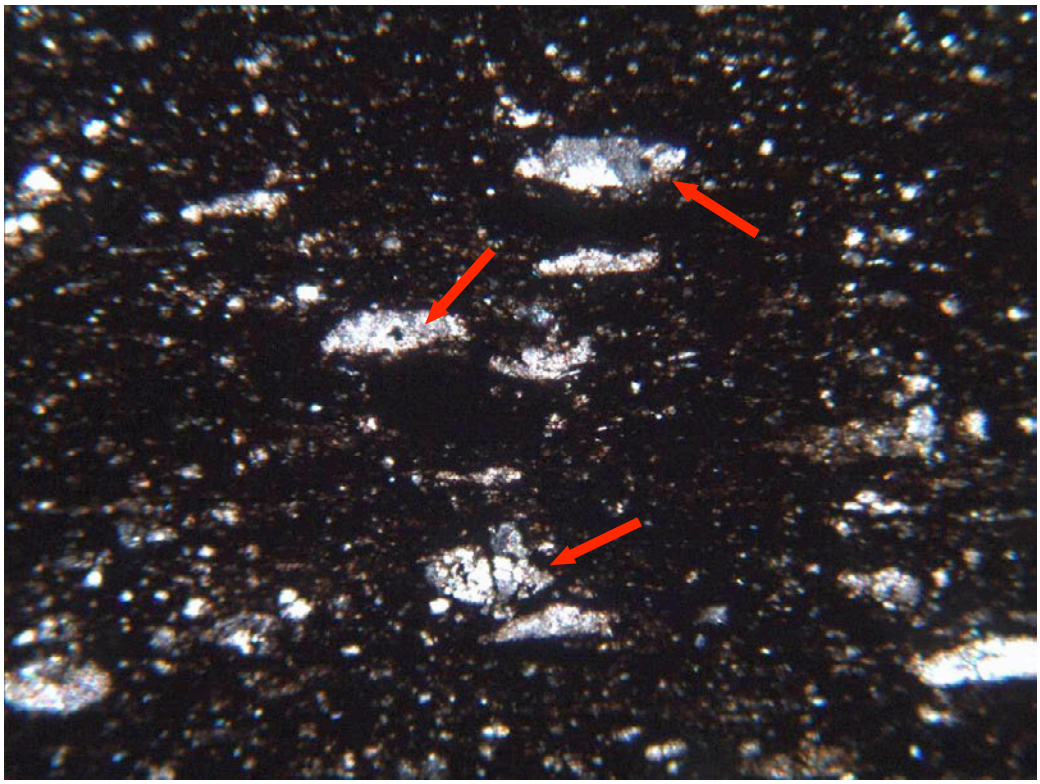

Figure 22. Photomicrograph of subfacies A_1. Note the compacted *Tasmanites* (algal cysts) (red arrows). Cross-polarized light. Field of view is 1mm across. 8612.5 ft.

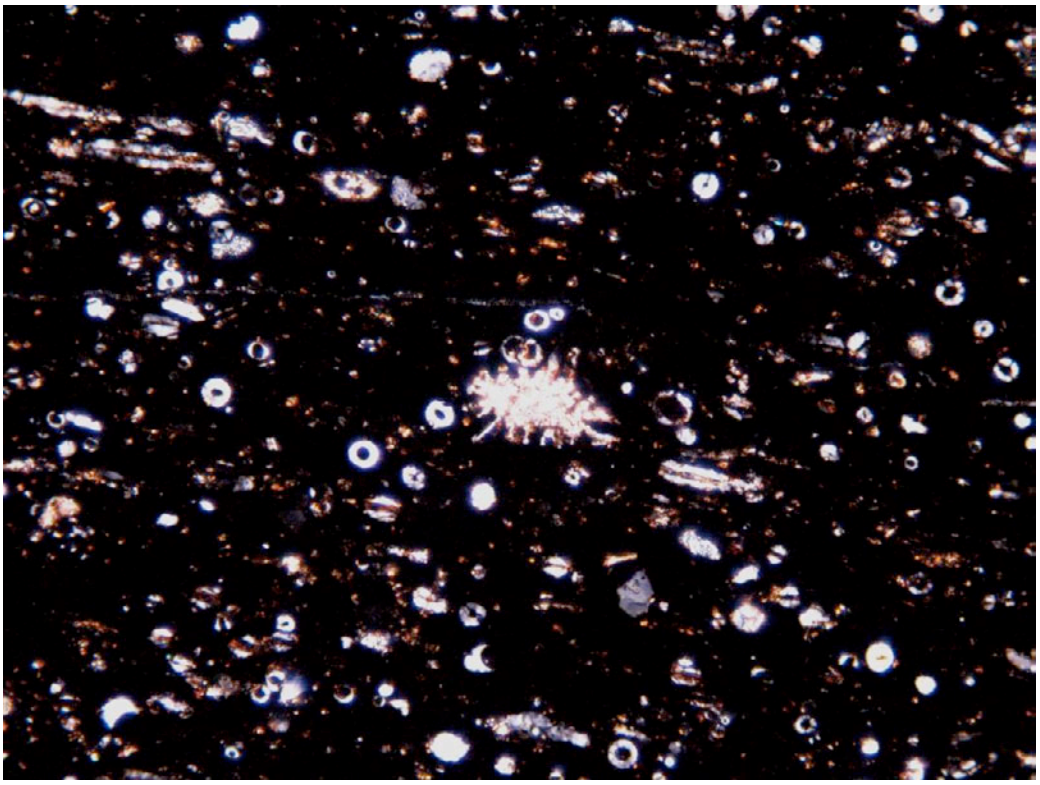

Figure 23. Photomicrograph of radiolarian among sponge spicules in subfacies A_1. Cross-polarized light. Field of view is 0.9mm across. 8497.5 ft.

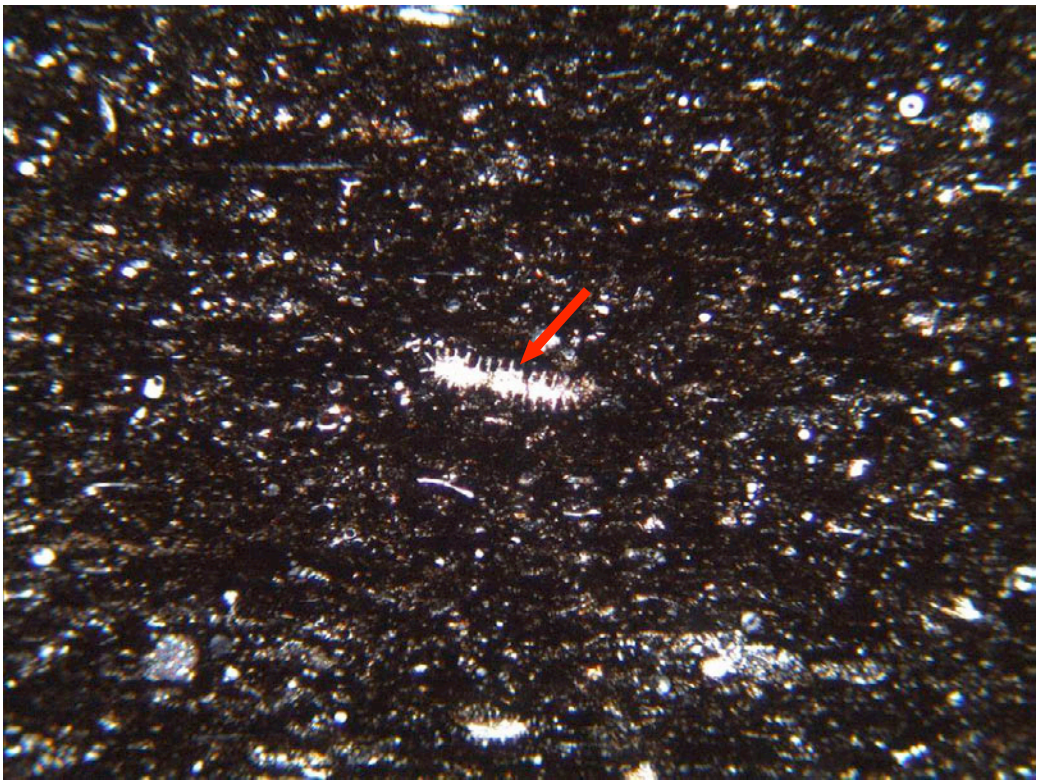

Figure 24. Photomicrograph of subfacies A_1. Notice the three radiolaria attached to each other (red arrow). Cross-polarized light. Field of view is 1mm across. 8577.8 ft.

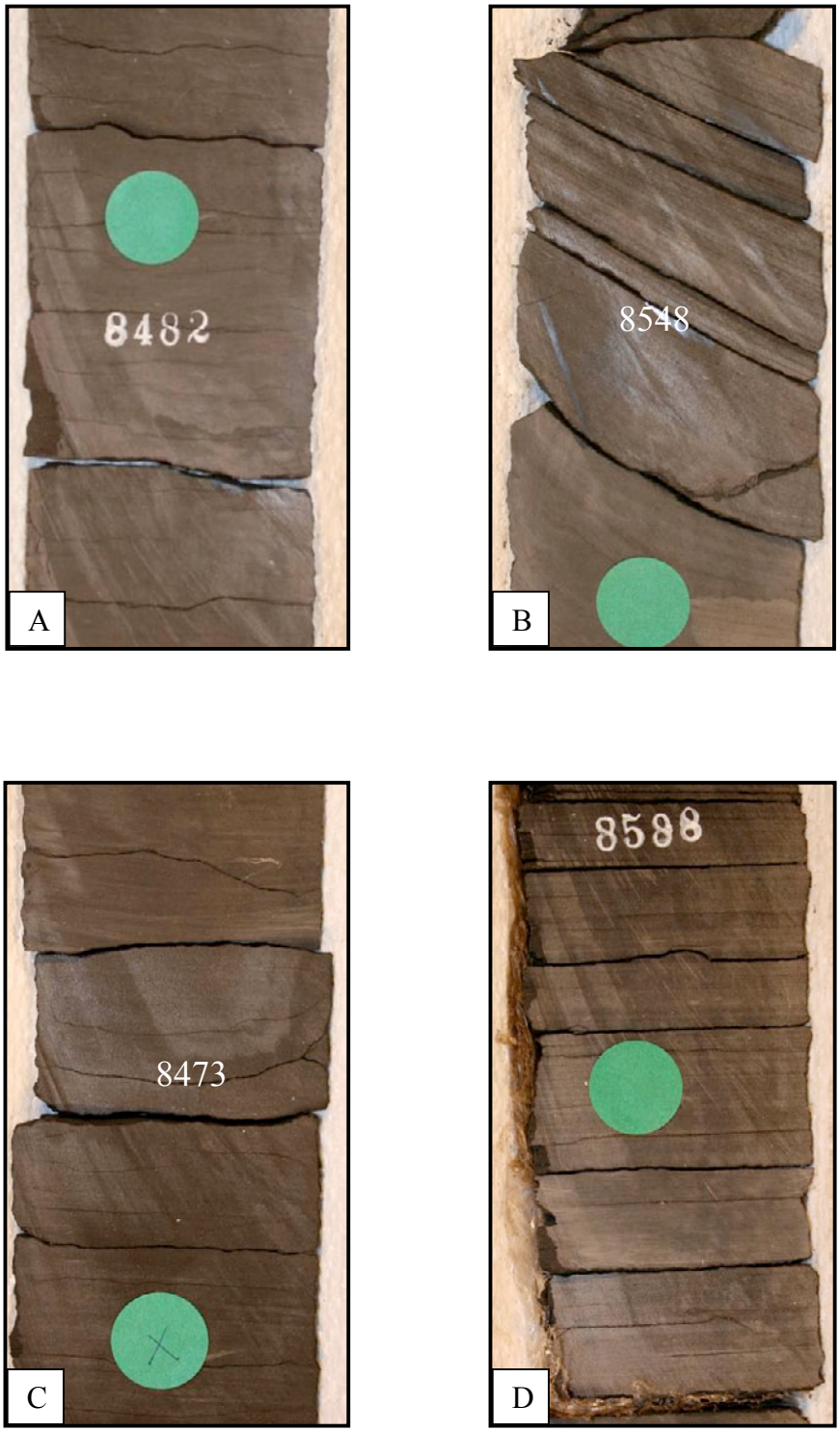

Figure 25. Core photos of subfacies A_2 consisting of dolomitic shale. Note the lighter color of the core compared to subfacies A_1 in Figure 16. Core is 6cm across.

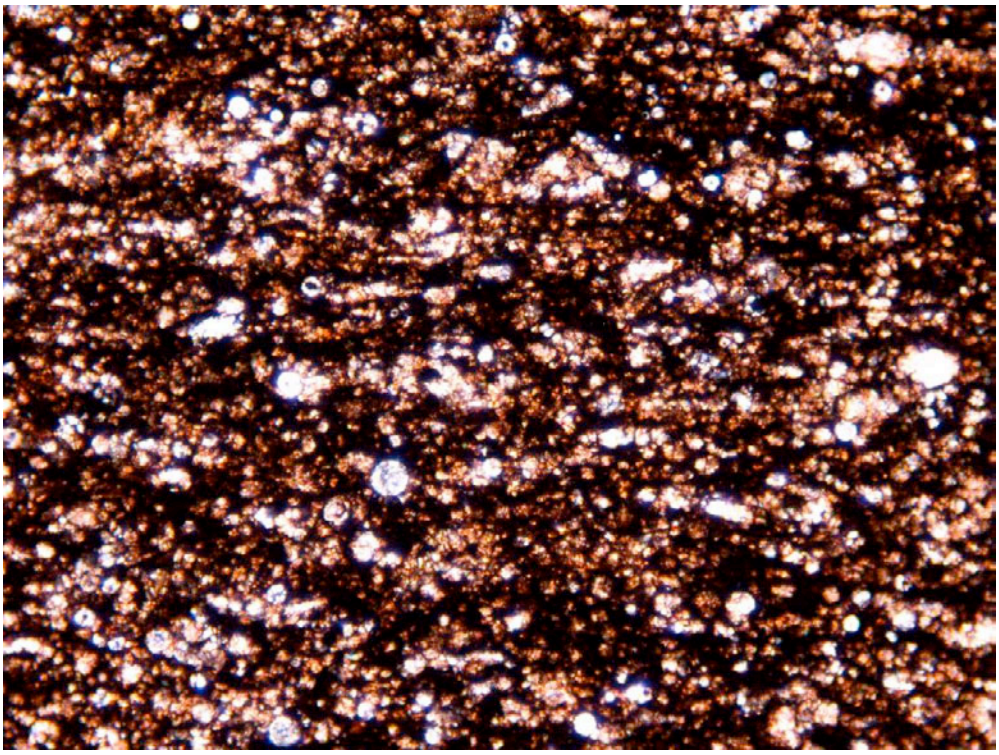

Figure 26. Photomicrograph of subfacies A_2 showing dolomite in the clay matrix. Sponge spicules were not completely replaced by dolomite. Cross-polarized light. Field of view is 0.9mm across. 8481.9 ft.

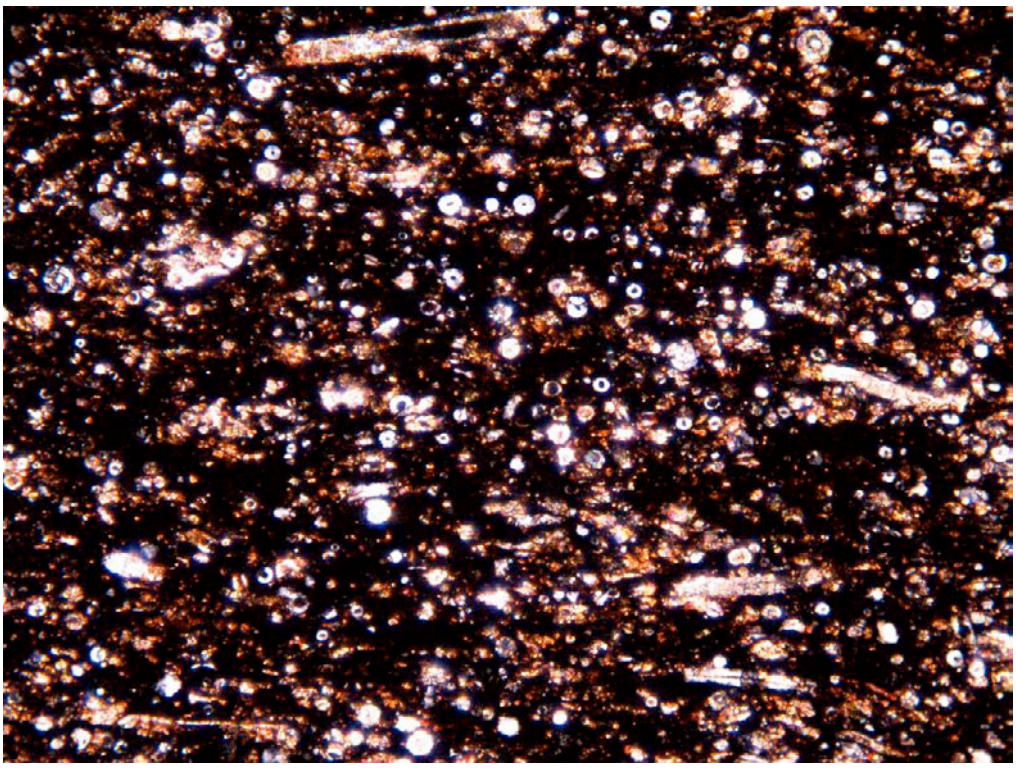

Figure 27. Photomicrograph of subfacies A_2 showing dolomite partially replacing the clay matrix. Cross-polarized light. Field of view is 0.9mm across. 8505.5 ft.

lower than that for A_1 (about 75 API) and the density porosity is higher (Figure 15). This subfacies is present throughout the entire core in thin intervals. Low gamma-ray response provides a means of calibrating core depths with log depths.

Subfacies A_3 is a claystone with pyrite and phosphate nodules. The clay is relatively structureless and sometimes fractured. Nodules of pyrite and phosphate are ellipsoidal to round in shape (Figure 28). Phosphatic nodules are typically replaced by pyrite in the center (Figures 29, 30). These nodules usually formed before compaction took place (Figure 29). On the well log, A_3, like A_1, has a high gamma-ray count, about 175 API (Figure 15). This facies is most common in the middle unit and the Barnett and is rarely present in the upper unit. Pyrite and phosphate nodules indicate this facies was deposited in a reducing environment.

Facies B

Facies B is a siltstone and contains three subfacies. Subfacies B_1 is a medium gray to grayish black, laminated, spiculitic siltstone. This subfacies has continuous, planar laminae (Figure 31). These laminae are defined by silt and clay alternating on a sub-millimeter scale (Figures 32-34). Calcite- and pyrite-filled fractures are common. Some shell fragments are also found in this facies. Rare clay-filled burrows are found at the top of some silty layers (Figure 35). Silt-sized grains are mainly sponge spicules (Figure 36). Subangular, medium to coarse quartz silt is present in small amounts (1-2%). The original opaline silica of the spicules has been replaced by chalcedony and also carbonate and pyrite. Compacted agglutinated forams made of microcrystalline quartz are also found in B_1. Sedimentary features seen in subfacies B_1 includes normal grading and small scale scour surfaces

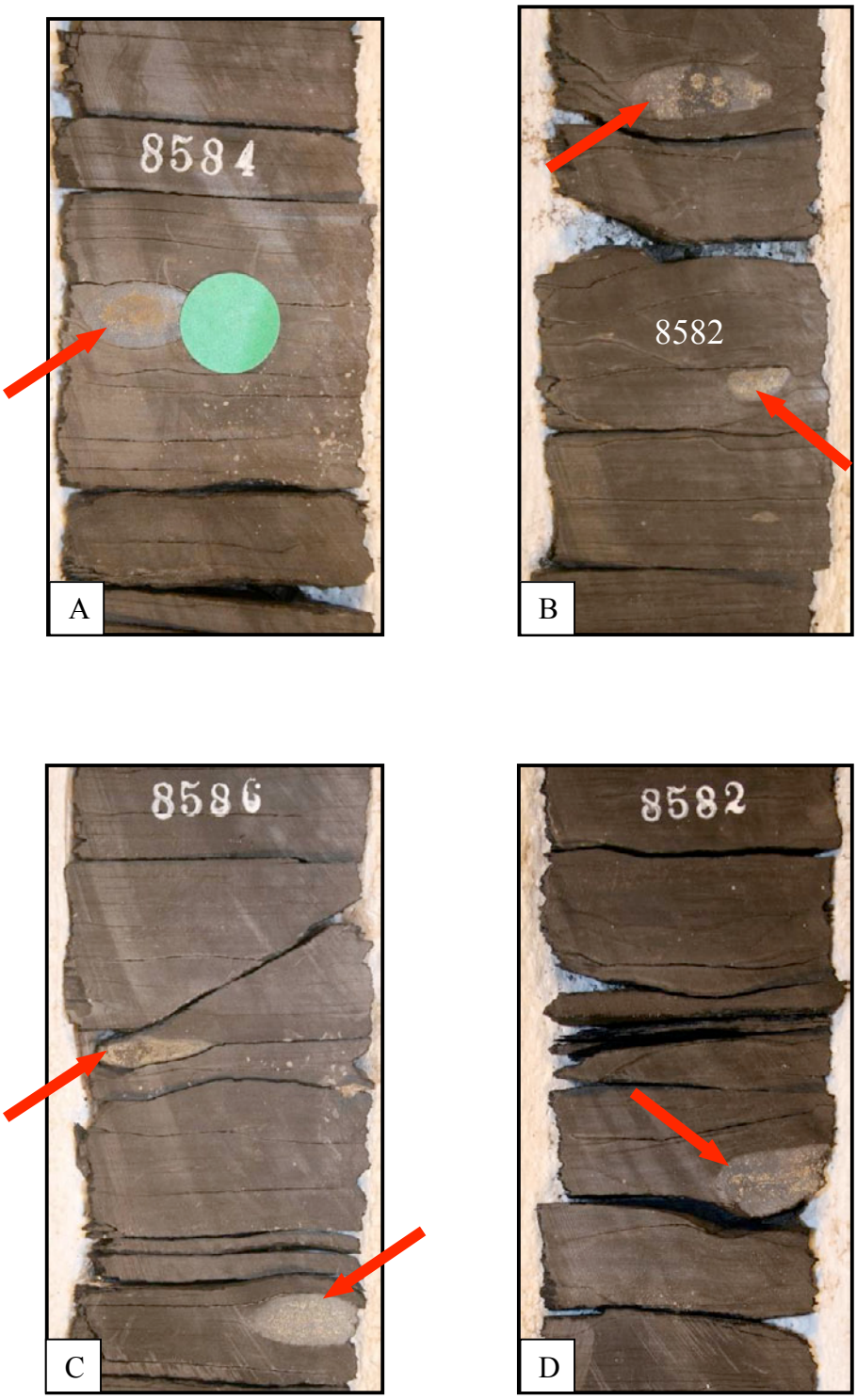

Figure 28. Core photos of Facies A_3. Pyrite and phosphate nodules indicated by red arrows. Core is 6cm across.

Figure 29. Ellipsoidal phosphate nodule with center replaced by pyrite. Plane light. Field of view is 2cm across. 8584.1 ft.

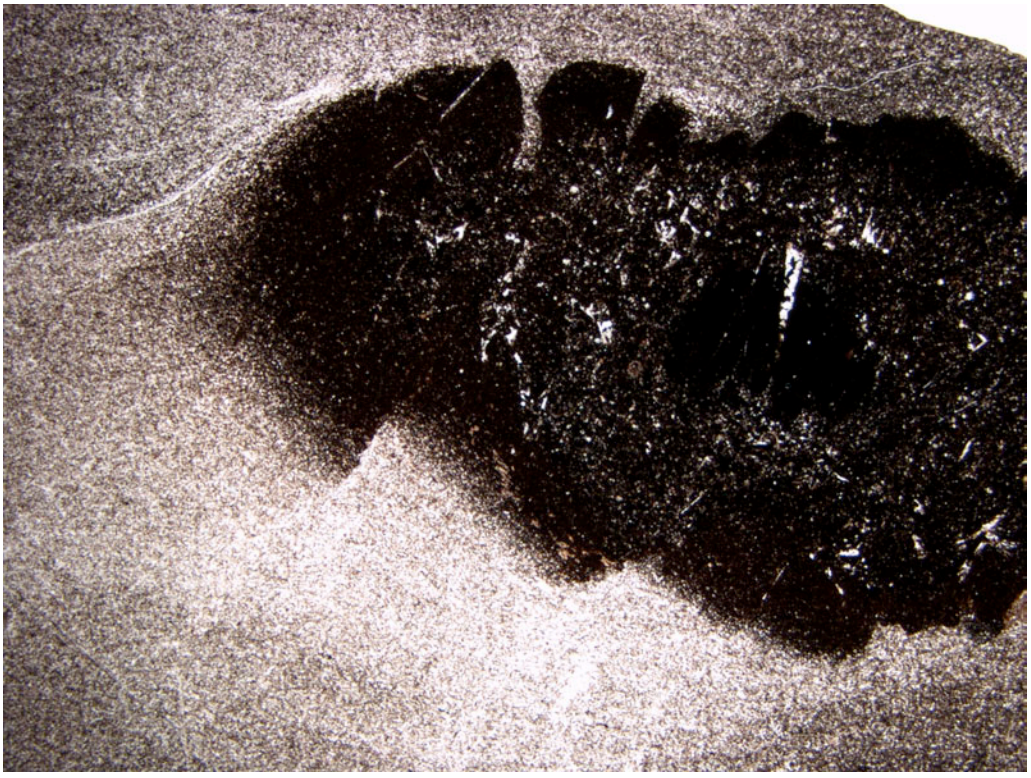

Figure 30. Irregular shaped pyrite and phosphate nodule. Plane light. Field of view is 2cm across. 8619.5 ft.

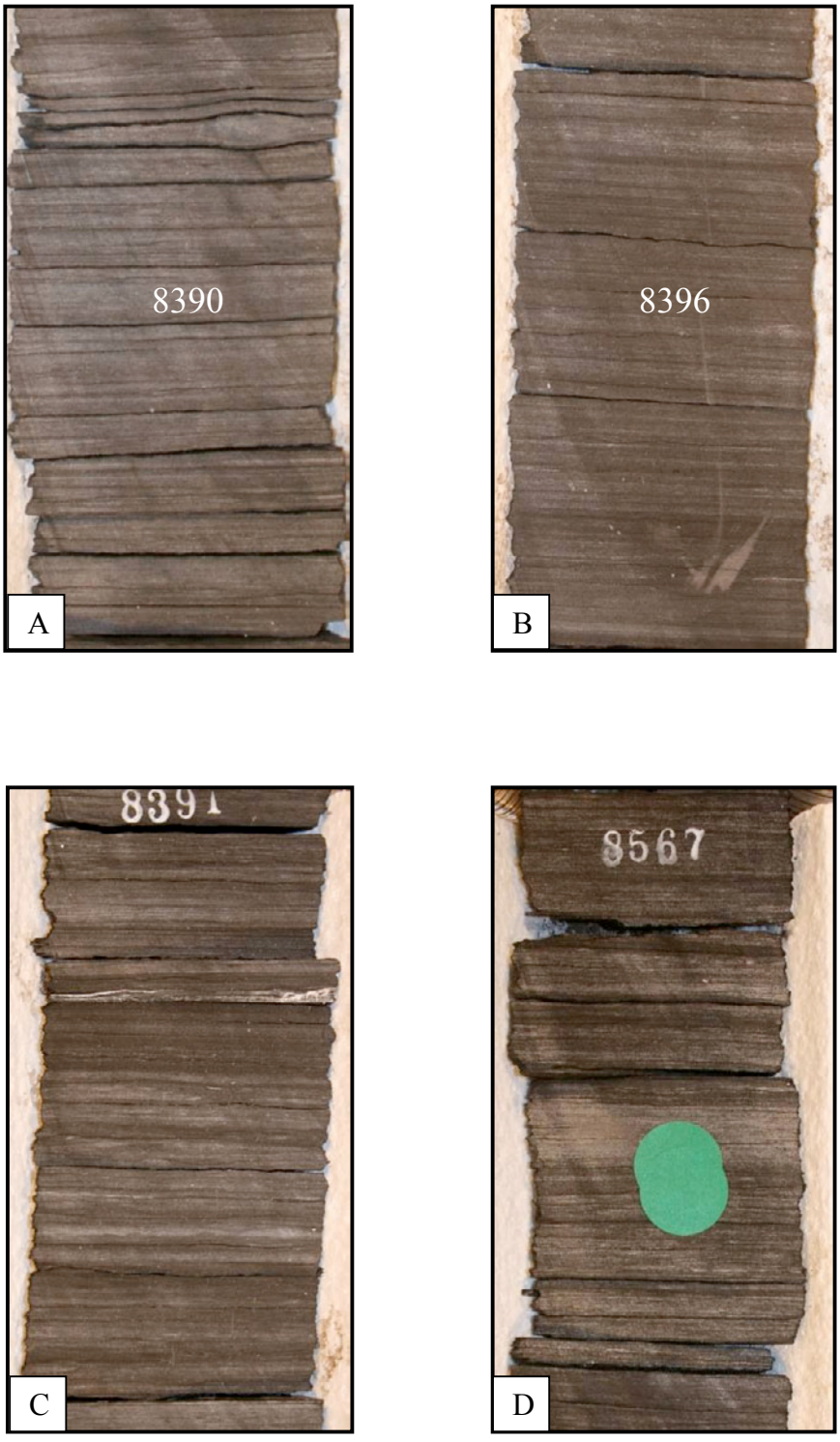

Figure 31. Core photos of Facies B_1 showing the alternating layers of dark clay and light-colored silt. Core is 6cm across.

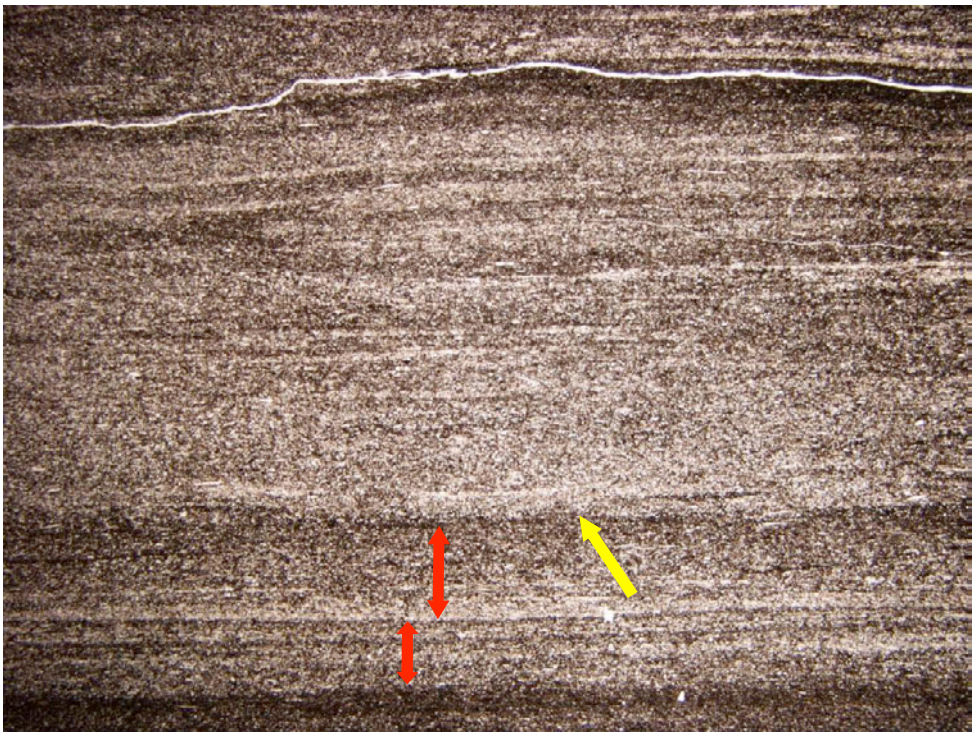

Figure 32. Photomicrograph of subfacies B_1 showing lighter colored layers of silt. Red arrows show normal grading. Yellow arrow points to scour surface. Plane light. Field of view is 2cm across. 8368.3 ft.

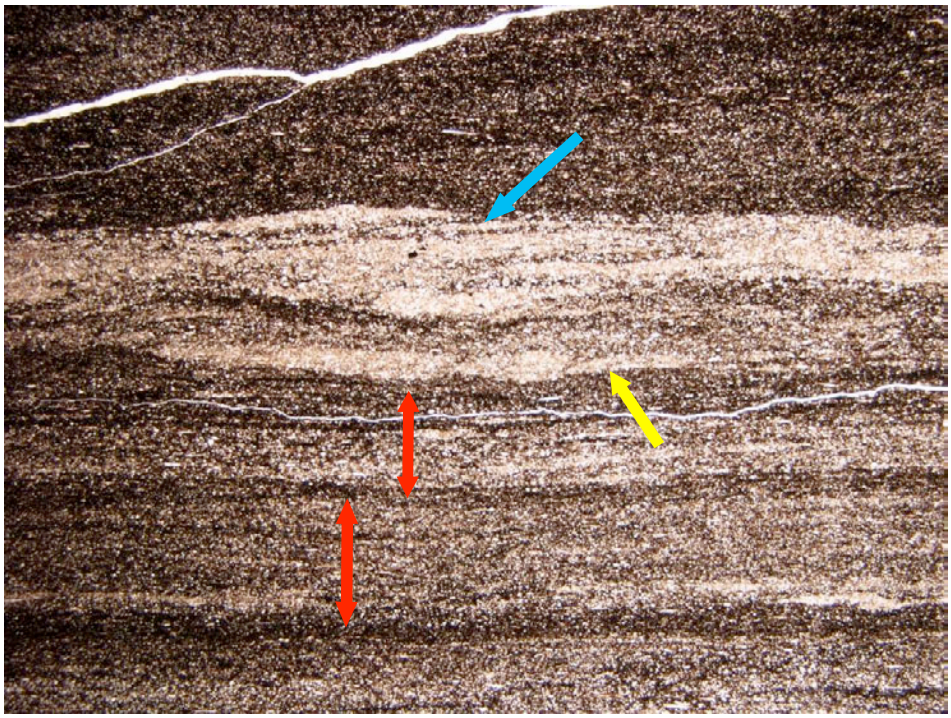

Figure 33. Photomicrograph of subfacies B_1 showing parallel and subparallel laminae. Red arrows show normal grading from a light silt to a dark clay. Scour surface is shown by the yellow arrow. Draped ripple cross-laminae shown by the blue arrow. Plane light. Field of view is 2cm across. 8387.5 ft.

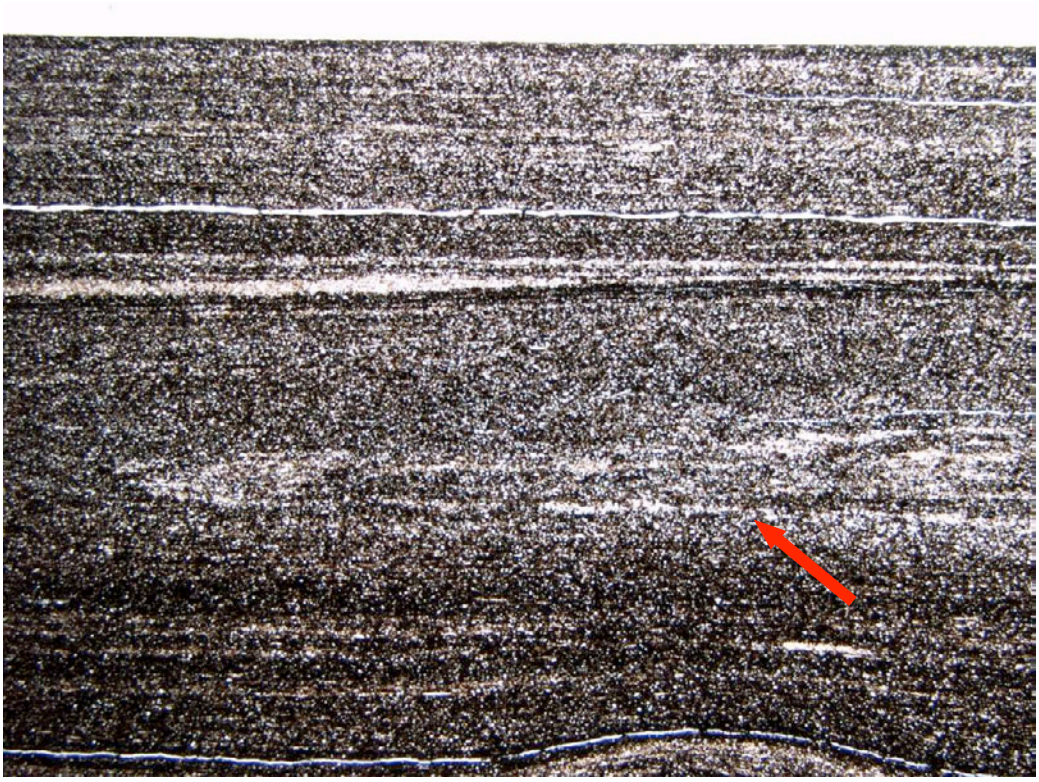

Figure 34. Photomicrograph of subfacies B_1. Note the parallel and subparallel laminae. Red arrow indicates a possible burrow. Plane light. Field of view is 2cm across. 8424.2 ft.

Figure 35. Photomicrograph of clay-filled burrow within the silt in subfacies B_1 (red arrow). Plane light. Field of view is 2cm across. 8565.9 ft.

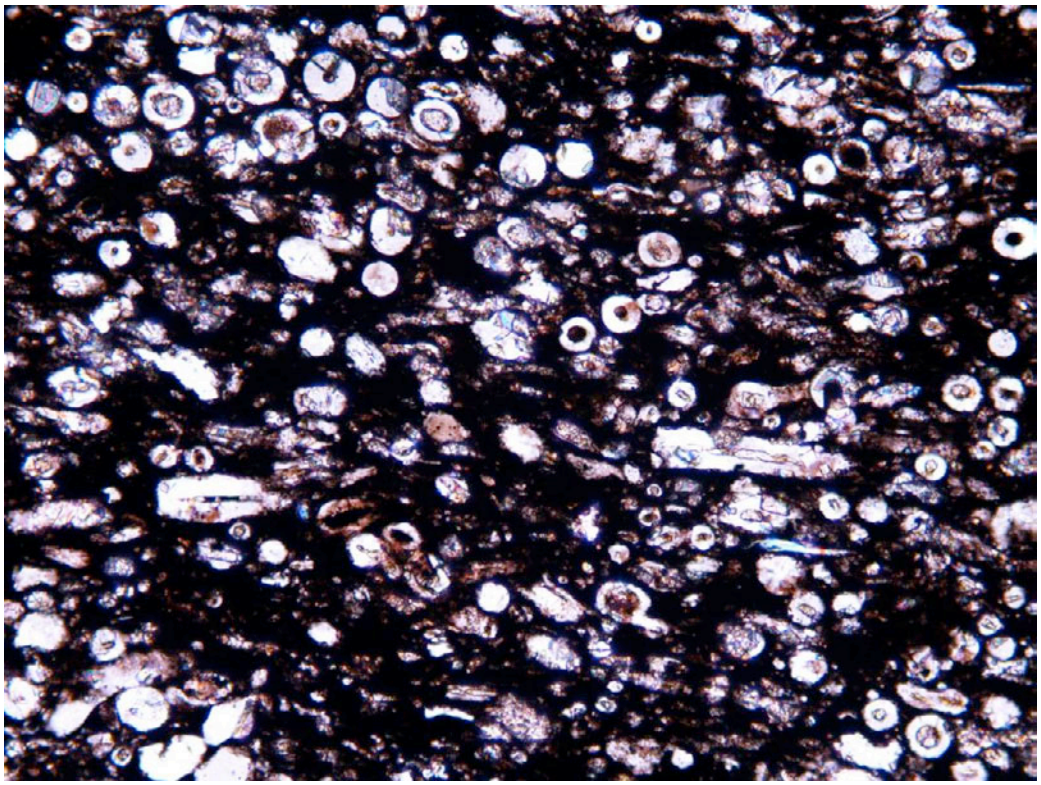

Figure 36. Photomicrograph of subfacies B_1 showing abundant sponge spicules. Cross-polarized light. Field of view is 0.9mm across. 8368.3 ft.

(Figure 33). Small phosphate nodules (≤3mm) are present, but occur sparingly (Figure 37). The gamma-ray response is low (about 75-90 API) and the density porosity is high (Figure 15). B_1 is present in each of the three sedimentary units, but is most common in the upper unit.

Subfacies B_2 is a medium gray to dark gray spiculitic siltstone (Figure 38). This subfacies has discontinuous, wavy, non-parallel laminae of silt and clay (Figures 39-41). Rare clay-filled burrows are present and typically occur on the top of silty layers (Figure 42). Fractures with calcite veins are present, but rare. Like B_1, the silt consists mostly of sponge spicules replaced by chalcedony, carbonate and pyrite. The detrital quartz concentration is 1-2% of the total silt. The well log response for B_2, like B_1, has a low gamma-ray response (95 API units) (Figure 15). This subfacies is present only in the upper unit.

Subfacies B_3 is a grayish black to black silty mudstone. Unlike subfacies B_1 and B_2, the silt-size grains consist mainly of subangular quartz. The clay matrix has a faint planar fabric and is partially replaced by carbonate (Figures 43, 44). Subfacies B_3 has a high gamma-ray response, approximately of 130-150 API (Figure 15). This facies is present only in the lowermost 25 ft of core.

Facies C

Facies C contains two subfacies, both of which are enriched in phosphate. Subfacies C_1 consists of thin, black streaks of phosphate in a clay matrix. The streaks are typically <2mm thick and consist of continuous to discontinuous layers of phosphate (Figure 45). In thin section, this facies is brown in plane light (Figures 46, 47). The log response for subfacies C_1 can be difficult to recognize since the layers are so thin. However, the presence

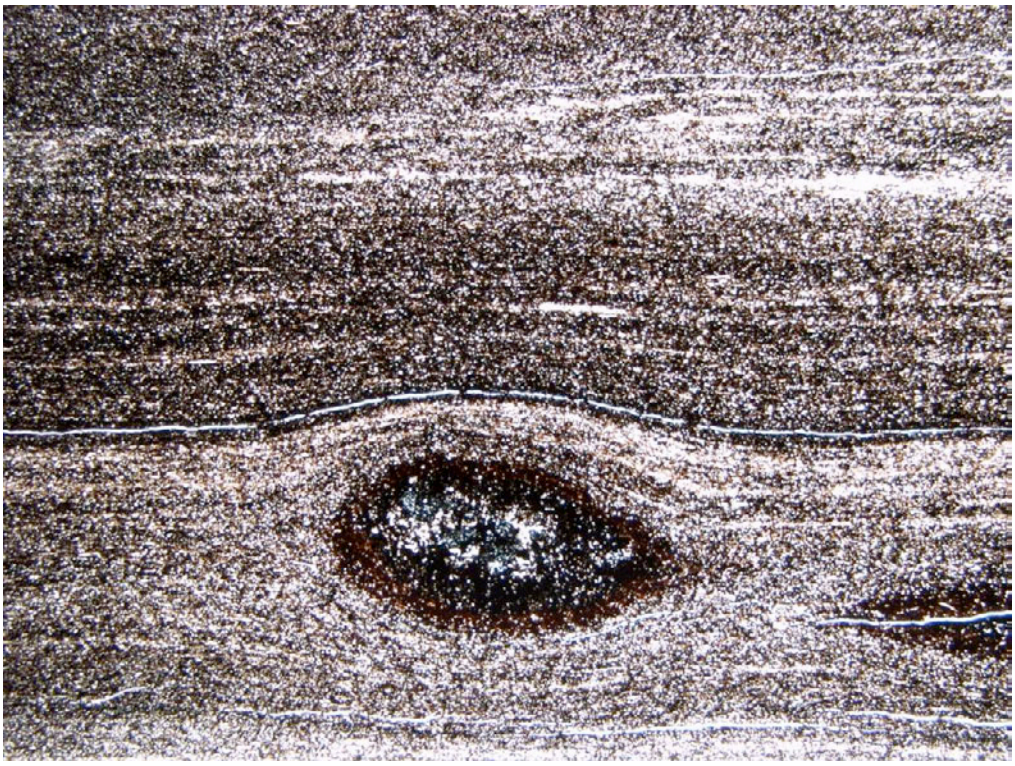

Figure 37. Photomicrograph of subfacies B_1 showing compaction of silt laminae around a phosphate nodule. Plane light. Field of view is 2cm across. 8424.2 ft.

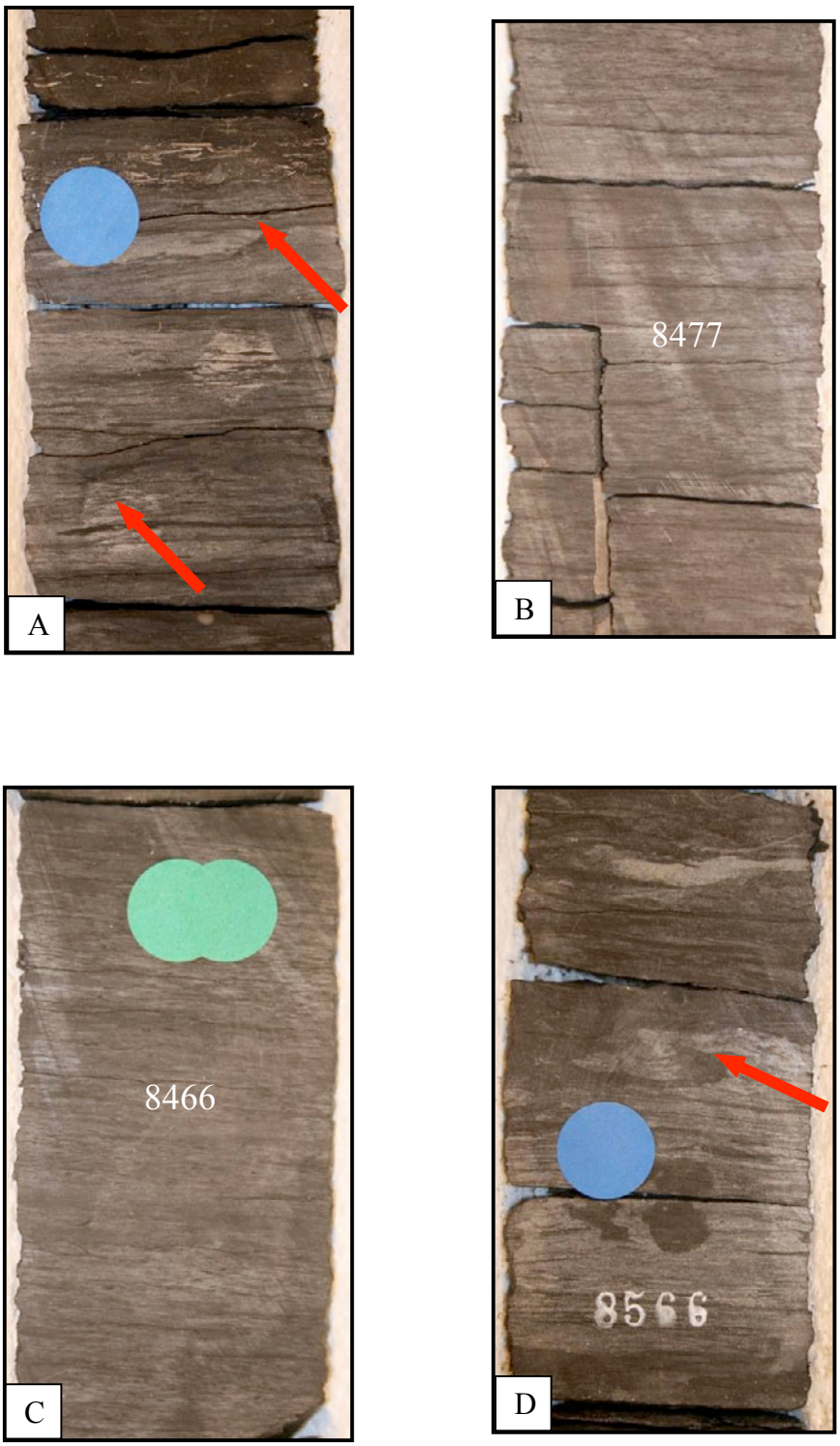

Figure 38. Core photos of subfacies B_2 showing wavy laminations. Red arrows point to burrows. Core is 6cm wide.

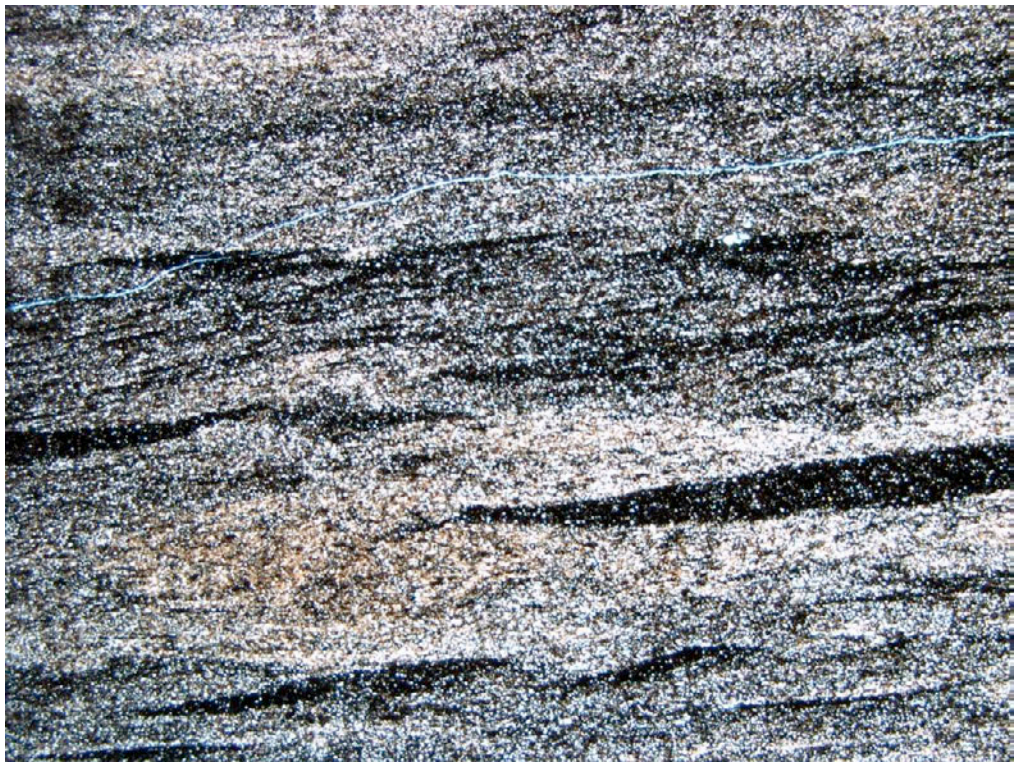

Figure 39. Photomicrograph of subfacies B_2 showing discontinuous clay and silt laminae. Plane light. Field of view is 2cm across. 8435.5 ft.

Figure 40. Photomicrograph of subfacies B_2. Notice the discontinuous clay and silt laminae. Red arrow points to a possible burrow. Plane light. Field of view is 2cm across. 8466.5 ft.

Figure 41. Photomicrograph of subfacies B_2 with discontinuous clay and silt laminae. Laminae are possibly burrowed. Plane light. Field of view is 2cm across. 8522.1 ft.

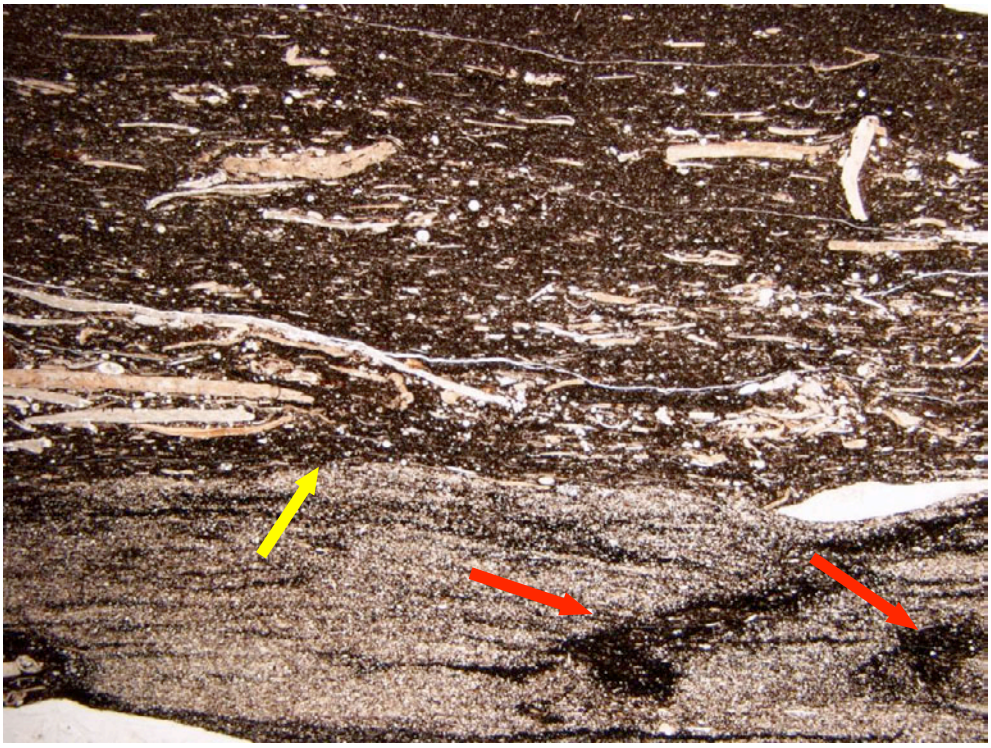

Figure 42. Photomicrograph of subfacies B_2 at the base of a shell layer. Contains wavy laminae of light colored silt and the clay-filled burrows (red arrows). Yellow arrow points to sharp boundary between the silt and the shell layer (Facies D). Plane light. Field of view is 2cm across. 8416.5 ft.

Figure 43. Photomicrograph of subfacies B_3, showing abundant detrital silt (yellow arrows) in a slightly dolomitic clay matrix. Cross-polarized light. Field of view is 1mm across. Notice larger grains of calcite (red arrows). 8642.8 ft.

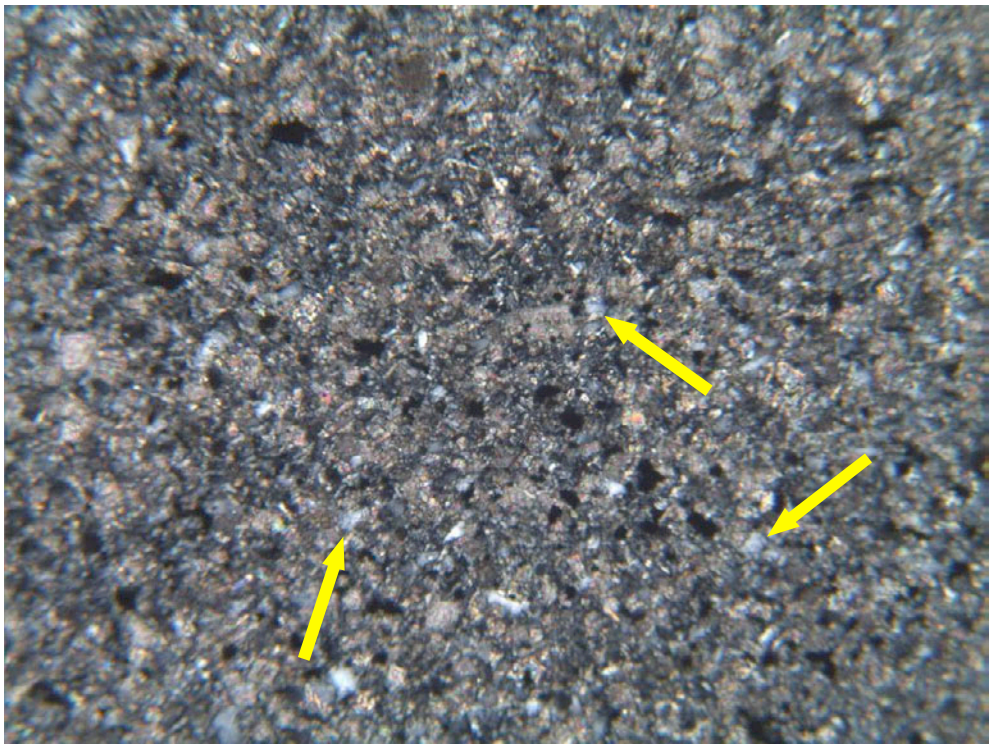

Figure 44. Photomicrograph of subfacies B_3. Note the increase in detrital silt (yellow arrows) in the dolomitic clay matrix. Cross-polarized light. Field of view is 1mm across. 8647.4 ft. Above the Barnett/Viola contact.

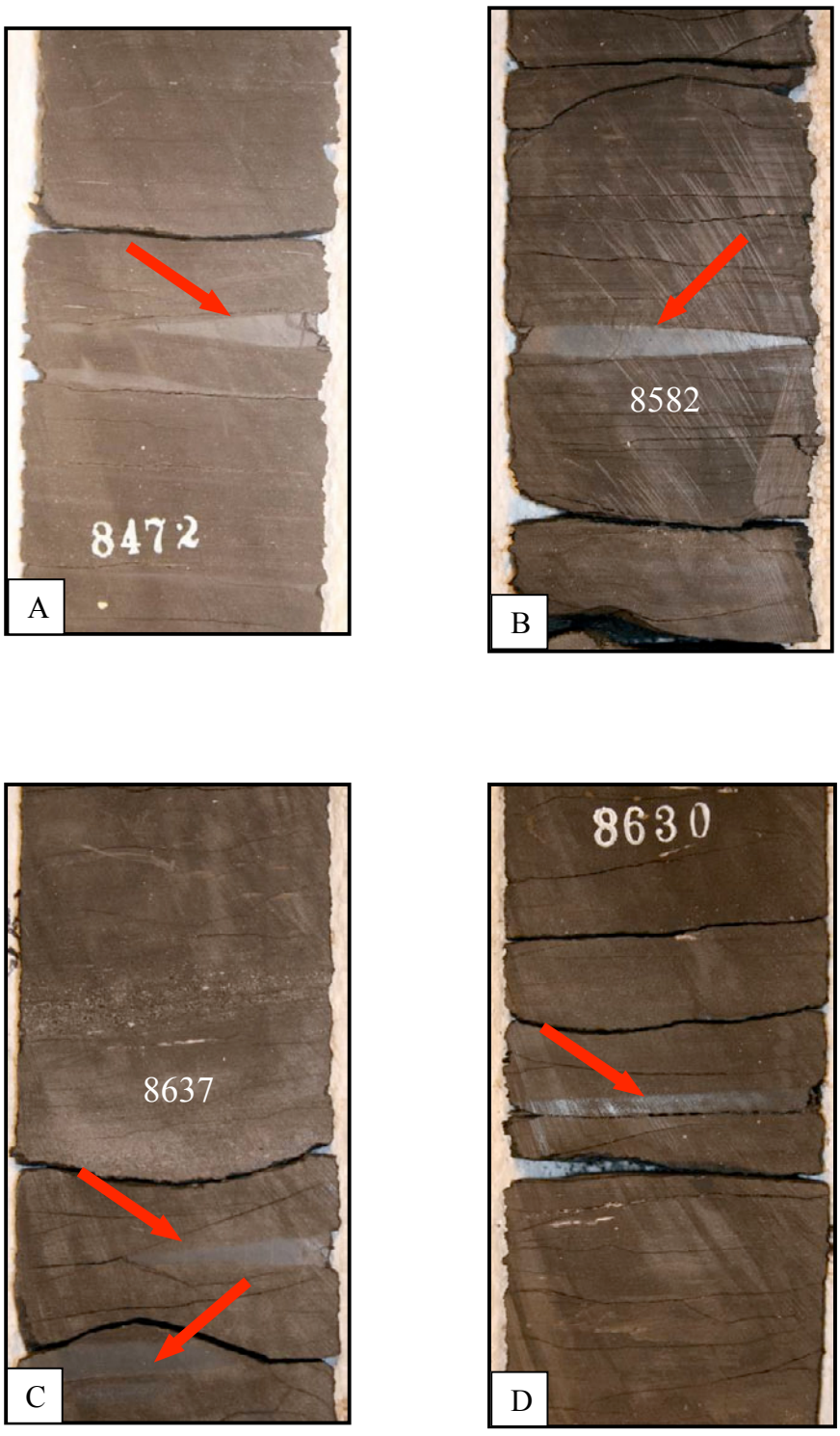

Figure 45. Core photos of subfacies C_1. Notice the phosphate streaks (red arrows). Core is 6cm wide.

Figure 46. Photomicrograph of subfacies C_1. Notice brown streaks of phosphate. Plane light. Field of view is 2cm across. 8586.5 ft.

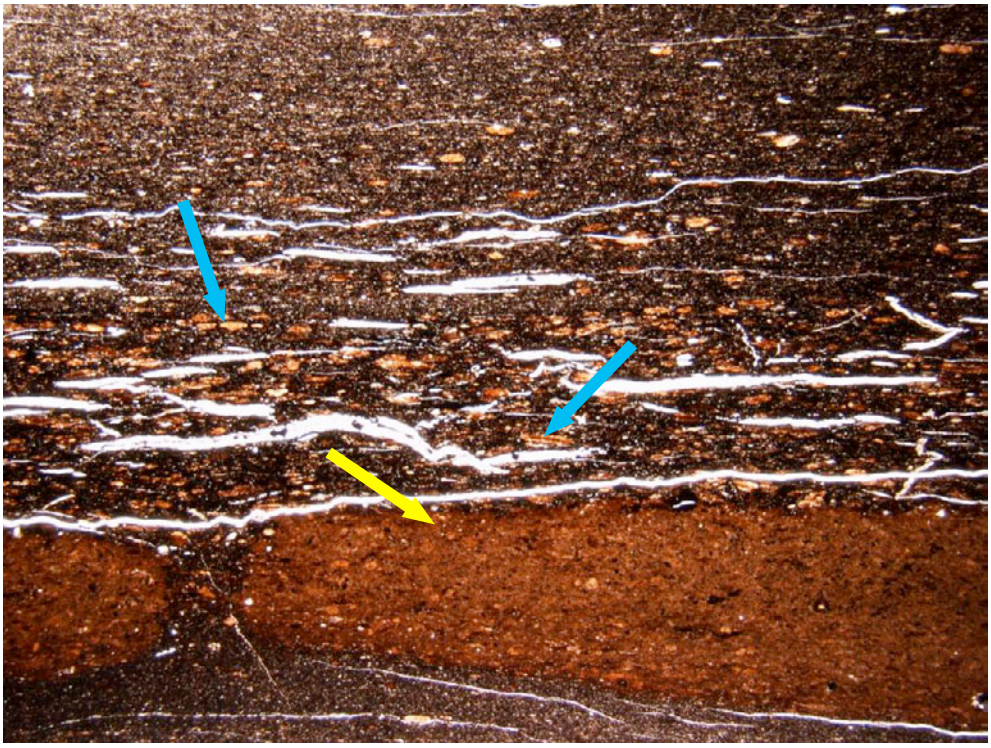

Figure 47. Photomicrograph of subfacies C_1. Note the brown phosphate streak (yellow arrow) along with the phosphate grains in the matrix (blue arrows). Plane light. Field of view is 2cm across. 8598.2 ft.

of subfacies C_1 and the occurrence of high gamma-ray responses appear to correlate somewhat, but this is not easy to determine (Figure 15). This facies is present in thin intervals throughout the cored interval.

Subfacies C_2 consists of grayish black, medium sand-sized (0.4mm) grains of phosphate in a clay matrix (Figure 48). Along with the phosphate, this subfacies contains cryptocrystalline argillaceous pellets (0.3mm- 0.5mm), sponge spicules, conodont fragments, and cherty bioclasts (Figures 49, 50). The gamma-ray response is high (greater than 150 API) (Figure 15). The abundance of phosphate in this facies causes the gamma-ray to read abnormally high due to the uranium content of phosphate. This facies is present only in the Barnett, particularly the top (Figure 15).

Facies D

Facies D consists of compacted shell fragments in a clay matrix (Figure 51). The layers (5mm-4cm thick) contain carbonate shell fragments replaced by chalcedony and euhedral pyrite (Figure 52). This facies is mostly matrix supported. Most of the shell fragments are of pelecypods (Figures 52, 53). Remains of conodonts (Figure 54), cephalopods, gastropods (Figure 55), crinoids (Figure 56) and sponges (Figure 57) are also present. Sponge spicules in the clay matrix are in places replaced by carbonate and pyrite. Phosphate grains are present, but not common within the shell layers (Figures 53, 58). Because the layers are so thin, Facies D is beyond the resolution of logging tools and shows no distinctive response (Figure 15). This facies is present in thin layers throughout the cored interval.

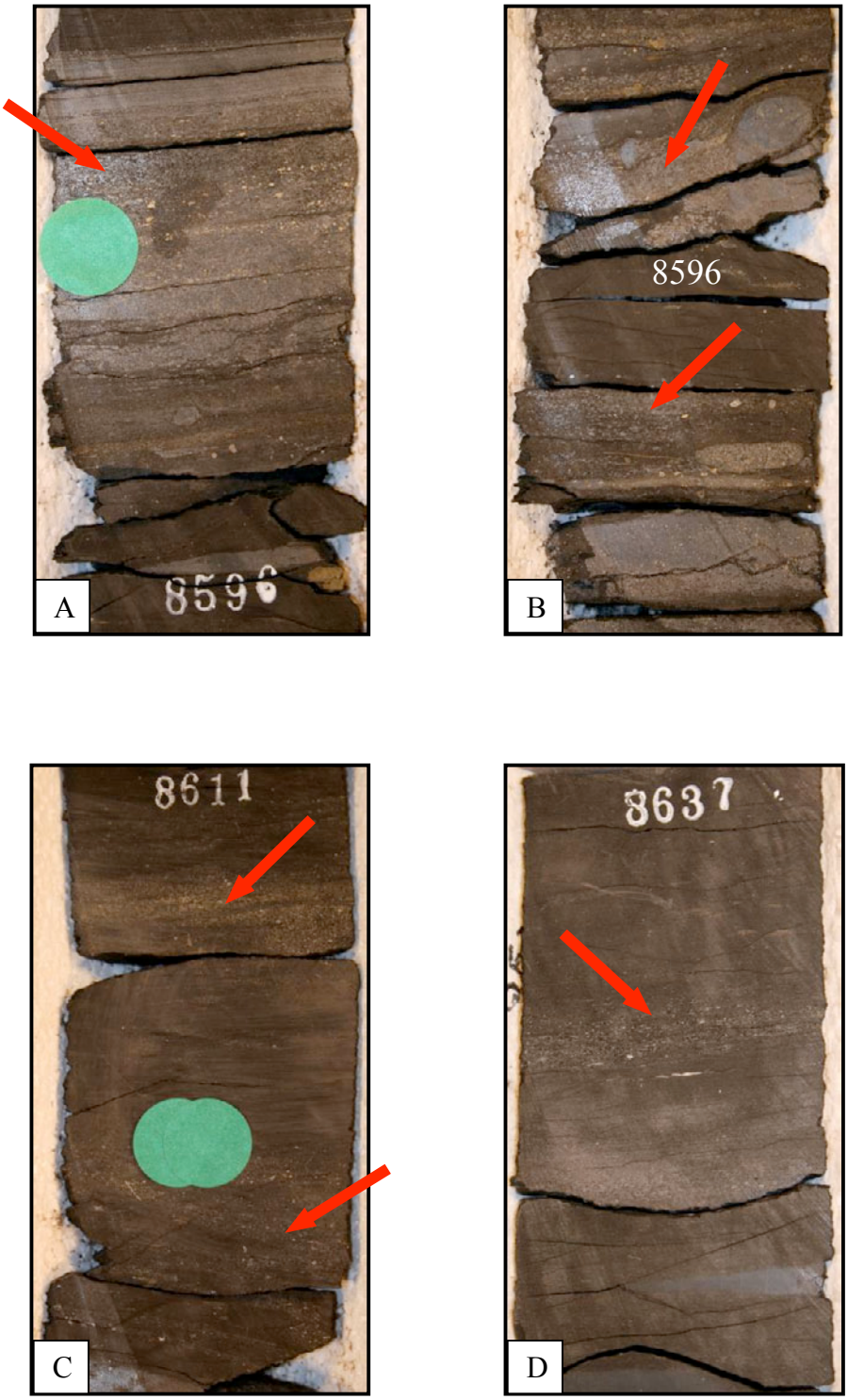

Figure 48. Core photos of Facies C_2. Arrows indicate sandy layers of phosphate. Core is 6cm wide.

Figure 49. Photomicrograph of Facies C_2. Notice the sand-sized phosphate grains, cherty bioclast (green arrow) and conodont fragments (yellow arrows). Cross-polarized light. Field of view is 9mm across. 8595.8 ft.

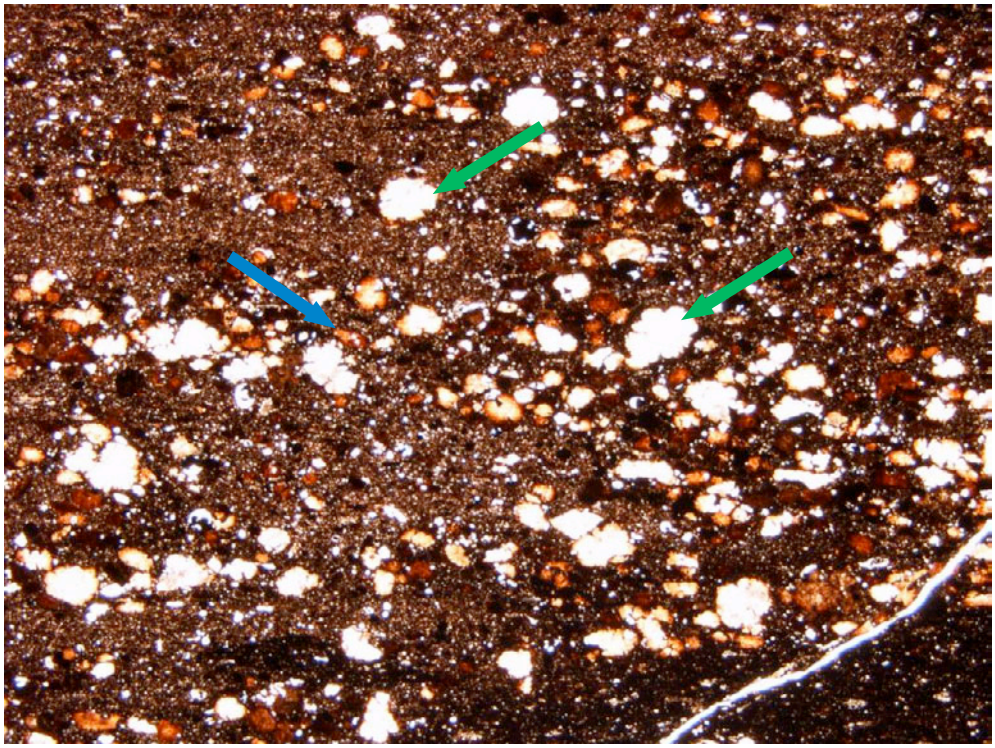

Figure 50. Photomicrograph of Facies C_2, showing sand-sized phosphate grains (blue arrow) and argillaceous pellets (green arrows). Cross-polarized light. Field of view is 9mm across. 8611.3 ft.

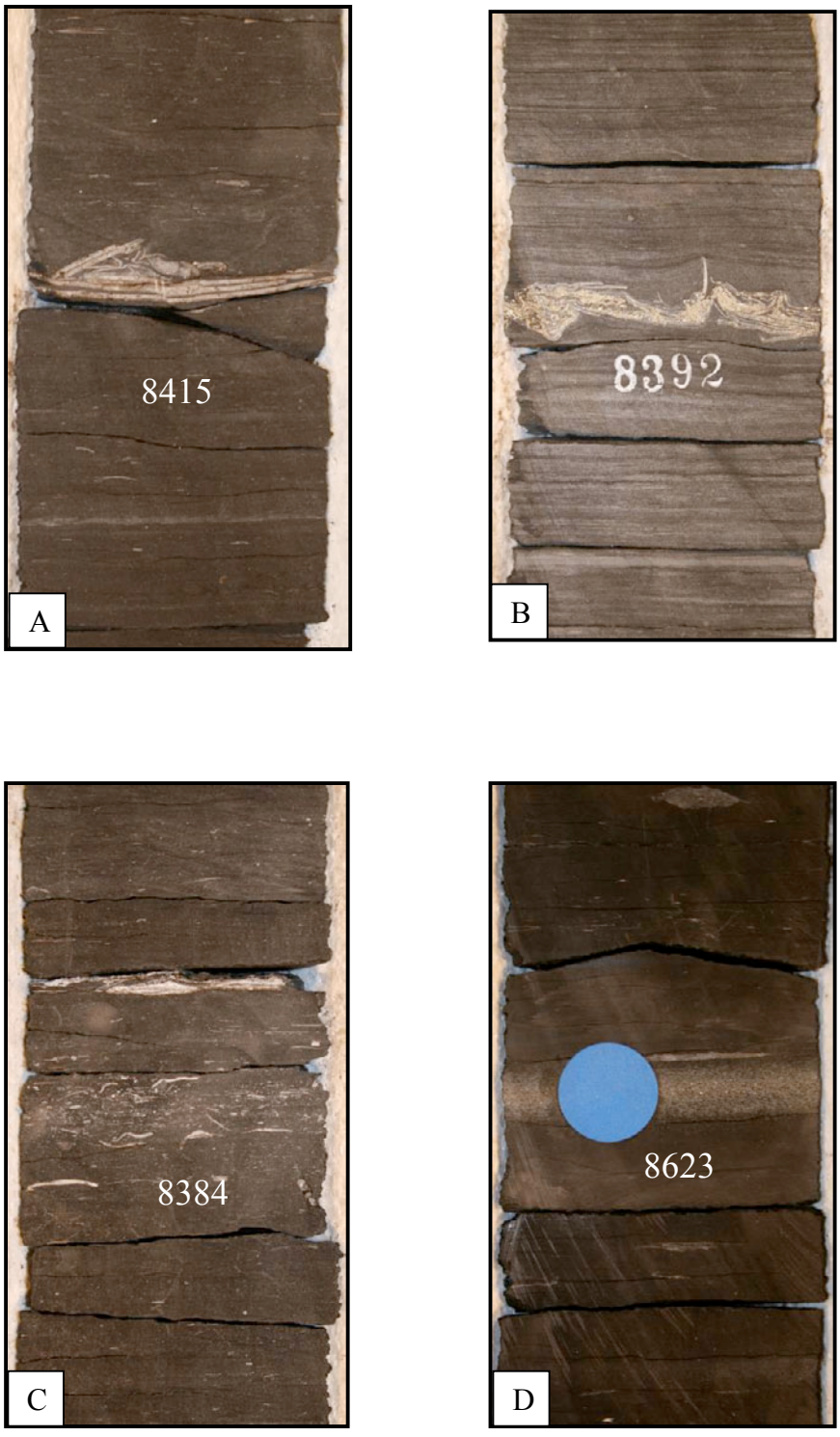

Figure 51. Core photos of Facies D. Note the various shell layers. Core is 6cm wide.

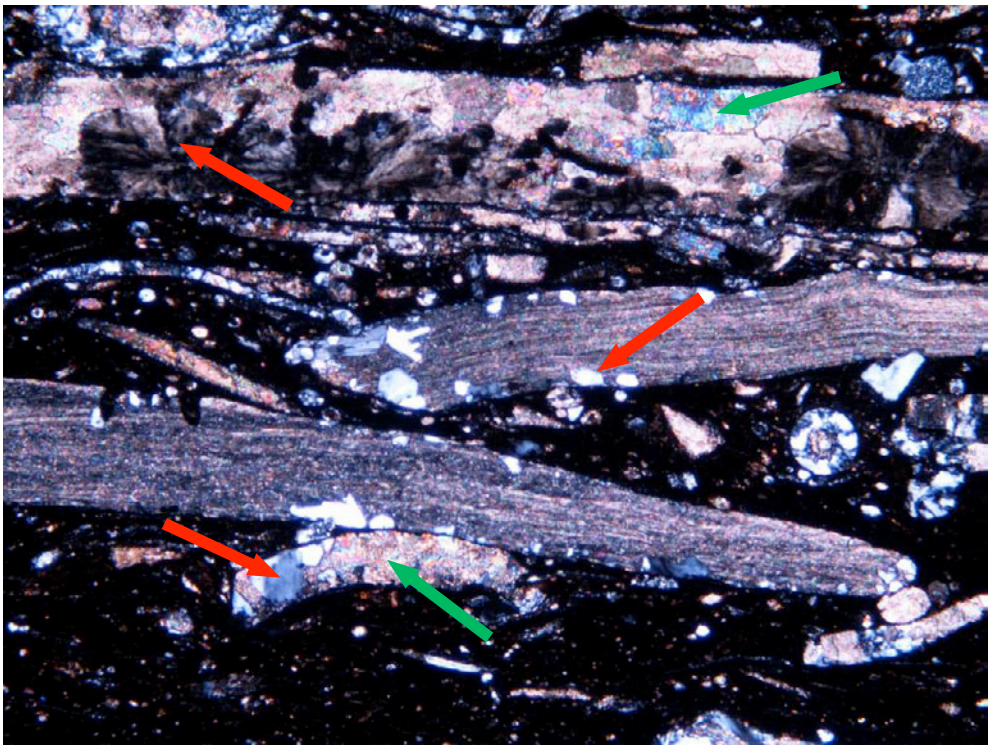

Figure 52. Photomicrograph of Facies D, showing calcite (green arrows) and chalcedony (red arrows) replacing the shell fragments. Cross-polarized light. Field of view is 2.2mm across. 8416.5 ft.

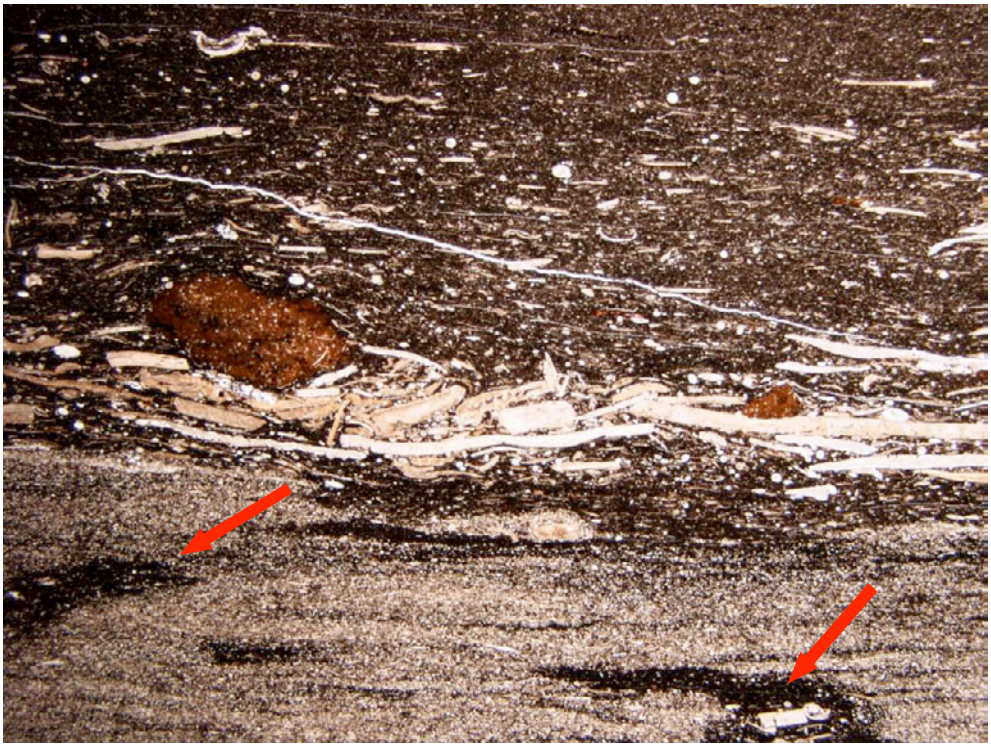

Figure 53. Photomicrograph of Facies D. Notice the various sizes of shell fragments along with phosphate grains. Red arrows show clay-filled burrows in Facies B in the lower part of view. Plane light. Field of view is 2cm across. 8416.5 ft.

Figure 54. Photomicrograph of Facies D, showing conodont fragment (red arrow). Plane light. Field of view is 2.2mm across. 8416.5 ft.

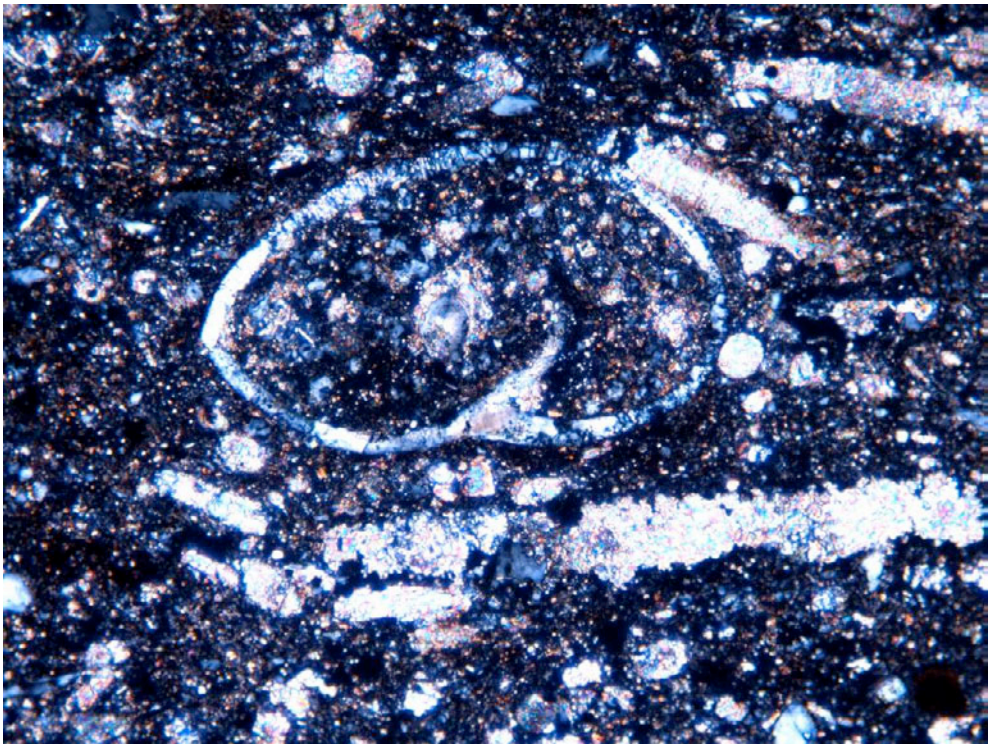

Figure 55. Photomicrograph of Facies D, showing gastropod shell replaced by dolomite and chalcedony. Cross-polarized light. Field of view is 0.9mm across. 8381.7 ft.

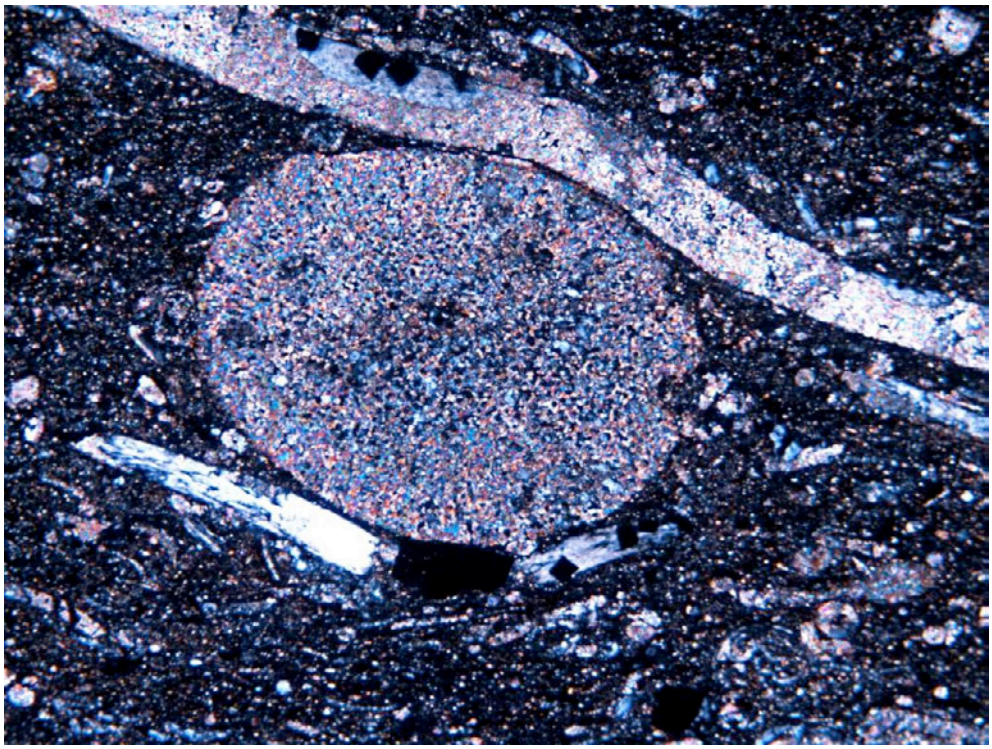

Figure 56. Photomicrograph showing pelecypod shell compacted around a crinoid fragment. Cross-polarized light. Field of view is 2.2mm across. 8381.7 ft.

Figure 57. Photomicrograph of Facies D, showing broken piece of sponge outlined by spicules (red arrow). Cross-polarized light. Field of view is 2.2mm across. 8428.2 ft.

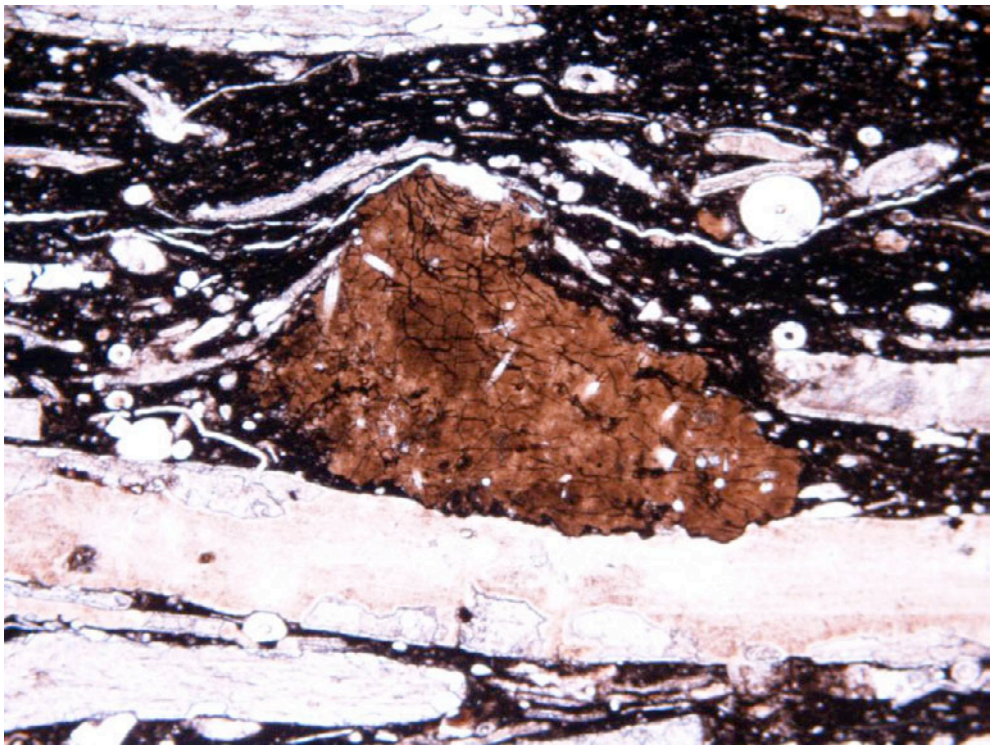

Figure 58. Photomicrograph of Facies D, showing compaction of the shells around a phosphate grain. Plane light. Field of view is 2.2mm across. 8416.5 ft.

Facies E

Facies E is a massive medium to light gray concretion (Figure 59). Calcite has replaced most of the matrix and silt grains. Relict sponge spicules, replaced with calcite, are present (Figures 60, 61). The gamma-ray response is very low (75 API) and the density porosity response is also low (Figure 15). Only a few concretions are found in the core. The low gamma-ray signature serves as a reference to calibrate the well log to the core.

Disturbed laminae

Although most of the cored interval has parallel laminae (Appendix 2), some intervals of the core show soft sediment deformation. In the Barnett, three feet (8616 ft- 8619 ft) of core is fractured and has disturbed laminae (Figure 62). In areas, the laminae are almost vertical. Several vertical calcite veins are also present within the interval. Parallel laminae are present above and below the disturbed interval.

Soft sediment deformation features are also present in the middle unit (Figure 63). Almost three feet of core (8548 ft- 8550 ft and 8558 ft) has subhorizontal laminae suggesting folding before significant lithification or compaction. Parallel laminae are also present above and below the disturbed intervals.

Geochemical Data

RockEval and TOC analyses were performed on a foot-by-foot basis on the EOG Gordon SWD core (Appendix 3). The values for S1 and S2 show low values (<1 mgHC/gR), which indicates that the thermal maturity for this interval is very high. As a result, Tmax values are unreliable. Because of the high thermal maturity of this interval, the only data that

Figure 59. Core photo of Facies E. Note the massive lighter colored carbonate. Yellow arrow shows the grading from carbonate to darker clay matrix. Core is 6cm wide.

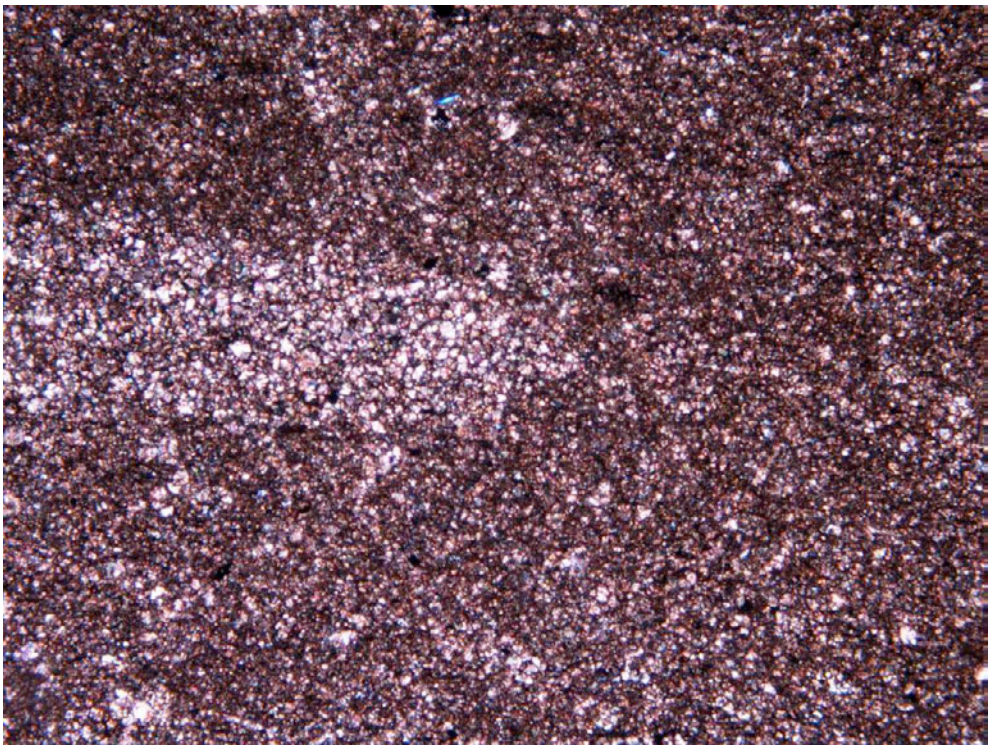

Figure 60. Photomicrograph of Facies E, showing calcite replacing the clay matrix. Cross-polarized light. Field of view is 2.2mm across. 8446.5 ft.

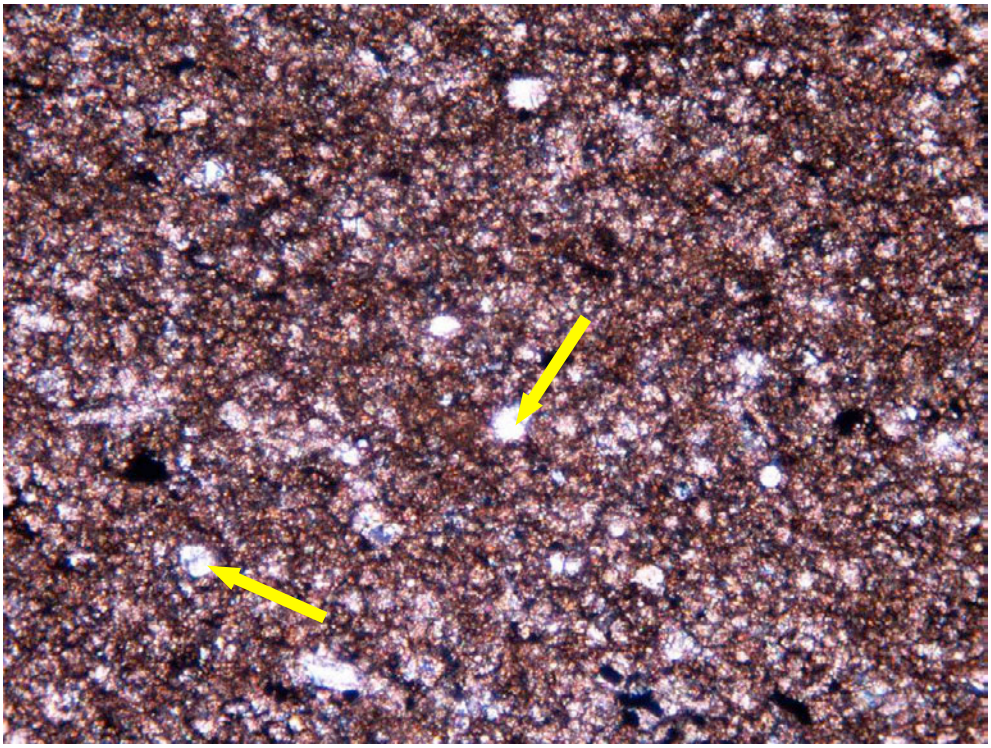

Figure 61. Photomicrograph of Facies E, showing calcite replacing the clay matrix. Notice the relict sponge spicules (yellow arrows). Cross-polarized light. Field of view is 0.9mm across. 8446.5 ft.

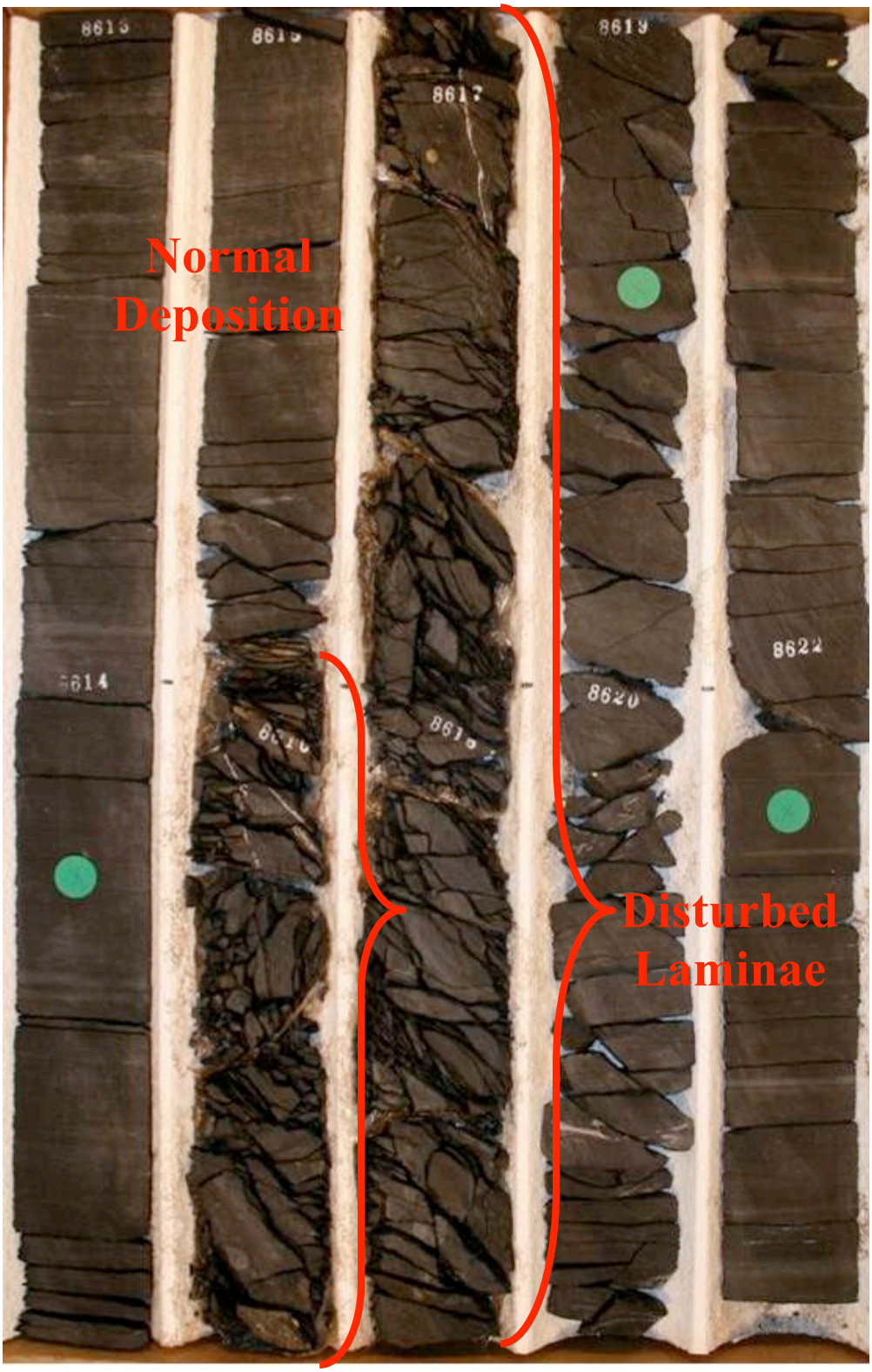

Figure 62. Core photo of disrupted bedding in the Barnett in interval shown in brackets.

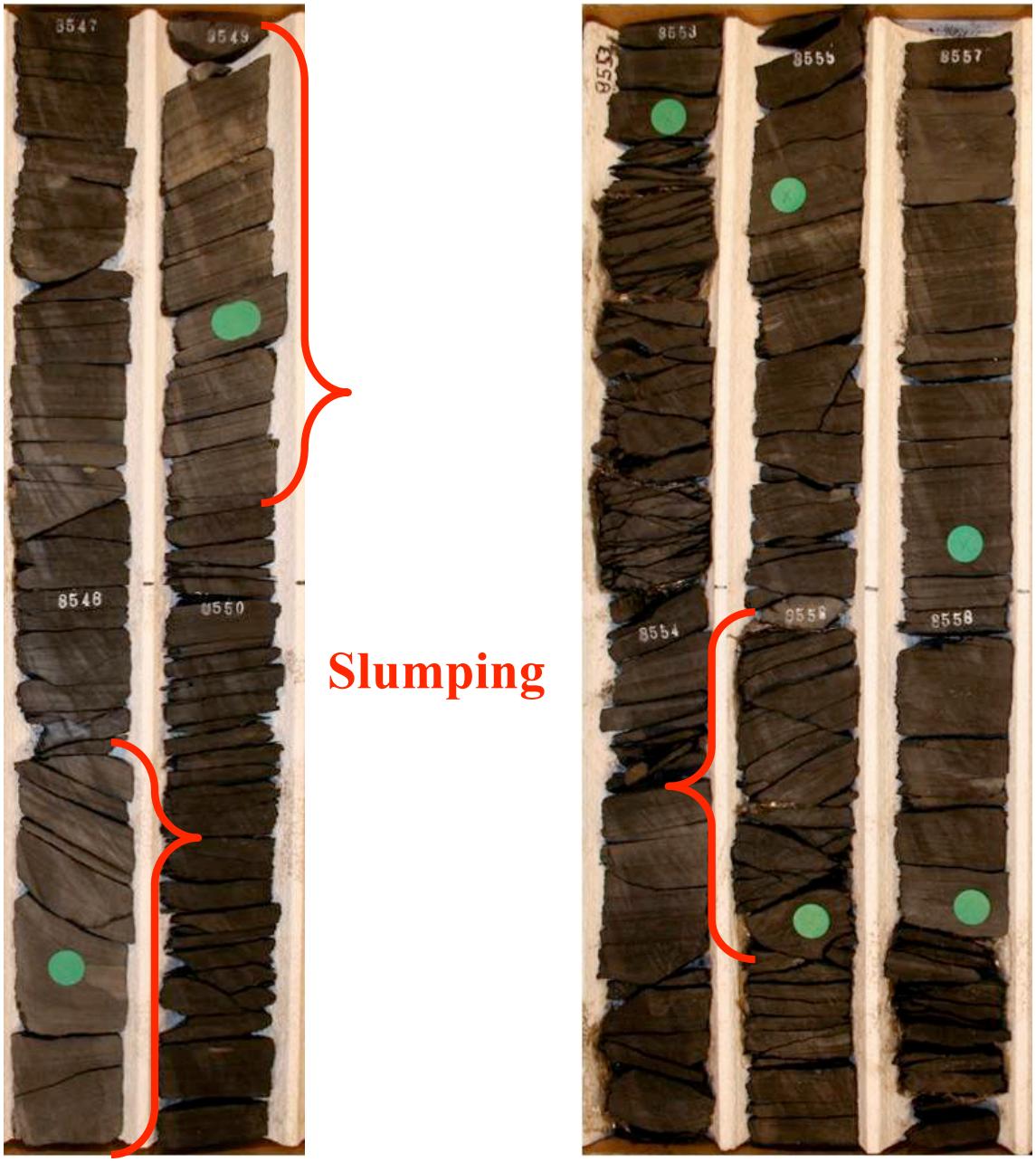

Figure 63. Core photo of disturbed bedding in the middle unit in intervals shown in brackets.

are useful for this study are the TOC analyses (D. Jarvie, personal communication). TOC values were much higher before burial and cracking of the hydrocarbons. TOC values in the EOG Gordon SWD core range from 0.77 to 8.89 wt%. The highest TOC values, as a rule, are seen in the upper part of the middle unit and the base of the upper unit (Figure 64). TOC values for the Barnett are lower. The TOC for the Barnett ranges from 1.69 to 7.29 wt% and averages about 3.92 wt%. In most cases, the high TOC values in the Barnett correspond to high gamma-ray peaks. The TOC values for the middle unit are higher, ranging from 0.077 to 8.89 wt% and averaging 4.48 wt% TOC. The upper unit has high TOC values at the base, which decrease upwards. The upper unit TOC values range from 1.22 to 4.23 wt%, averaging 2.62 wt% TOC. High TOC values in the upper unit occur at gamma-ray peaks, although the peaks are lower in magnitude. Although high TOC values correlate with gamma-ray peaks, the magnitude of the TOC peak is not always directly proportional to the magnitude of the gamma-ray peak in the core.

Log Analysis

Three separate sedimentary units were identified and mapped throughout Johnson County and parts of Hill, Hood, Somervell and Bosque counties. Paleontological work needs to be undertaken to establish the ages of these units.

Cross section A-A' (Figure 65) extends across the study area from northwest to southeast. A correlatable resistivity marker is used as a datum. The northernmost well is the EOG 2H Two-O-Five and the southernmost well is the EOG Gordon SWD (Figure 7). The three sedimentary units are shown on the section. These units were identified by a change in overall gamma-ray response. This cross section also shows the internal stratigraphy in each

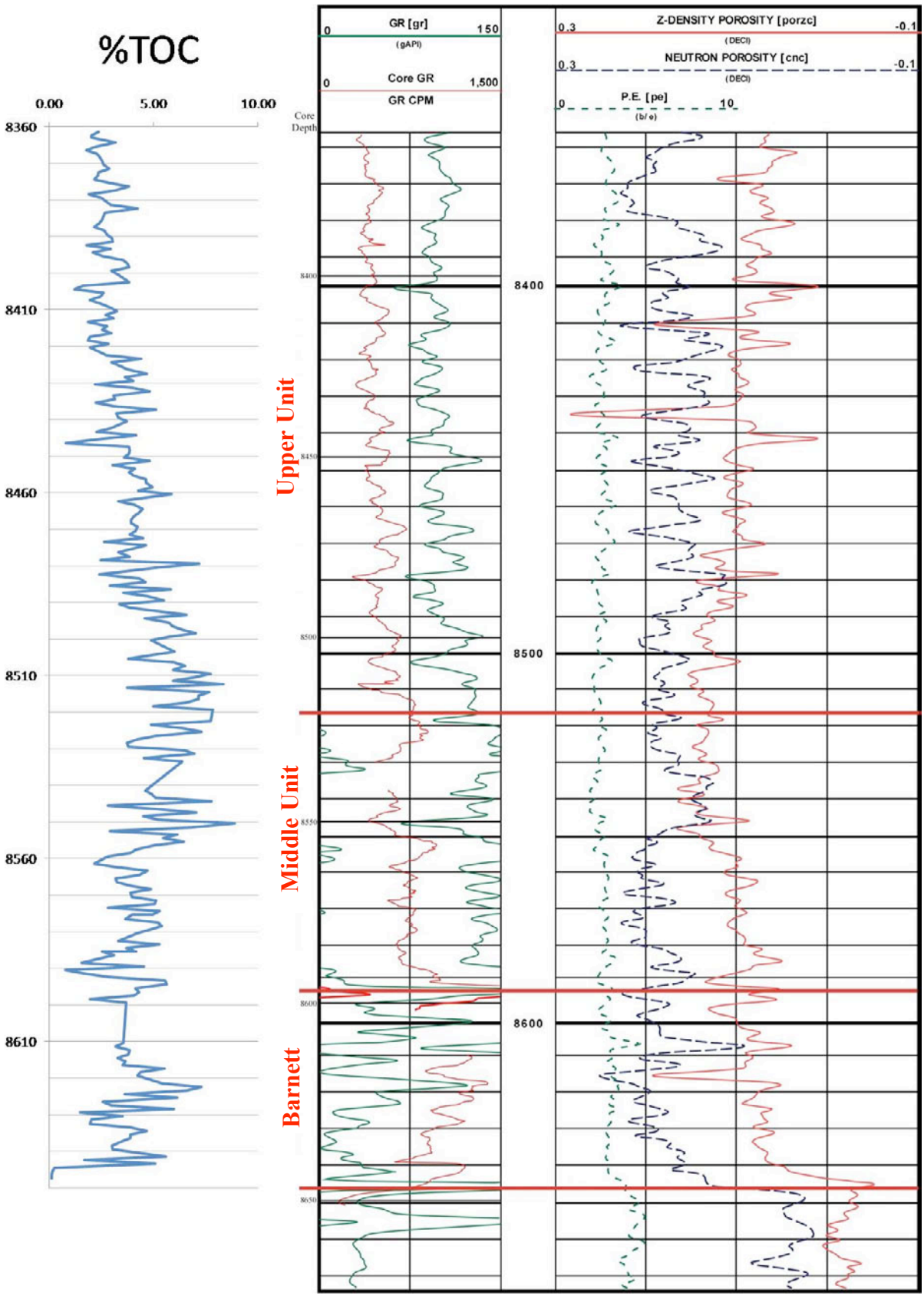

Figure 64. TOC versus depth in the EOG Gordon SWD.

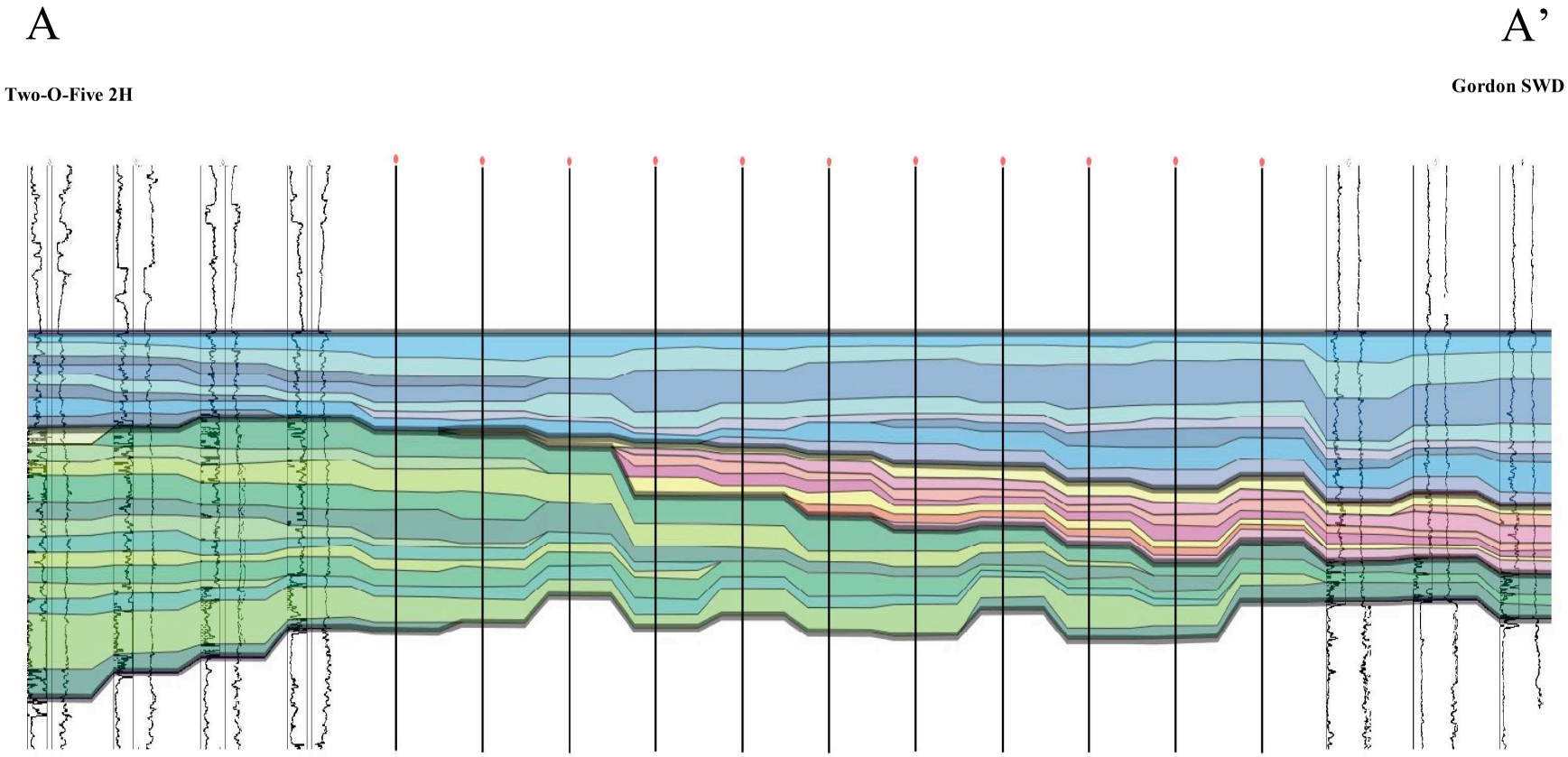

Figure 65. Cross section A-A’ from the EOG 2H Two-O-Five well in Johnson County to the EOG Gordon SWD well in Hill County (Figure 7). The green colors show the Barnett Shale, the red colors show the middle unit and the blue colors show the upper unit. See Figure 66 for the map showing the location of the cross section. Due to proprietary data, several logs are not displayed in the cross section.

of these units. The Barnett is the thickest in Johnson County and thins into Hill County, while the middle unit and upper unit are thinner in Johnson County and thicker in Hill County.

Barnett Shale

The Barnett ranges in thickness from 505 ft in Johnson County and thins to about 30 ft in Hill County (Figure 66). The thickest part of the Barnett trends from southwest to northeast. Other maps published on the Fort Worth basin show the Barnett to be 300 ft thick in Hill County (Figure 67). The interpretation of the data in this study proves otherwise. Other authors who mapped the Barnett as a thick in this area, possibly included the middle unit with the Barnett. Cross section A-A' is oriented axial to distal to the deposition of the Barnett. The internal stratigraphic units of the Barnett thicken in a northwest direction. In addition, the lateral extent of stratigraphic units decreases northward within the Barnett. In the EOG Gordon SWD well log (Figure 14), the Barnett is about 50 ft thick. The gamma-ray log response is high for the Barnett in Hill County.

The Barnett dips to the east toward the Ouachita front (Figure 68). The structure contours parallel the trend of the dominant structural feature in this area, the Ouachita fold-thrust belt, which trends due north-south. The contours on the isopach map cross the structure contours at a high angle, consistent with the fact that movement of the thrust-belt began in the Mississippian and continued through the Middle Pennsylvanian (Walper, 1982).

Middle unit

The middle unit is thickest in Johnson County, closest to the Ouachita fold-thrust belt, and quickly thins to the west (Figure 69). It has a maximum thickness of 223 ft and pinches

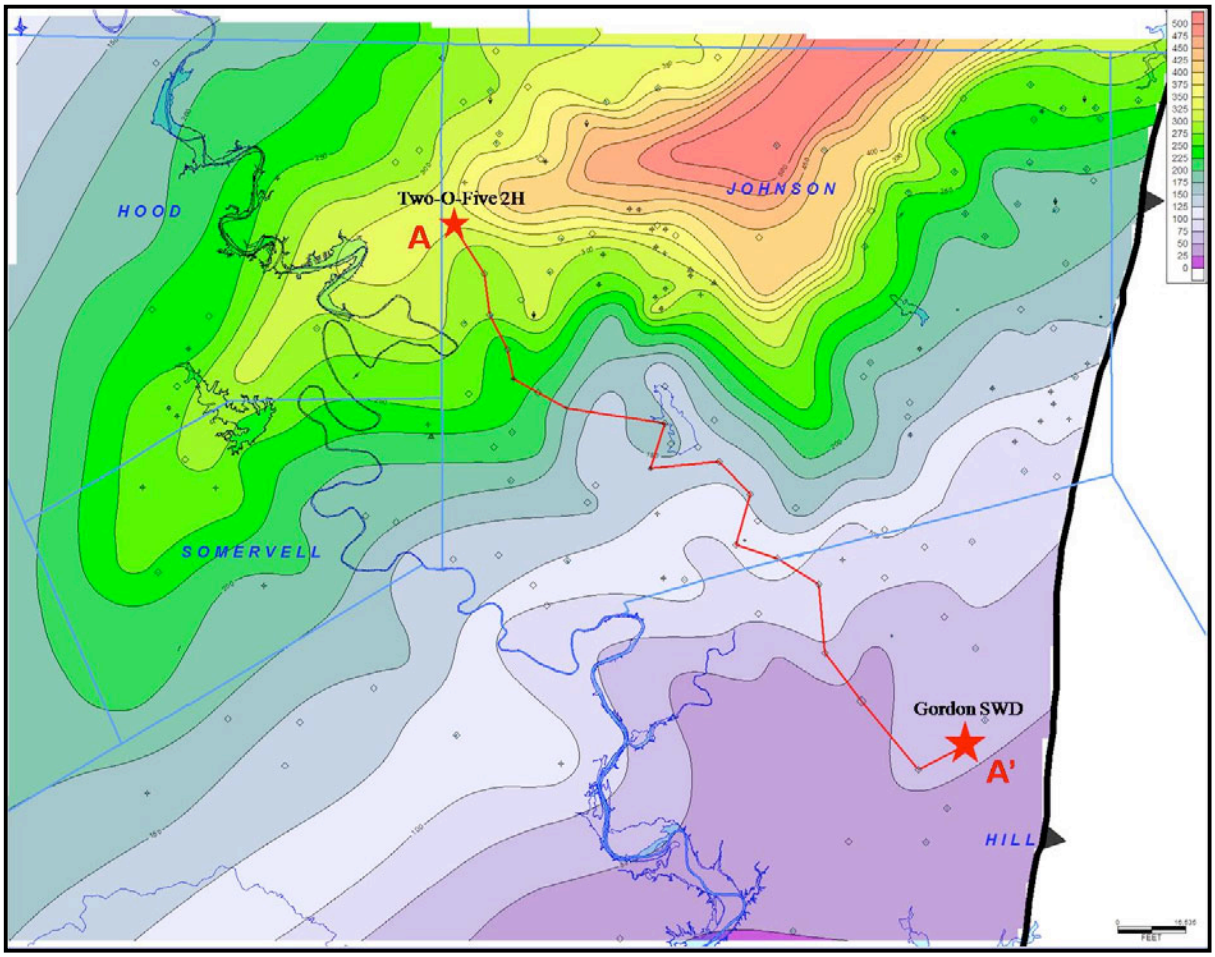

Figure 66. Isopach map of the Barnett Shale. Contour interval, 25ft.

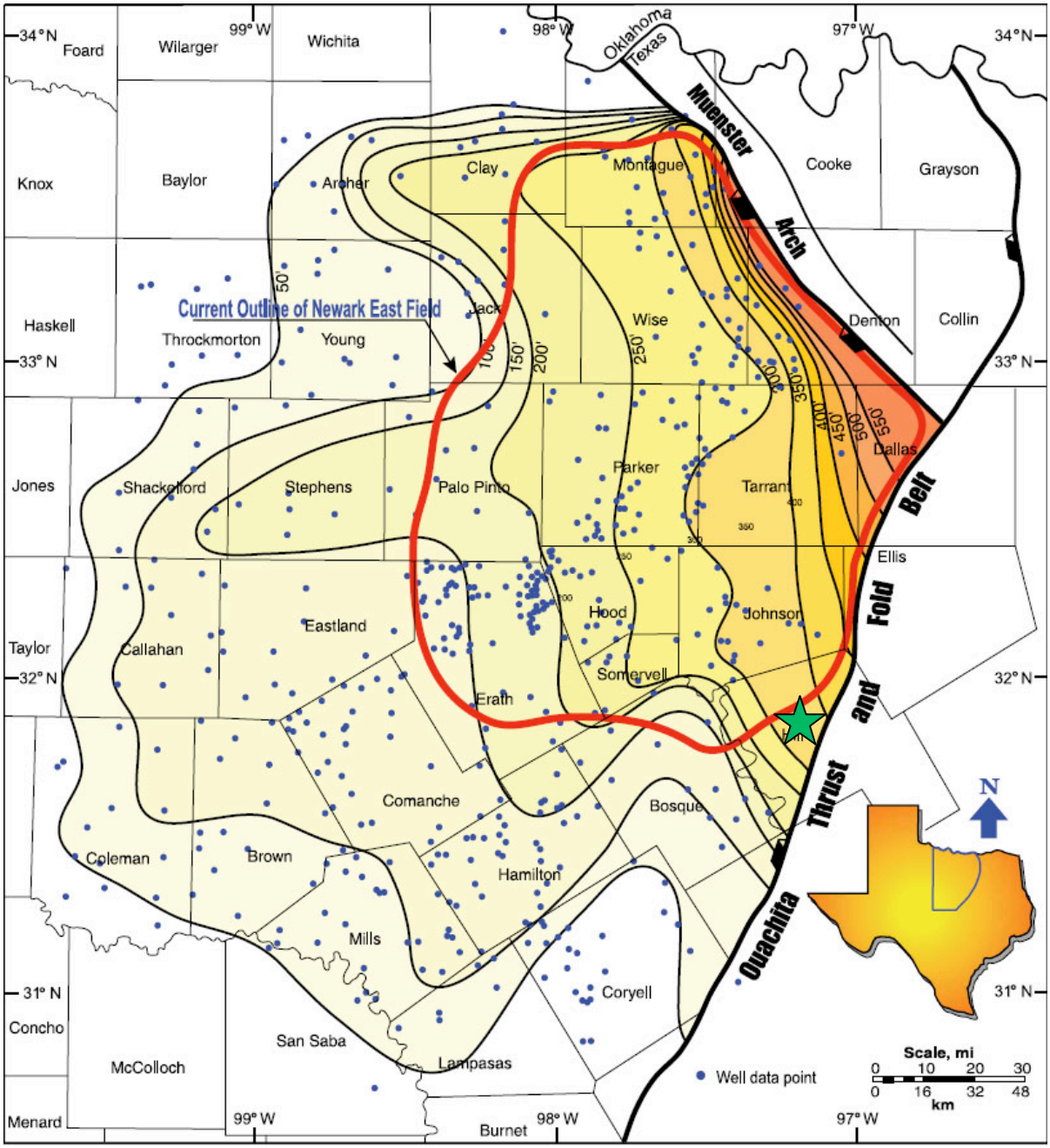

Figure 67. Isopach map of the Barnett in the Fort Worth basin. The green star shows the location of the EOG Gordon SWD. From Zhao et al. (2007).

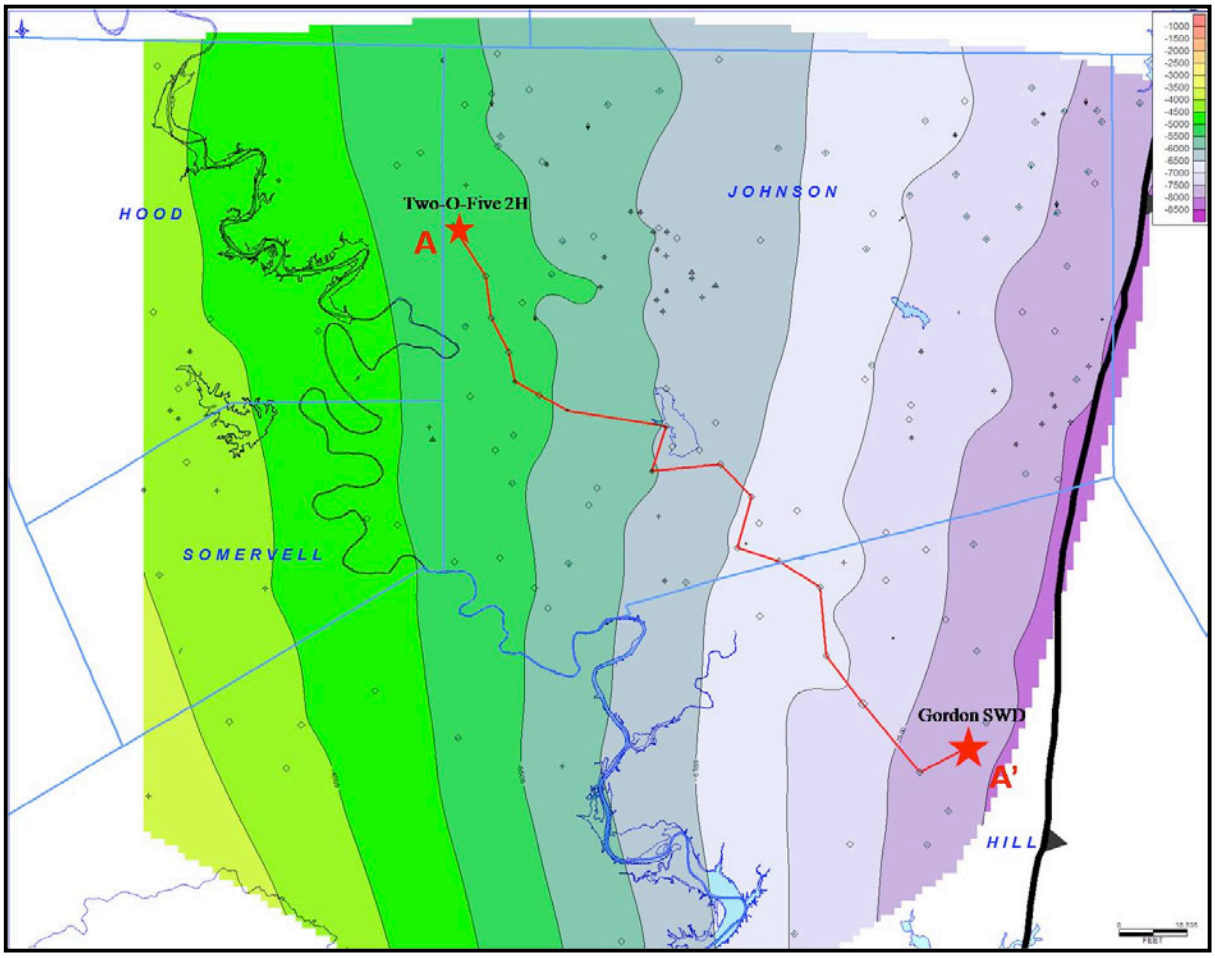

Figure 68. Structure contour map on the top of the Barnett Shale. Contour interval, 500 ft.

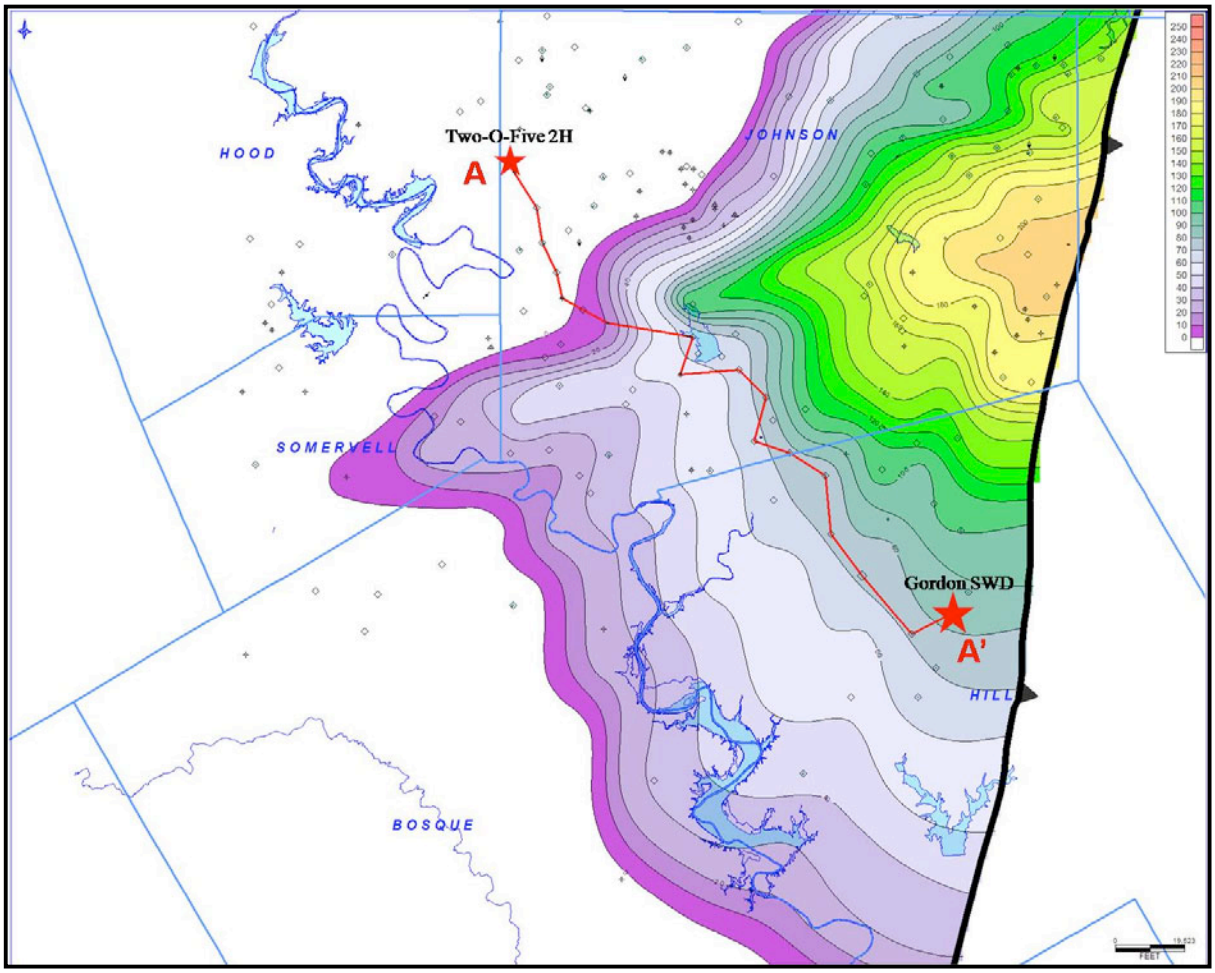

Figure 69. Isopach map of the middle unit. Contour interval, 10 ft.

out to the west. The middle unit is about 75 ft thick in the EOG Gordon SWD well log. It onlaps the Barnett from east to west (Figure 65). The gamma-ray response is high, but it generally has a lower API count than the Barnett, averaging around 115 API units.

The structure on the top of the middle unit is the same as on top of the Barnett (Figure 70). The north- to south-trending structure contours parallel the Ouachita fold-thrust belt. The isopach map of the middle unit shows a depositional trend parallel to structure. Comparison of the isopach and structure maps of the middle unit and Barnett shows that a change in location of the source area took place during the accumulation of the middle unit.

Upper unit

The upper unit is thickest closest to the Ouachita fold-thrust belt in Hill County (Figure 71). It reaches a thickness of 236 ft and thins to the west to approximately 115 ft in Hood, Somervell and Bosque counties. The upper unit onlaps the middle unit and the Barnett. The upper unit is thin (about 70 ft) in Johnson County, where the middle unit reaches its greatest thickness. The upper unit is about 220 ft thick in the EOG Gordon SWD well. The gamma-ray response for the upper unit is much lower than in both the middle unit and the Barnett, averaging about 95 API units.

DISCUSSION AND INTERPRETATION

Environment of Deposition

The facies in the core were deposited in deep-water, marine environments. An organic-rich mudstone or claystone is the basic lithology for all of the facies. Slight

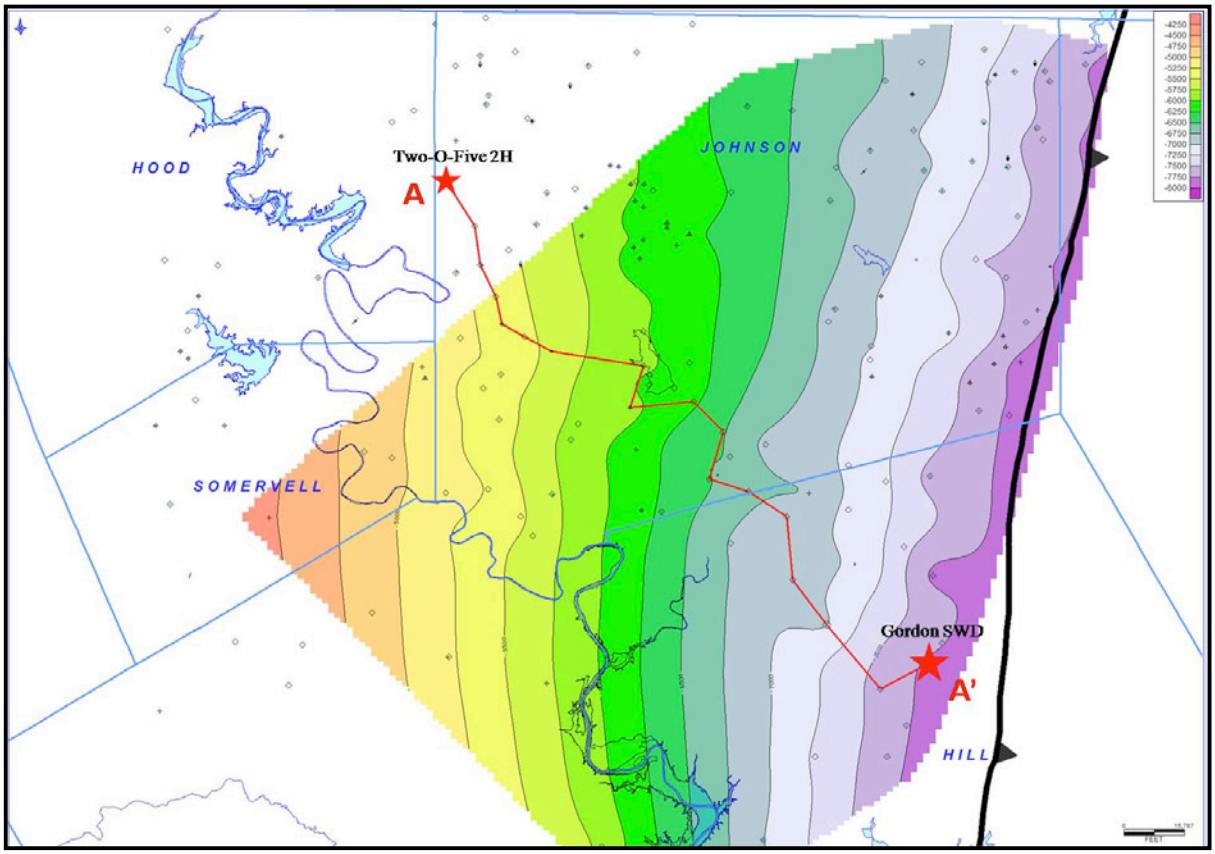

Figure 70. Structure map on the top of the middle unit. Contour interval, 250ft.

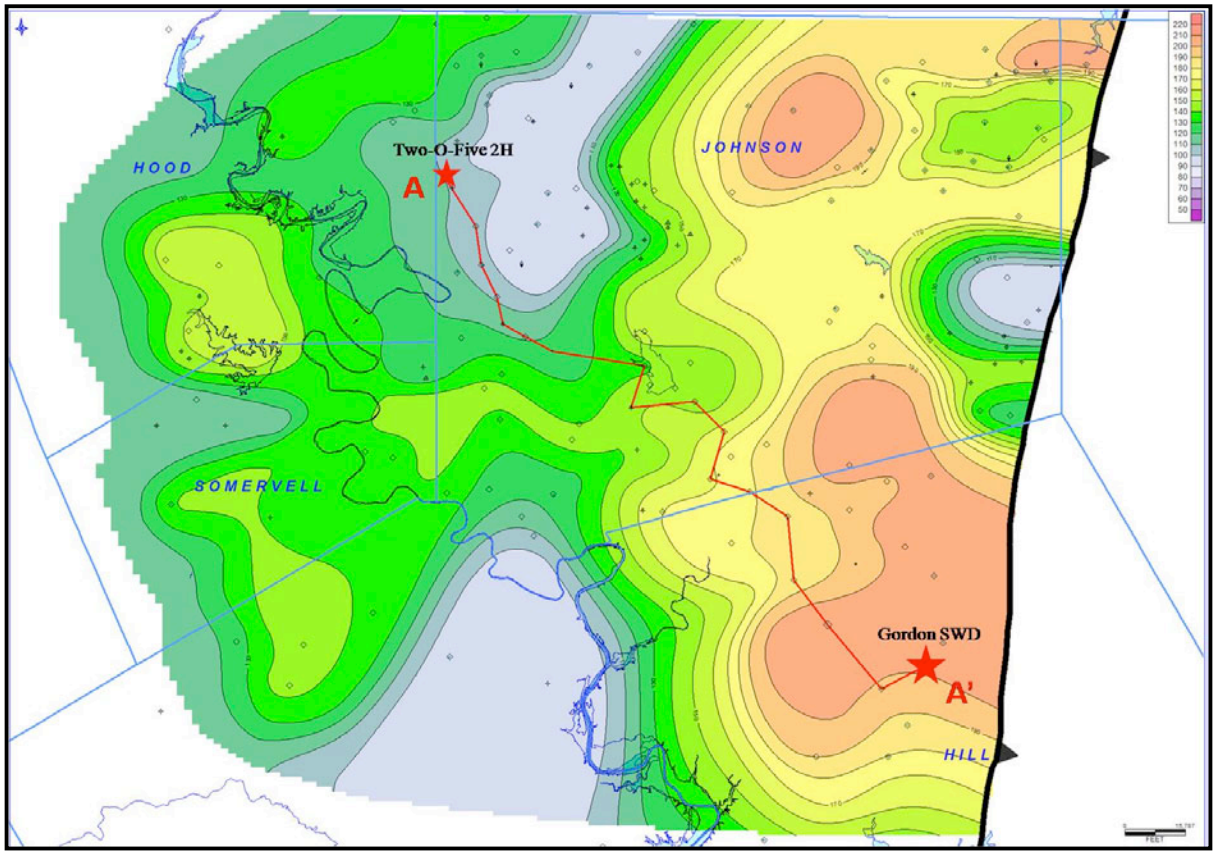

Figure 71. Isopach map of the upper unit. Contour interval, 10 ft.

differences arise from changes in the relative proportions of detrital material and levels of diagenetic alteration.

Facies A

Facies A is an organic-rich mudstone or claystone. It was deposited in deep, quiet waters, where sedimentation was low. Sedimentation was primarily a result of hemipelagic settling of clay particles along with pelagic organisms such as agglutinated forams, sponge spicules and *Tasmanites*, which are marine algal cysts (Loucks and Ruppel, 2007). This facies is present throughout the cored interval. However, it is most abundant in the lower portion of the core, primarily in the middle unit and Barnett.

Subfacies A_2 is a dolomitic mudstone or claystone, which indicates diagenetic alteration possibly due to the conversion of smectite to illite and the addition of magnesium from organic material (McHargue and Price, 1982). The dolomitic shales often occur just above a clay-rich zone with high TOC.

Subfacies A_3, a claystone with pyrite and phosphate nodules, is indicative of a reducing environment and indicates an anoxic depositional environment. The pyrite and phosphate nodules formed before compaction had taken place, because the surrounding laminae show compaction around the nodules. Phosphate nodules of this type generally form below the sediment-water interface at a depth of 5-20cm. In anoxic conditions, the dissolution of iron oxyhydroxides in the sediment liberates iron and phosphate, which is reprecipitated slowly in the shallow subsurface (Hoffman et al., 1998). This facies is found mostly in the middle unit and the Barnett.

Facies B

Facies B is a siltstone deposited in a more proximal setting than facies A. Facies B_1 and B_2 are laminated siltstones. The silt-sized grains are mainly sponge spicules inferred to have been deposited from low-density turbidity currents flowing off nearby shoals. These deposits of low-density turbidity currents or series of multiple turbidity currents range in thickness from 1-2 cm up to 20 cm. Small-scale scour surfaces and normal grading from light silt to a dark clay are common in B_1 and B_2, which coincide respectively with Td and Tc in the Bouma sequence (Lowe, 1982). The parallel to subparallel laminae of B_1 result from the waning of turbulent flow and deposition from suspension clouds of a density flow. B_2 has discontinuous wavy laminations resulting from currents traveling from up on the shelf into the basin, possibly due to slope failure, storm events or minor changes in sea level. Burrowing is common in this facies. Turbidity currents of this type, which are inferred to have originated from up on the shelf, have the ability to briefly oxygenate the bottom water. Organisms swept from the shelf by turbidity currents are brought into the basin. These organisms begin to burrow, and then die when anoxia sets back in. Both facies B_1 and B_2 suggest a proximal setting and are found mostly in the upper unit.

Subfacies B_3 is a mudstone. Most of the silt-sized grains in B_3 are detrital quartz floating in a calcareous clay matrix. This facies is present only at the base of the Barnett, which is near a regional unconformity. The detrital silt grains could be related to the unconformity. During prolonged exposure of the shelf, erosion could have created silt-sized detrital grains. As sea level began to rise during the Barnett, this silt sediment may have been suspended, carried into the basin and re-deposited in the Barnett. Alternatively, the quartz silt could be wind-blown material. The quartz grains are floating in the matrix, which suggests

suspension settling. Angular, silt-sized quartz grains are likely to collect during periods of very low sedimentation when the influx of clay material is very low.

Facies C

Facies C is similar to phosphatic intervals recognized in the Barnett Shale by Papizis (2005), Loucks and Ruppel (2007), Hickey and Henk (2007), and Singh et al. (2008). Thin layers of subfacies C_1 are inferred to represent periods of non-deposition and the formation of phosphatic hardgrounds on the sea floor. These phosphatic hardgrounds are found throughout the core, but are more common in the Barnett and the middle unit. The phosphate is an early authigenic phase that cemented the hardground (Papizis, 2005). Phosphate hardgrounds can form on the slope as a result of upwelling and record hiatuses associated with low sedimentation rates.

Subfacies C_2 contains sand-sized grains of phosphate. The phosphate grains were probably derived from phosphatic hardgrounds and transported downslope from higher up on the shelf during periodic storm events. Subfacies C_2 is interpreted to have formed during maximum flooding where sedimentation rates are low in the deep part of the basin. Sedimentation of clay particles in subfacies C_2 is greatly reduced, allowing phosphate pellets to be reworked along this surface. Biogenic sediments such as sponge spicules and conodont fragments are also common in this interval. Further up on the shelf, in the EOG 2H Two-O-Five core, the same subfacies has pellets of glauconite coated with phosphate. The coated grains and the presence of glauconite suggest a more shelfal environment. Contour currents (described by Loucks and Ruppel (2007)) may have reworked the grains, creating the coated grains. Subfacies C_2 occurs at the top of the Barnett and can be correlated throughout the

basin as a second-order maximum flooding surface on top of the Barnett. Smaller, less pronounced intervals of subfacies C_2 in the Barnett may have originated from periods of low sedimentation. The subparallel laminae suggest these layers were deposited from contour currents. These surfaces can be identified as short-lived starvation surfaces associated with third-order changes in sea level.

Facies D

Layers of shell fragments comprise facies D. The shell layers of the upper unit consist of pelecypod fragments. These can be interpreted to be remnants of debris flows from up on the shelf (Loucks and Ruppel, 2007). This facies is present mostly in the upper unit, which suggests the shells were transported from a nearby shelf or reef deposits. Phosphate grains associated with hardgrounds may be rip-up clasts deposited in the fossil layers.

Facies E

Facies E are calcareous concretions. These concretions formed before significant compaction took place. Elsewhere, carbonate concretions are common in the Barnett (Bunting, 2007). However, in the EOG Gordon SWD core, only a few concretions are present.

Depositional Model— Advancing Thrust

Barnett Shale

The isopach map of the Barnett (Figure 66) indicates a source area from the northeast, where it is the thickest, and trending northeast-southwest. The Barnett in Hill County

represents a basinal setting (Figure 72A). The Barnett was deposited above the Ordovician section and is back-stepping, from the southeast to the northwest (Figure 65). The gamma-ray response is very high on the EOG Gordon SWD well log, which is due to the combination of phosphate and organic matter content. This indicates the Barnett was deposited in an anoxic, starved basin setting. The top of the Barnett has an extremely high gamma-ray count and relatively high organic matter content (5.61 wt% TOC) and represents a condensed section. The corresponding subfacies C_2 indicates that the top of the Barnett is a maximum flooding surface. The distribution of subfacies C_2 shows several minor surfaces associated with third- or fourth-order sea level changes in the Barnett. The relatively lower TOC values for the Barnett could be explained by a lack of productivity of organics in the deep basin. At the maximum flooding surface, the surface area for life to flourish on the shelf is increased. The anoxic basinal waters provided ideal conditions for the preservation of organic matter. However, if productivity is not at a maximum in the overlying waters, then lesser amounts of available organic matter will be available to be preserved.

During the Late Mississippian, the Ouachita fold-thrust belt was being thrusted onto the Laurentian craton (Walper, 1982). Although the location of the thrust belt was further away at this point, deformed bedding in the core (Figure 62) indicates that slumping was occurring. Slumping associated with an unstable shelf can be triggered from earthquakes associated with tectonic movement. Moreover, at the top of this interval, the laminae return to horizontal. The increased pyrite at the top of the interval indicates starvation in the anoxic basin and suggests normal deposition returned above the disturbed section.

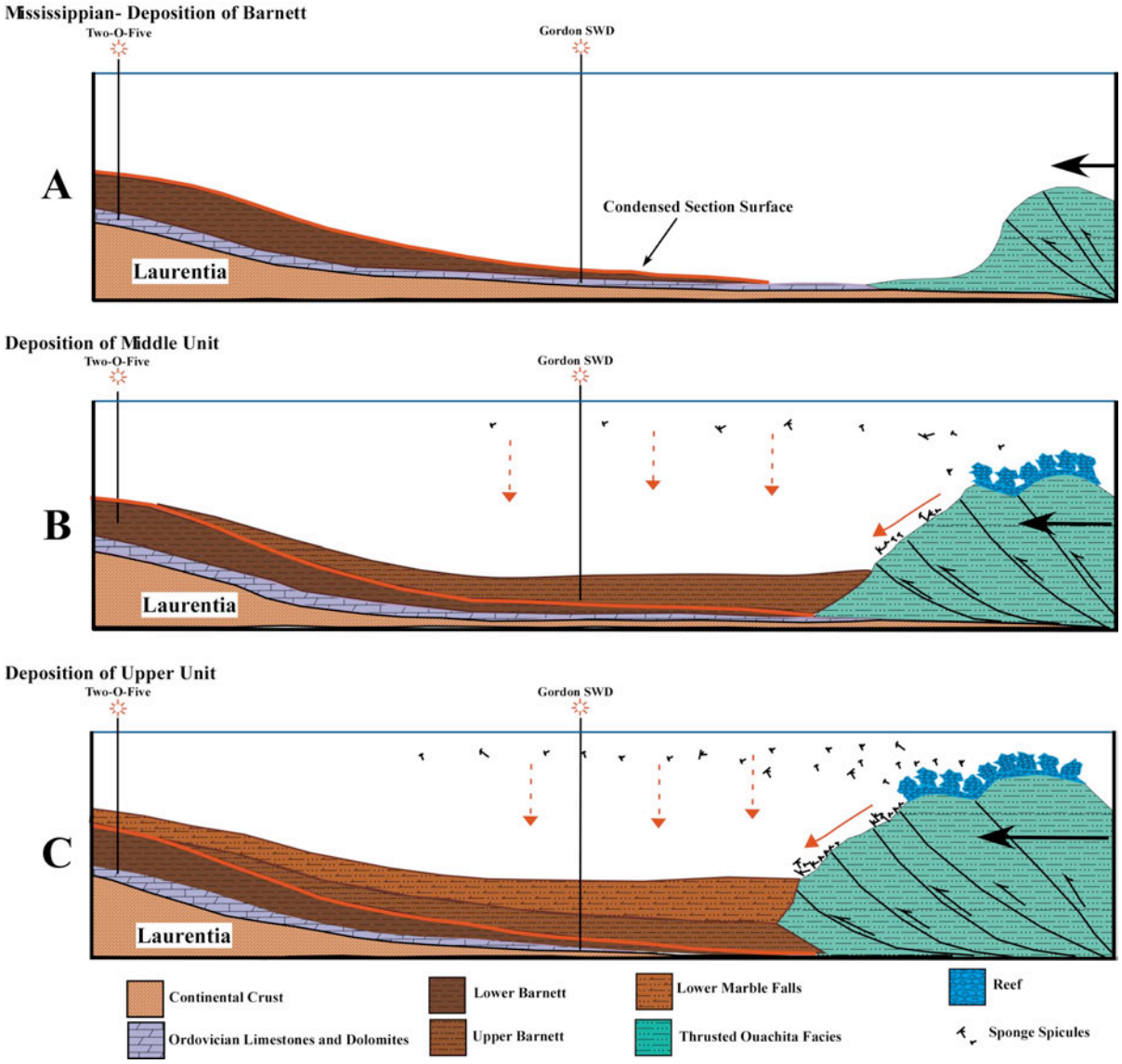

Figure 72. Interpretation of the depositional environment for the Barnett Shale, middle unit and upper unit in Hill County.

Middle unit

The middle unit indicates a change in location of source area (Figure 69). The change in source area was due to the advancement of the Ouachita fold-thrust belt, which provided a different sediment source (Figure 72B). The main depocenter for the middle unit was in eastern Johnson County (Figure 69). The middle unit onlaps the Barnett from the east to the west, thinning from the base (Figure 65). The middle unit consists mostly of subfacies A_1 and A_3. These are clay-rich units containing pyrite and phosphate nodules. These facies indicate the middle unit was deposited in low energy, deep, anoxic waters.

An increase in subfacies B_1 suggests the approach of the thrust belt. Subfacies B_1 is made up almost entirely of siliceous sponge spicules, which were probably derived from a reef growing on the approaching accretionary wedge (Figure 72B). Based on the prograding relationships, these spicules can travel long distances and sedimentation was due to either rain out from the water column or turbidity currents. Clay-filled burrows in the silt facies are a possible indication of brief oxygenation of the bottom water due to turbidity currents.

The middle unit shows high gamma-ray counts on well logs. However, the gamma-ray reading is not as high as it is in the Barnett because of the elevated silt content. The highest TOC values in the EOG Gordon SWD core are in the middle unit suggesting that productivity in the overlying waters must have been high. Upwelling of bottom waters promotes blooms of life on the shelf margin. The presence of clay, pyrite and phosphate nodules in this interval indicates periods of anoxic conditions, which are favorable in preserving the organic matter. Movement from the Ouachita fold-thrust belt during the deposition of the middle unit is seen in core. Folding and inclined bedding may result from tectonic movements during deposition (Figure 63).

Upper unit

In the depositional model of the upper unit (Figure 72C), influx of sediment continued from the Ouachita fold-thrust belt, but in a larger volume (Figure 71). The depocenter from the upper unit shifted to eastern Hill County, depositing only a thin layer over the middle unit in Johnson County. The upper unit onlaps the middle unit and the Barnett, but remains relatively continuous (Figure 65). This shift in deposition was likely due to tectonics. As the Ouachita thrust front advanced, the thrust belt depressed the crust, which resulted in the shift of the depocenter.

The upper unit gamma-ray response is low, which is due to the increase in silt content. The upper unit consists of alternating intervals of subfacies A_1, B_1 and B_2. The increase in silty facies is due to the proximity of the Ouachita fold-thrust belt. The silt is primarily siliceous sponge spicules with only a small amount of detrital quartz. Sponge spicules are derived from a reef, which was situated on the Ouachita fold-thrust belt, and transported westward. The increase in subfacies B_2 indicates the presence of turbidity currents. Burrows are also present at the top of some silt layers in the upper unit and could indicate sediment-gravity flows oxygenating the sediment surface. Layers of shell fragments (Facies D) are also common in the upper unit. The shell debris is inferred to have originated from turbidity currents and debris flows from the nearby fold-thrust belt.

The basal part of the upper unit has high TOC content, which quickly decreases. The higher TOC is in the clay-rich interval, which is part of the distal basinal facies formed during progradation of the upper unit. A fall in relative sea level between the middle unit and the upper unit affected the location of oxygenated waters. The middle unit was deposited in anoxic conditions. The upper unit was gradually exposed to oxygenated waters, which

coincides with low TOC and makes the presence of burrowing organisms living in the substrate possible. Introduction of oxygenated waters lowered the preservation potential of organic matter.

Smithwick Shale

Several descriptions of the Smithwick Shale in the Llano region are similar to the spiculitic shales of the middle and upper units. The name "Smithwick Shale" has been applied to many shale units in the Llano region. Several publications on the Smithwick show a wide variety of observations. For example, McBride and Kimberly (1963) describe the Smithwick from a locality in the Llano region as a dark gray claystone interbedded with sandstone. They observed very few sponge spicules. However, Kier et. al. (1979) and Erlich and Coleman (2005) describe the Smithwick Formation from several localities in outcrop in central Texas as a micro-laminated, spiculitic shale, rich in TOC, containing phosphate, calcareous fossils, and plant fragments. This description of the Smithwick Shale in central Texas corresponds to the description of the middle and upper units in this study.

The Smithwick Shale spans the lower to middle Pennsylvanian in the Fort Worth basin (Figure 6). These shales are interpreted to be deposited in a low energy, outer shelf to upper slope environment (Erlich and Coleman, 2005). Kier et. al. (1979) and Erlich and Coleman (2005) describe the Smithwick Shale as a transitional slope unit between the Marble Falls to the west and prodelta deposits to the east. It is the lateral equivalent of the Upper Marble Falls member. The advancing Ouachita fold-thrust belt caused drowning of the Marble Falls carbonate platform. As deposition of the Marble Falls carbonates moved

westward, the basinal facies (Smithwick Shale) followed, eventually overlying the carbonate platform (Erlich and Coleman, 2005).

Although descriptions of the Smithwick Shale are similar to the middle and upper units, the onlapping relationships do not correspond. The spiculitic shales of the middle and upper units were not deposited from the Marble Falls platform to the west, according to the isopach maps. The onlapping nature of the strata indicates the spiculitic shale was sourced from the Ouachita fold-thrust belt. A regional study of the Marble Falls in the southern part of the Fort Worth basin could clear up the debate on the lithostratigraphic relationship between the middle and upper units to the Smithwick Shale. A biotratigraphic study of the middle unit and the upper unit would also help determine the age of the spicule-rich shales.

Analogue- Island of Barbados

Barbados is a coral-capped, non-volcanic island on the eastern edge of the Caribbean plate (Taylor and Mann, 1991) (Figure 73). It is the only island on the Barbados ridge, which is a part of the Barbados accretionary prism. This accretionary wedge formed on the Caribbean plate as the North American plate is subducted beneath it. The volcanic arc of the Lesser Antilles is inboard of the accretionary prism. Barbados is formed of intensely folded and faulted Paleocene to Eocene marine rocks, which outcrop in the Scotland District. These sediments are dominantly clastic turbidite sequences interbedded with clay and gravelly sands. The folds may be part of a larger zone of active folding that extends over an area of 5,500 km^2 at the Barbados Ridge Complex. Eighty-five percent of the island is covered in terraces of uplifted Pleistocene coral that reach 90m in thickness (Cleary et al., 1984). The two most prominent terraces on Barbados indicate rise and fall of sea level during the

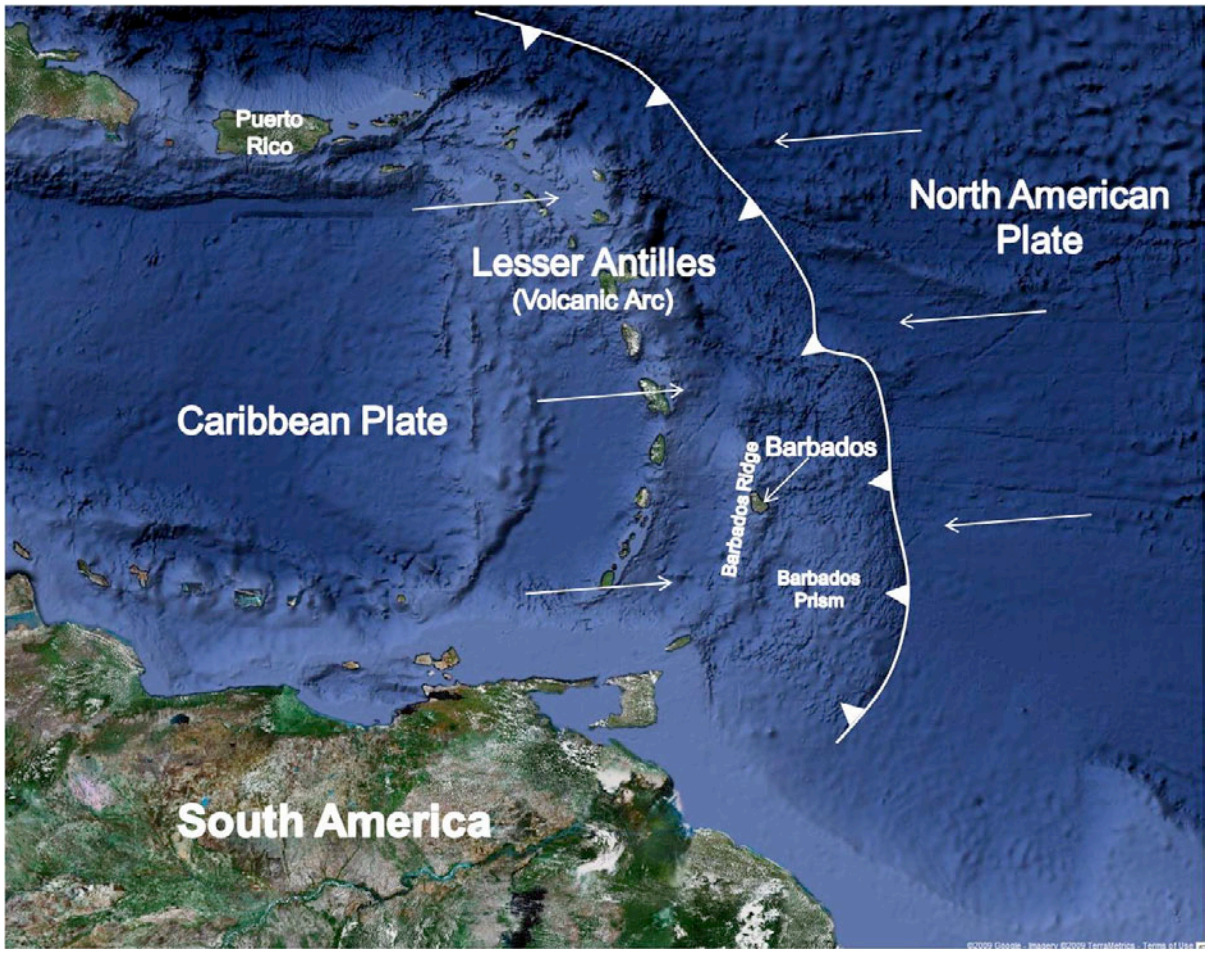

Figure 73. Plate configuration of the Caribbean. The North American plate is being subducted beneath the Caribbean plate. Barbados is an island resulting from the folding and uplift of the growing accretionary wedge. Modified from http://maps.google.com/

Quaternary (Taylor and Mann, 1991). The change in relative sea level is due to both eustacy and tectonic uplift. Rates of uplift on Barbados vary from 0.07 to 0.44 mm/yr (Taylor and Mann, 1991). The coral reefs on Barbados, an active accretionary wedge, are an analogue for sponge buildups on the approaching Ouachita fold-thrust belt in the Fort Worth basin in the Paleozoic.

Sequence Stratigraphy

The three sedimentary units identified and mapped throughout Johnson and Hill counties show a change in deposition due to the advance of the Ouachita fold-thrust belt. The Barnett was derived from the northeast, while the middle unit and upper unit were derived from the approaching fold-belt to the east. A relative sea level curve for sediments in the EOG Gordon SWD was created using organic content derived from TOC and the gamma-ray curve (Figure 74). High organic matter corresponds to higher sea level and low organic matter corresponds to a fall in sea level (Bohacs, 1990; Creaney and Passey, 1993). The EOG Gordon SWD shows a rise in relative sea level in the Barnett, and then a gradual fall through the middle unit and upper unit. The change in relative sea level is inferred to be due to a combination of eustacy and tectonism.

Barnett Shale

The relative change in sea level in the Barnett is inferred to be due to eustacy. The Barnett was deposited during a second-order highstand (Ross and Ross, 1988). The Barnett shows a retrogradational stacking pattern indicating it is a part of the transgressive systems tract. Several parasequences representing prograding highstand deposits are present in the

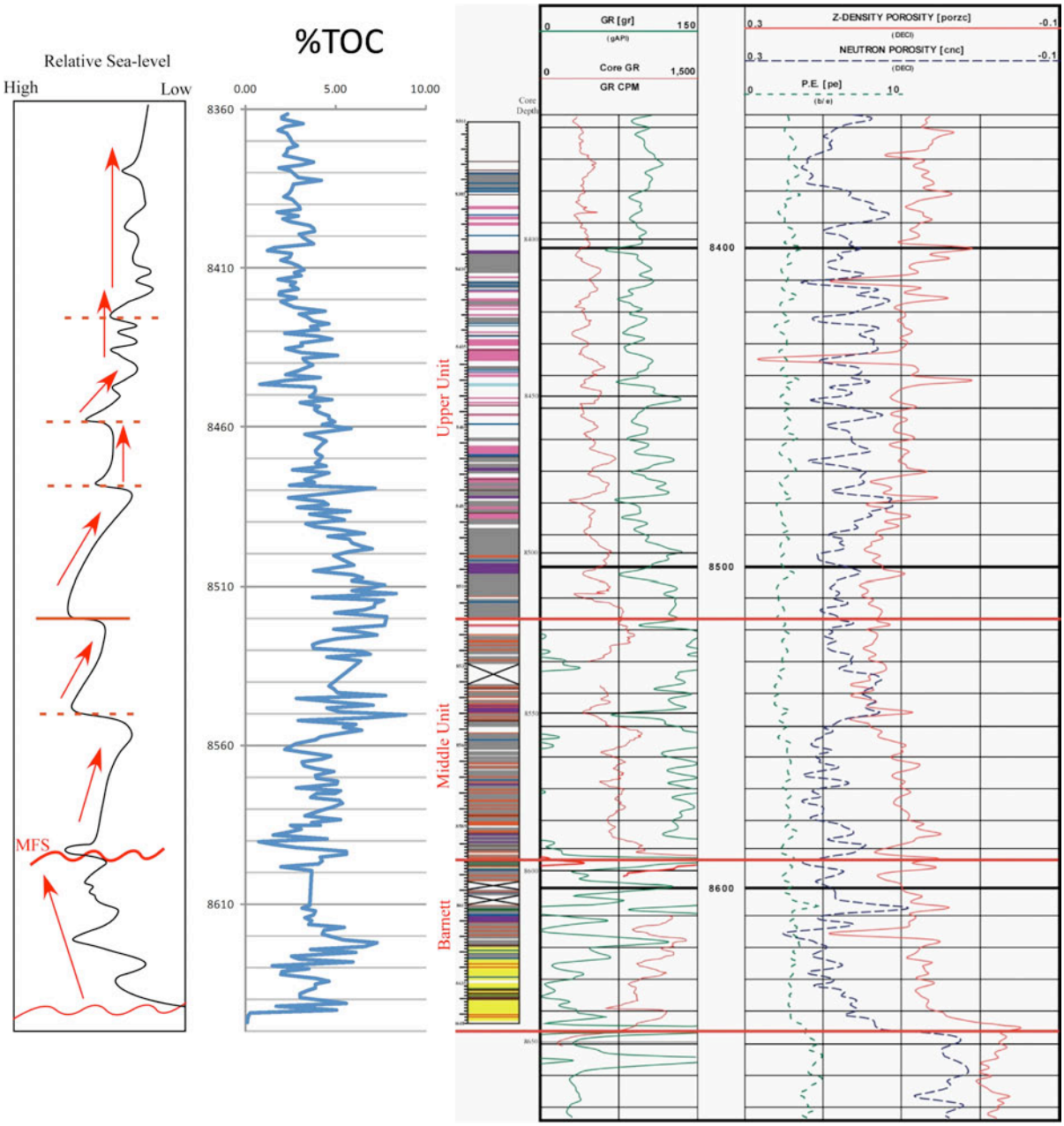

Figure 74. Relative change in sea level curve for the EOG Gordon SWD interpreted from TOC and gamma-ray log. MFS refers to the maximum flooding surface.

Barnett. The facies distribution in the Barnett shows several starvation surfaces. At a depth of 8,640 ft, a small rise in sea level concentrated several phosphate hardgrounds and sandy phosphate layers. This interval is also characterized by high gamma-ray counts. At about 8,620 ft depth, high gamma-ray, high TOC and the presence of a phosphate hardground are indicative of a rise in sea level. At the top of the Barnett, the maximum flooding surface is traceable and has a distinct petrographic signature. Subfacies C_2 is a sandy phosphate layer that is indicative of a starved sedimentation surface. Rise in sea level has trapped sediments further on the shelf. This surface is both a maximum flooding surface and a nondepositional unconformity. This unconformity does not represent the sequence-bounding, erosional unconformity associated with a change from a highstand systems tract to a lowstand systems tract. It is a time stratigraphic surface that marks the maximum flooding of the shelf. The Barnett in the EOG Gordon SWD shows an overall deepening signature related to a rise in sea level.

Middle unit

The middle unit represents a time when sedimentation patterns changed. Eustatic sea level was high during the Mississippian (Figure 75). The deposition of Marble Falls carbonates was followed by a fall in sea level during the Early Pennsylvanian. Locally, Johnson and Hill counties became a depocenter for turbidity currents from the Ouachita fold-thrust front. The uplift of the fold-thrust belt provided a source for prograding sedimentation from the east. However, sediment supply from the low-density turbidity currents was not large enough to cause a relative fall in sea level alone. Eustacy was likely the driving factor. A rise in sea level occurred shortly thereafter, drowning the Marble Falls carbonate

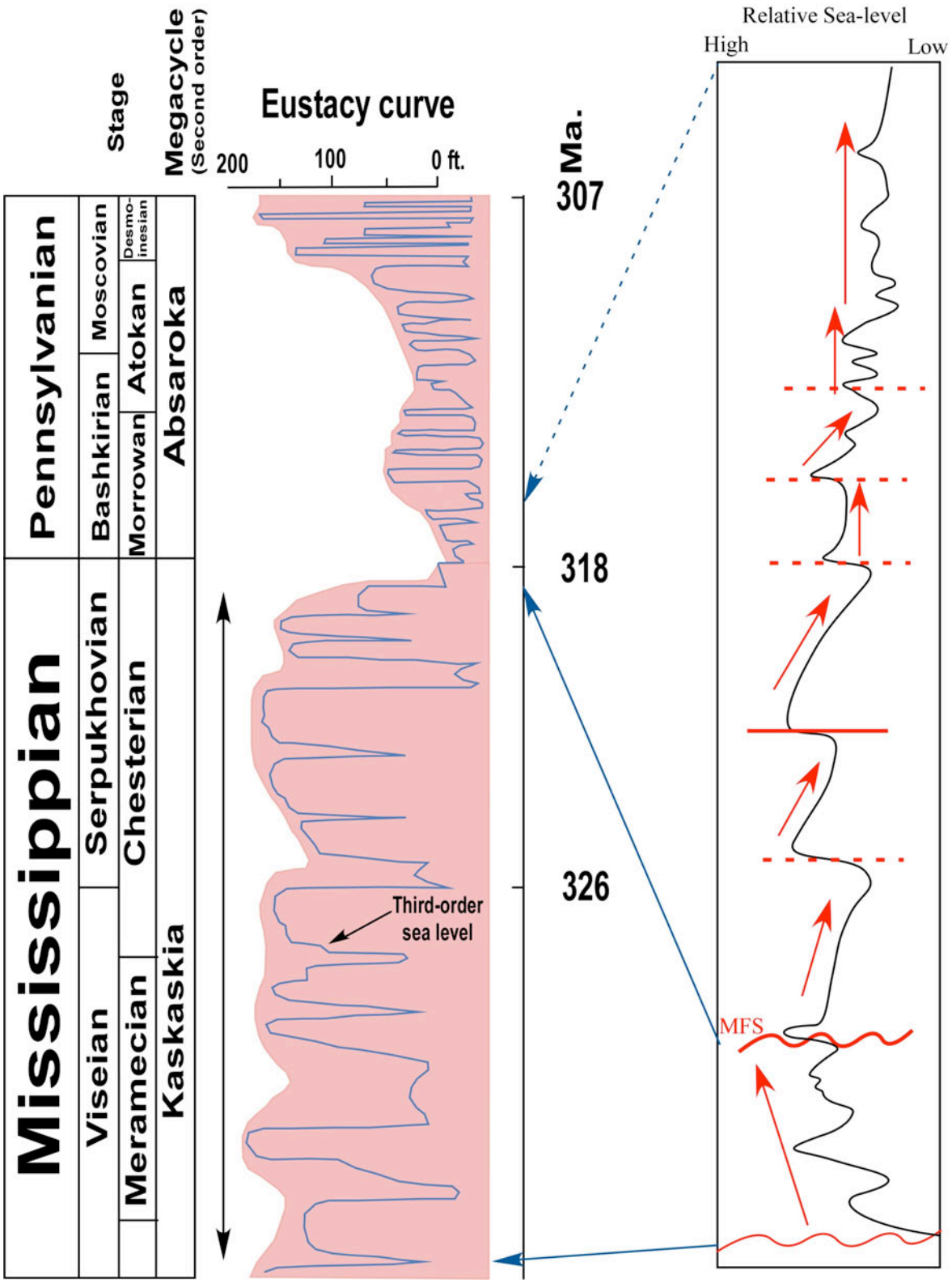

Figure 75. Eustatic sea level curve compared to interpreted sea level curve for the EOG Gordon SWD. MFS refers to the maximum flooding surface.

platforms. The rise in sea level is due to a combination of eustacy and subsidence associated with the advancing fold-thrust belt.

The middle unit contains two distinct parasequences of prograding deposits. It begins with an aggradational to progradational pattern indicative of an early highstand systems tract. At the top of the first parasequence, the facies change from a clay-rich mudstone (subfacies A_1) to a cleaner, siltier facies (subfacies B_1). The deposition of the silty facies is due to increased sediment supply from the thrust front. Following the deposition of this facies, a period of low sedimentation associated with a rise in sea level lead to concentration of organic matter and phosphate, which also correspond to a high gamma-ray response. The next parasequence in the middle unit is another prograding deposit with a coarsening upwards signature. The top of the middle unit marks the flooding surface on top of this parasequence. The late Mississippian to Early Pennsylvanian eustatic curve matches well with the sea level curve of the EOG Gordon SWD created from the TOC and gamma-ray curve (Figure 75). Higher-order changes in sea level are inferred to be due to regional tectonics. The stacking pattern and the aggrading and prograding deposits in the middle unit show that it is a highstand deposit.

Upper unit

The upper unit is characterized by an overall coarsening upwards signature. A decrease in TOC and lower gamma-ray response likely corresponds to a lowering in sea level. Sedimentation rates from turbidity currents would not be large enough to cause a drop in sea level. Eustacy is likely the mechanism for a change in relative sea level.

The increased sediment prograded into the basin, downlapping and onlapping the Barnett and middle unit. The base of the upper unit is a flooding surface, which is high in TOC. Sponge spicules are inferred to have been brought to the basin by turbidity currents flowing off the Ouachita fold-thrust belt. Continued aggradation in response to turbidity currents triggered by tectonism is typical of the upper unit. The several parasequences in the upper unit associated with subfacies B_1, B_2, and D suggest pulses of sedimentation from the Ouachita fold-thrust belt.

The change in relative sea level for the middle and upper units is likely due to eustacy. The ages of the units are unknown, however, Early Pennsylvanian is suspected. The relative sea level curve for middle and upper units in the EOG Gordon SWD likely compares to the fall in eustacy from the Mississippian to the Pennsylvanian (Figure 75). However, higher-order changes of sea level are due to regional tectonics.

SUMMARY AND CONCLUSIONS

Eustacy is the dominating factor in the change in sea level during the deposition of the Barnett. The retrogradational stacking pattern is typical of the TST. The Barnett in Hill County is thin and the presence of pyrite and phosphate nodules suggests an anoxic depositional setting. The high preservation potential for organic matter in the Barnett is not coupled with high organic matter content, suggesting relatively low productivity in the overlying ocean waters.

A condensed section or starvation surface found at the top of the Barnett indicates a period of maximum flooding. This surface is traceable across the study area and correlates to the condensed facies in the EOG 2H Two-O-Five. The condensed facies has a distinct sandy

phosphatic character and marks the top of the Barnett. Although the TOC values are not a maximum at this point, a peak in organic matter is present at the condensed section interval. The gamma-ray spike associated with the condensed section corresponds to a high uranium content in the phosphate as well as the increased organic matter.

The onset of deposition of the middle and upper units is marked by a change in source area as sediment was being shed off the Ouachita fold-thrust belt. The middle unit is mostly a silty mudstone with pyrite and phosphate nodules suggesting an anoxic, basinal setting. The abundance of sponge spicules in the silt layers suggests a nearby source. The onlapping relationship of the middle and upper units on the Barnett suggests the silt was coming from a reef growing on the fold-thrust belt. The stacking pattern for the middle unit is dominantly progradational. The change in sea level was due to eustacy, whereas higher orders of relative change in sea level cycles are controlled by tectonism. TOC is high in the clay-rich facies. High organic matter content in the middle unit suggests high productivity in the overlying oceanic waters. The anoxic, basinal setting during the deposition of the middle unit was conducive to preserving the available organic matter.

The upper unit formed as a result of continued deposition from the Ouachita fold-thrust belt. A fall in eustacy was the dominating control on change in relative sea level. Higher order changes in sea level were due to pulses of tectonism in the advancing fold-belt. The upper unit is a spicule-rich mudstone deposited by turbidity currents. The silt-rich layers indicate a close proximity to the reef growing on the Ouachita fold-thrust belt. The decrease in pyrite and phosphate and the increase in burrows in silt layers suggest the upper unit was deposited in dysoxic to oxic waters. TOC values gradually decrease upward from the base of the upper unit, indicating a drop in eustacy and increased sedimentation rate.

A high gamma-ray response corresponds with, in most instances, the concentration of organic matter and phosphatic facies in the EOG Gordon SWD. The magnitude of the gamma-ray response, the amount of TOC and presence of phosphate are not directly related. However, the general trends in the three parameters correspond to one another. The vertical resolution of the gamma-ray tool is coarser than thin units recognized in core. Isolated thin phosphatic hardgrounds and calcareous shell layers are difficult to recognize on well logs.

Relative change in sea level in the Fort Worth basin resulted from the interplay of tectonism and eustacy. Subsidence, sedimentation and eustacy are all factors that are difficult to discriminate. A biostratigraphic study would help constrain the ages of the sedimentary units. Future work on this is needed and is fundamental to understanding the Paleozoic stratigraphy in Hill County.

REFERENCES

Bohacs, K.M., 1990, Sequence stratigraphy of the Monterey Formation, Santa Barbara County; integration of physical, chemical, and biofacies data from outcrop and subsurface, American Association of Petroleum Geologists Bulletin, vol. 74, p. 614.

Bunting, P., 2007, Petrographic Analysis of the Barnett Shale in the Fort Worth Basin. M.S. thesis, Texas Christian University, Fort Worth, Texas, 101 p.

Cleary, W.J., H.A. Curran, and P.A. Thayer, 1984, Barbados Ridge: Inner slope sedimentation. SEPM (Society for Sedimentary Geology), vol. 54, p. 527-540.

Creaney, S. and Q.R. Passey, 1993, Recurring patterns of total organic carbon and source rock quality within a sequence stratigraphic framework, American Association of Petroleum Geologists Bulletin, vol. 77, p. 386-401.

Doveton, J.H. and D.F. Merriam, 2004, Borehole petrophysical chemostratigraphy of Pennsylvanian black shales in the Kansas subsurface, Chemical Geology, vol. 206, p. 249-258.

Erlich, R.N. and J.L. Coleman Jr., 2005, Drowning of the Upper Marble Falls carbonate platform (Pennsylvanian), central Texas: A case of conflicting “signals”?, Sedimentary Geology, vol. 175, p. 479- 499.

Herbin, J.P., C. Muller, J.R. Geyssant, F. Melieres, I.E. Penn, and Y., 1993, Group, Variation of the distribution of organic matter within a Transgressive System Tract: Kimmeridge Clay (Jurrassic), England, In Katz, B. and L.M. Pratt, eds., AAPG Studies in Geology, vol. 37, p. 67-100.

Hesselbo, S.P. and J.M. Huggett, 2001, Glaucony in ocean-margin sequence stratigraphy (Oligocene-Pliocene, offshore New Jersey, U.S.A.; ODP Leg 174A), Journal of Sedimentary Research, vol. 71, no. 4, p. 599-607.

Hickey, J.J. and B. Henk, 2007, Lithofacies summary of the Mississippian Barnett Shale, Mitchell 2 T.P. Sims well, Wise County, Texas, American Association of Petroleum Geologists Bulletin, v. 91, p. 437- 443.

Hoffman, D.L., T.J. Algeo, J.B. Maynard, M.M. Joachimski, J.C. Hower, and J. Jaminski, 1998, Regional and stratigraphic variation in bottomwater anoxia in offshore core shales of Upper Pennsylvanian cyclothems from the Eastern midcontinent shelf (Kansas), U.S.A. In Schieber, J., W. Zimmerle, and P.S. Sethi, eds., Shales and Mustones I: Basin Studies, Sedimentology, and Paleontology. E. Schweizerbart, Stuttgart, p. 243-269.

Kier, R.S., L.F. Brown, Jr. and E.F. McBride, 1979, The Mississippian and Pennsylvanian (Carboniferous) systems in the United States- Texas, U.S. Geological Survey Professional Paper 1110-S, p.S1-S45.

Krumbein, W.C. and L.L. Sloss, 1951, Stratigraphy and Sedimentation, W.H. Freeman and Company, San Francisco, 660 p.

Loucks, R.G. and S.C. Ruppel, 2007, Mississippian Barnett Shale: Lithofacies and depositional setting of a deep-water shale-gas succession in the Fort Worth Basin, Texas, American Association of Petroleum Geologists Bulletin, v. 91, p. 579-601.

Loutit, T.S., J. Hardenbol, P.R. Vail, and G.B. Baum, 1988, The key to age determination and correlation of continental margin sequences, In Wilgus, C.K., B.S. Hastings, C.G.

St. C. Kendall, H.W. Posamentier, C.A. Ross, and J.C. Van Wagoner, eds., Sea level Changes: An Integrated Approach, SEPM (Society for Sedimentary Geology) Special Publication 42, p. 183-212.

Lowe, D.R., 1982, Sediment gravity flows: II. Depositional models with special reference to the deposits of high-density turbidity currents. Journal of Sedimentary Petrology, vol. 52, p. 279-297.

Macquaker, J.H.S., R.L. Gawthorpe, K.G. Taylor, and M.J. Oates, 1998, Heterogeneity, stacking patterns and sequence stratigraphic interpretation in distal mudstone successions: Examples from the Kimmeridge Clay Formation, U.K., In Schieber, J., W. Zimmerle, and P.S. Sethi, eds., Shales and Mustones I: Basin Studies, Sedimentology, and Paleontology. E. Schweizerbart, Stuttgart, p.163-186.

McBride, E.F., and J.E. Kimberly, 1963, Sedimentology of the Smithwick Shale (Pennsylvanian), eastern Llano region, Texas, American Association of Petroleum Geologists Bulletin, vol. 47, p.1840-1854.

McHargue, T.R. and R.C. Price, 1982, Dolomite from clay in argillaceous or shale-associated marine carbonates, Journal of Sedimentary Petrology, vol. 52, p. 873-886.

Mitchum, R.M. and P.R. Vail, 1977, Seismic stratigraphy and global changes in sea level; Part Seven: Seismic stratigraphic interpretation procedure, In Payton, C.E., ed., Seismic Stratigraphy,- applications to hydrocarbon exploration: AAPG Memoir, p. 135-143.

Odin, G.S. and R. Letolle, 1980, Glauconitization and phospatization environments: A tentative comparison, In Bentor, Y.K., ed., SEPM (Society for Sedimentary Geology) Special Publication 29, p. 227-237.

Papizis, P.K., 2005, Petrographic characterization of the Barnett Shale, Fort Worth Basin, Texas: M.S. Thesis, University of Texas at Austin, Austin, Texas, 142 p.

Pollastro, R.M., 2007, Total petroleum system assessment of undiscovered resources in the giant Barnett Shale continuous (unconventional) gas accumulation, Fort Worth Basin, Texas, American Association of Petroleum Geologists Bulletin, v. 91, p.551-578.

Posamentier, H.W. and G.P. Allen, 1997, Siliciclastic Sequence Stratigraphy; Concepts and applications. SEPM (Society for Sedimentary Geology) Concepts in Sedimentology and Paleontology, vol. 7, 210 p.

Ross, C.A. and J.R.P. Ross, 1988, Late Paleozoic transgressive-regressive deposition, In Wilgus, C.K., B.S. Hastings, C.G. St. C. Kendall, H.W. Posamentier, C.A. Ross, and J.C. Van Wagoner, eds., Sea level Changes- An Integrated Approach SEPM (Society for Sedimentary Geology) Special Publication 42, p. 227-247.

Schieber, J., 1998, Sedimentary features indicating erosion, condensation, and hiatuses in the Chattanooga Shale of Central Tennessee: Relevance for sedimentary and stratigraphic evolution. In Schieber, J., W. Zimmerle, and P.S. Sethi, eds., Shales and Mustones I: Basin Studies, Sedimentology, and Paleontology. E. Schweizerbart, Stuttgart, p. 187-215.

Schutter, S.R., 1998, Characteristics of shale deposition in relation to stratigraphic sequence systems tracts. In Schieber, J., W. Zimmerle, and P.S. Sethi, eds., Shales and Mustones I: Basin Studies, Sedimentology, and Paleontology. E. Schweizerbart, Stuttgart, p. 79-108.

Singh, P., R. Slatt, W. and Coffey, 2008, Barnett Shale- unfolded: Sedimentology, sequence stratigraphy, and regional mapping, Gulf Coast Association of Geological Societies

Transactions, vol. 58, p.777-796.

Slatt, R., P. Singh, R.P. Philp, K.J. Marfurt, and Y. Abousleiman, 2008, Workflow for stratigraphic characterization of unconventional gas shales, (Society of Petroleum Engineers) SPE 119891.

Taylor, F.W., and P. Mann, 1991, Late Quaternary folding of coral reef terraces, Barbados, Geology, vol. 19, p. 103-106.

Vail, P.R., R.M. Mitchum Jr., and S. Thompson, III, 1977, Seismic stratigraphy and global changes in sea level; Part Three: Relative changes in sea level from coastal onlap, in Payton, C.E., ed., Seismic Stratigraphy,- applications to hydrocarbon exploration: American Association of Petroleum Geologists Memoir 26, p. 63-81.

Vail, P.R., and W.W. Wornardt Jr., 1991, An integrated approach to exploration and development in the 90's; well log/seismic sequence stratigraphy analysis, American Association of Petroleum Geologists Bulletin, vol. 75, p. 1541.

Van Wagoner, J.C., R.M. Mitchum, K.M. Campion and V.D. Rahmanian, 1990, Siliciclastic sequence stratigraphy in well logs, cores and outcrops: Concepts for high resolution correlation of time and facies, American Association of Petroleum Geologists Methods in Exploration Series, 55 p.

Van Wagoner, J.C., H.W. Posamentier, R.M. Mitchum, P.R. Vail, J.F. Sarg, T.S. Loutit and J. Hardenbol, 1988, An overview of the fundamentals of sequence stratigraphy and key definitions, In Wilgus, C.K., B.S. Hastings, C.G. St. C. Kendall, H.W. Posamentier, C.A. Ross, and J.C. Van Wagoner, eds., Sea level Changes- An Integrated Approach SEPM (Society for Sedimentary Geology) Special Publication 42, p. 39-45.

Walker, R.G., 1992, Facies, facies models and modern stratigraphic concepts. In Walker, R.G. and N.P. James, eds., Facies Models: Response to Sea Level Change, Geological Association of Canada, p. 1-14.

Walper, J.L., 1982, Plate tectonic evolution of the Fort Worth Basin, In Martin, C.A., ed., Petroleum geology of the Fort Worth basin and Bend arch area: Dallas Geological Society, p. 237-251.

Wignal, P.B., 1994, Black Shales: Oxford Science, Oxford, U.K., 127 p.

Zhao, H., N.B. Givens, and B. Curtis, 2007, Thermal maturity of the Barnett Shale determined from well-log analysis, American Association of Petroleum Geologists Bulletin, v. 91, p. 535-549.

APPENDICES

Appendix 1: Detailed Core Description

Appendix 2: Core Photos

Appendix 3: Geochemical Data Table

Appendix 1

Detailed Core Description

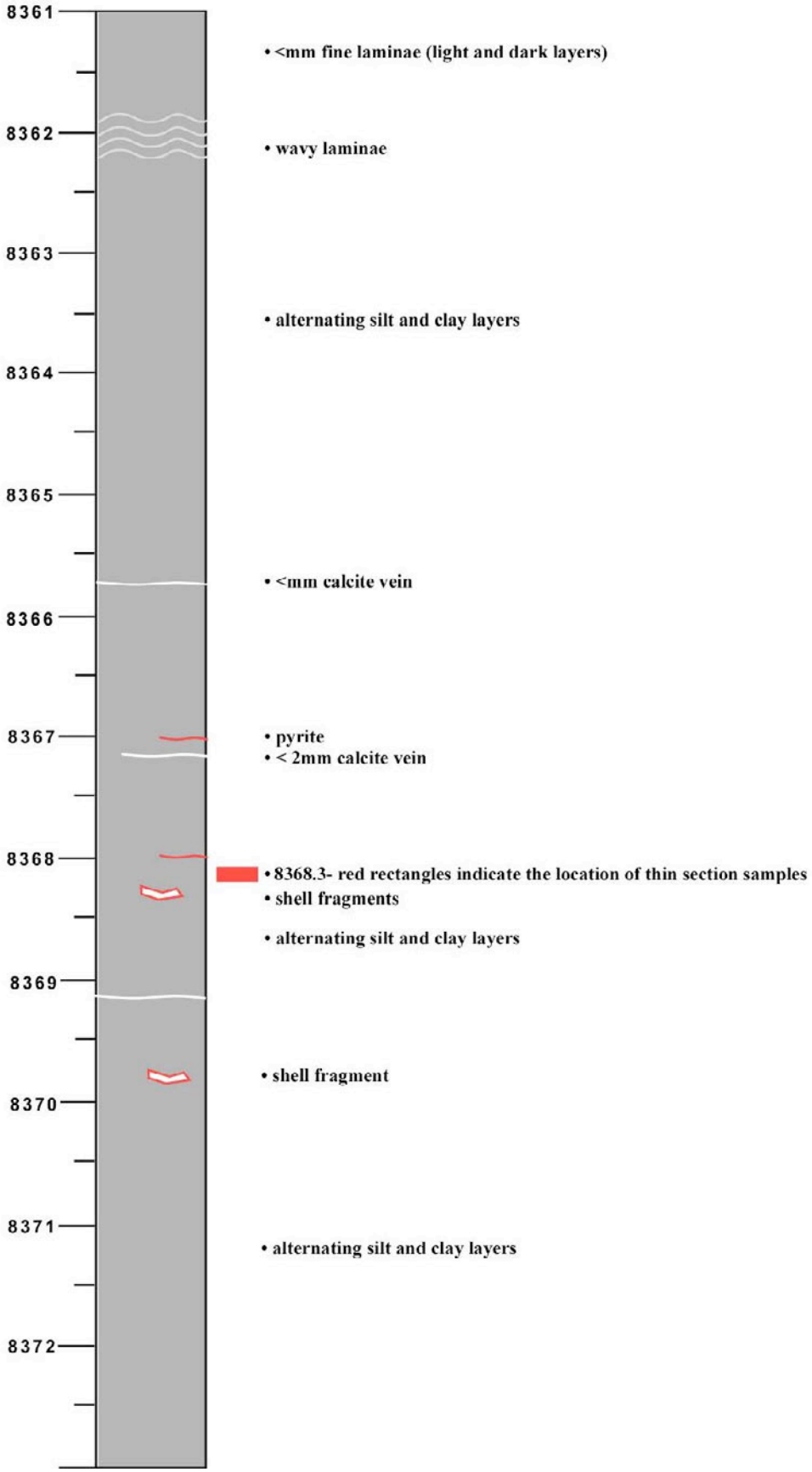
8361
8362
8363
8364
8365
8366
8367
8368
8369
8370
8371
8372
• <mm fine laminae (light and dark layers)
• wavy laminae
• alternating silt and clay layers
• <mm calcite vein
• pyrite
• < 2mm calcite vein
• 8368.3- red rectangles indicate the location of thin section samples
• shell fragments
• alternating silt and clay layers
• shell fragment
• alternating silt and clay layers

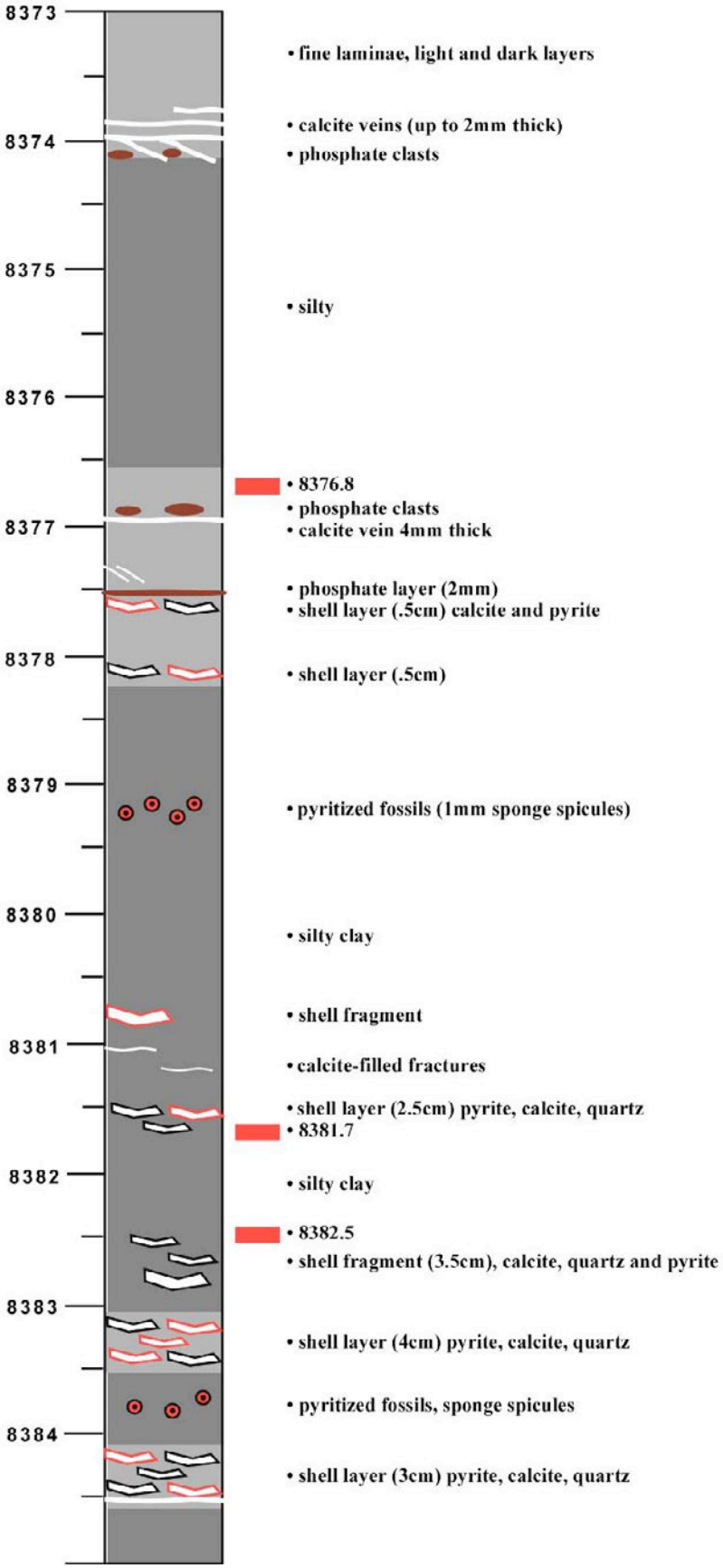
8373
8374
8375
8376
8377
8378
8379
8380
8381
8382
8383
8384
• fine laminae, light and dark layers
• calcite veins (up to 2mm thick)
• phosphate clasts
• silty
• 8376.8
• phosphate clasts
• calcite vein 4mm thick
• phosphate layer (2mm)
• shell layer (.5cm) calcite and pyrite
• shell layer (.5cm)
• pyritized fossils (1mm sponge spicules)
• silty clay
• shell fragment
• calcite-filled fractures
• shell layer (2.5cm) pyrite, calcite, quartz
• 8381.7
• silty clay
• 8382.5
• shell fragment (3.5cm), calcite, quartz and pyrite
• shell layer (4cm) pyrite, calcite, quartz
• pyritized fossils, sponge spicules
• shell layer (3cm) pyrite, calcite, quartz

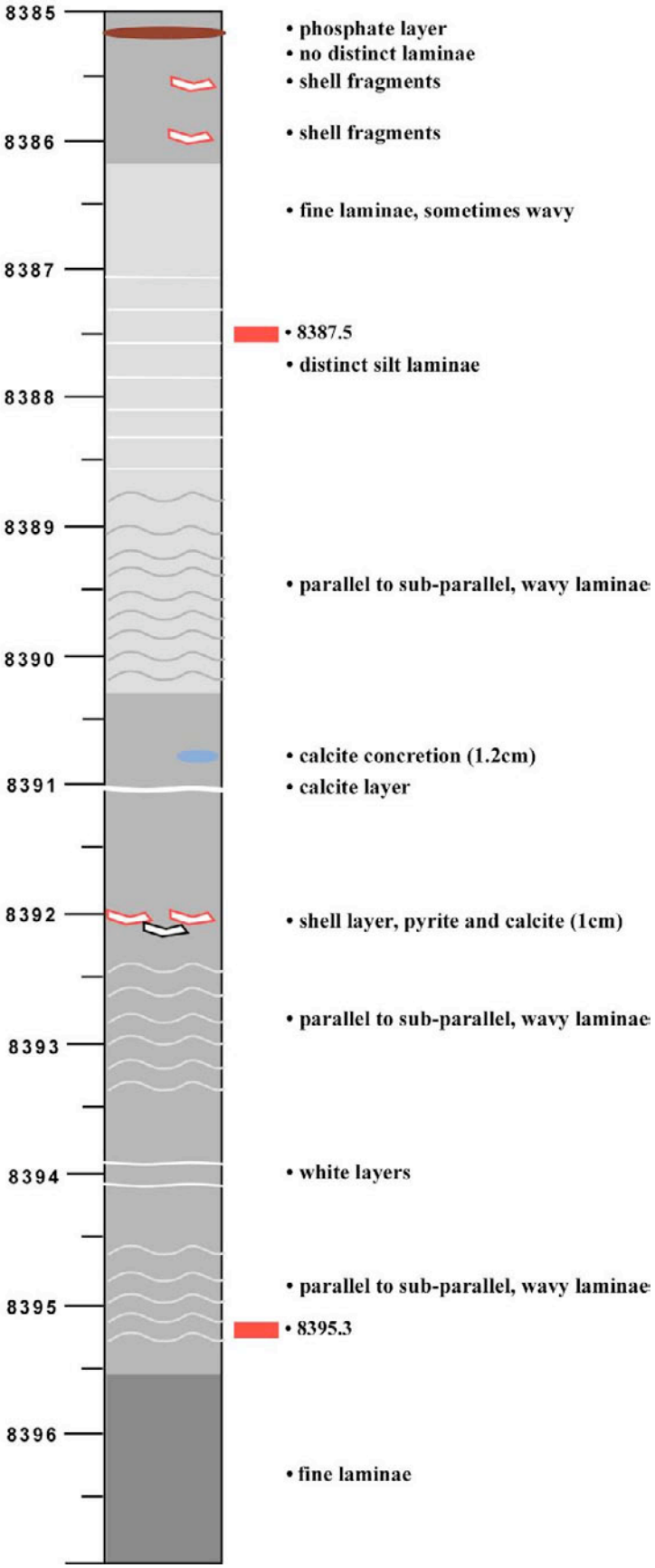
8385
8386
8387
8388
8389
8390
8391
8392
8393
8394
8395
8396
• phosphate layer
• no distinct laminae
• shell fragments
• shell fragments
• fine laminae, sometimes wavy
• 8387.5
• distinct silt laminae
• parallel to sub-parallel, wavy laminae
• calcite concretion (1.2cm)
• calcite layer
• shell layer, pyrite and calcite (1cm)
• parallel to sub-parallel, wavy laminae
• white layers
• parallel to sub-parallel, wavy laminae
• 8395.3
• fine laminae

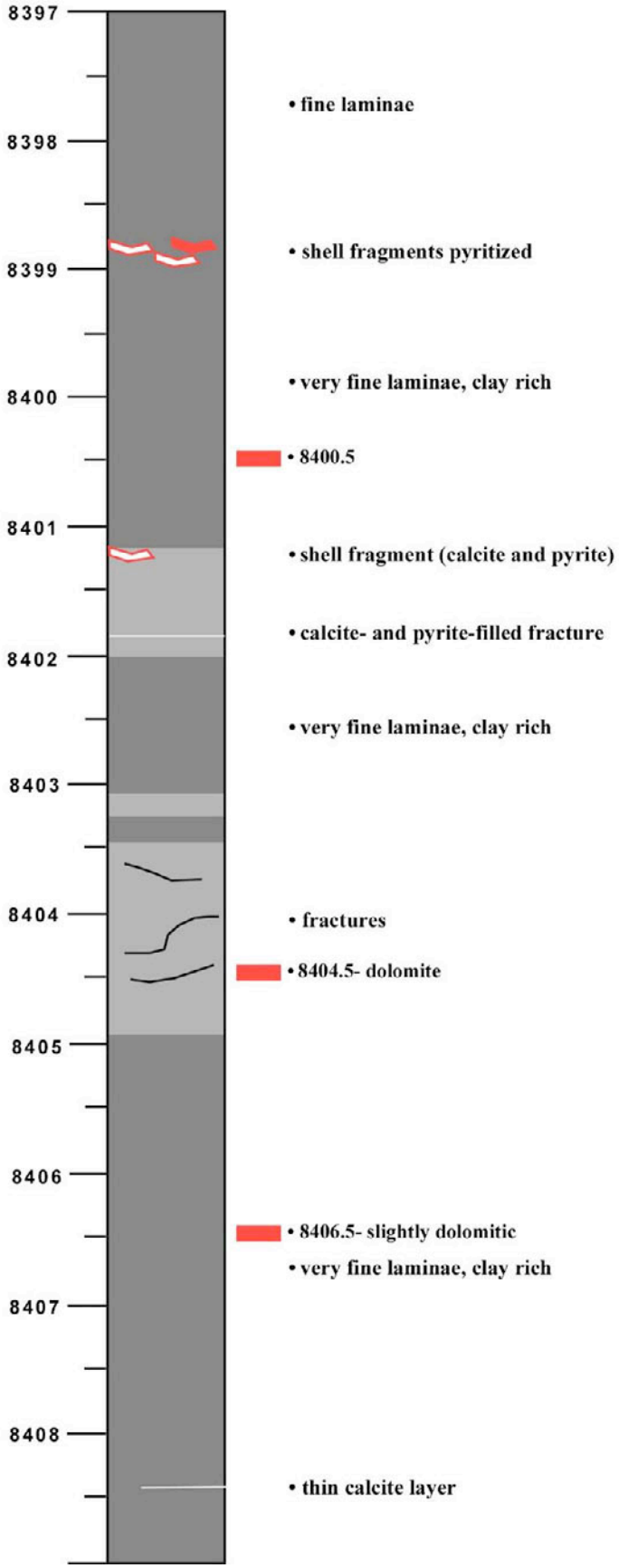
8397
8398
8399
8400
8401
8402
8403
8404
8405
8406
8407
8408
• fine laminae
• shell fragments pyritized
• very fine laminae, clay rich
• 8400.5
• shell fragment (calcite and pyrite)
• calcite- and pyrite-filled fracture
• very fine laminae, clay rich
• fractures
• 8404.5- dolomite
• 8406.5- slightly dolomitic
• very fine laminae, clay rich
• thin calcite layer

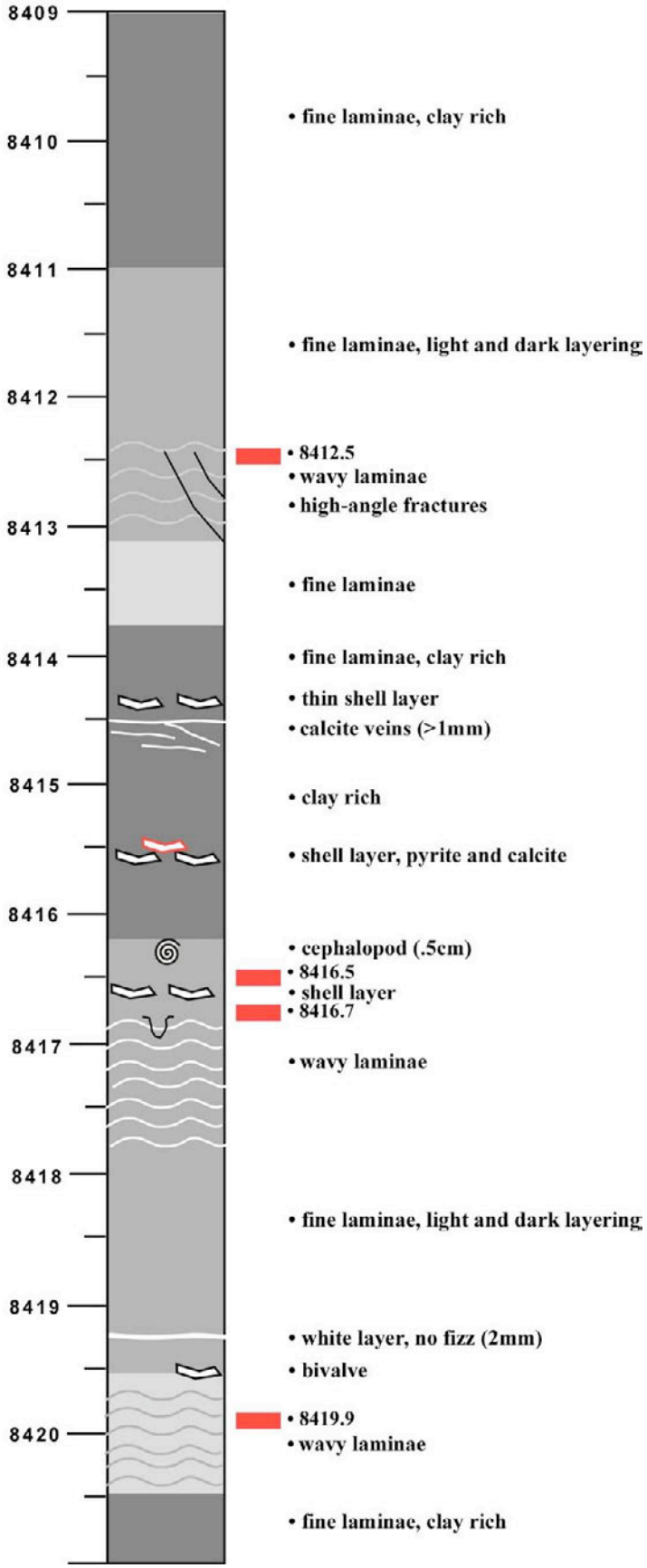
8409
8410
8411
8412
8413
8414
8415
8416
8417
8418
8419
8420
• fine laminae, clay rich
• fine laminae, light and dark layering
• 8412.5
• wavy laminae
• high-angle fractures
• fine laminae
• fine laminae, clay rich
• thin shell layer
• calcite veins (>1mm)
• clay rich
• shell layer, pyrite and calcite
• cephalopod (.5cm)
• 8416.5
• shell layer
• 8416.7
• wavy laminae
• fine laminae, light and dark layering
• white layer, no fizz (2mm)
• bivalve
• 8419.9
• wavy laminae
• fine laminae, clay rich

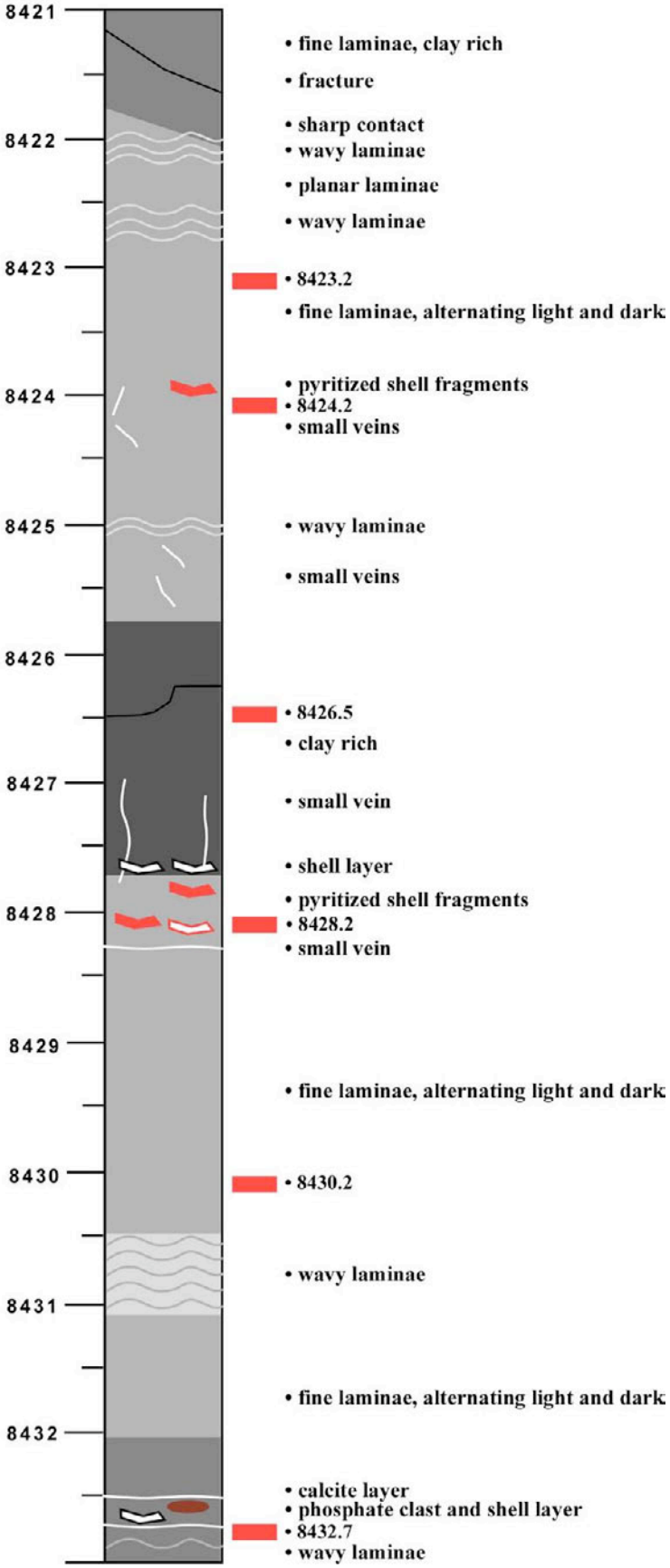
8421
8422
8423
8424
8425
8426
8427
8428
8429
8430
8431
8432
• fine laminae, clay rich
• fracture
• sharp contact
• wavy laminae
• planar laminae
• wavy laminae
• 8423.2
• fine laminae, alternating light and dark
• pyritized shell fragments
• 8424.2
• small veins
• wavy laminae
• small veins
• 8426.5
• clay rich
• small vein
• shell layer
• pyritized shell fragments
• 8428.2
• small vein
• fine laminae, alternating light and dark
• 8430.2
• wavy laminae
• fine laminae, alternating light and dark
• calcite layer
• phosphate clast and shell layer
• 8432.7
• wavy laminae

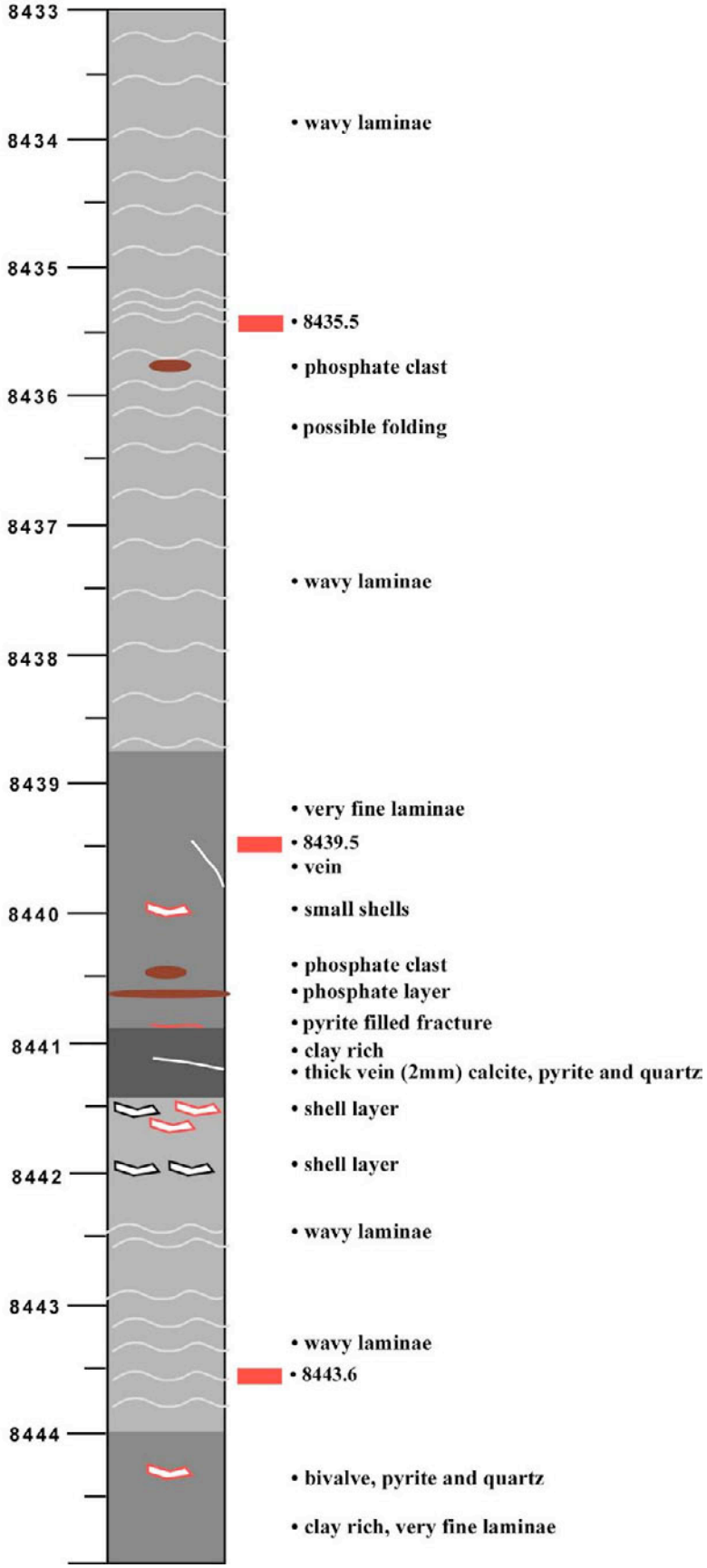
8433
8434
8435
8436
8437
8438
8439
8440
8441
8442
8443
8444
• wavy laminae
• 8435.5
• phosphate clast
• possible folding
• wavy laminae
• very fine laminae
• 8439.5
• vein
• small shells
• phosphate clast
• phosphate layer
• pyrite filled fracture
• clay rich
• thick vein (2mm) calcite, pyrite and quartz
• shell layer
• shell layer
• wavy laminae
• wavy laminae
• 8443.6
• bivalve, pyrite and quartz
• clay rich, very fine laminae

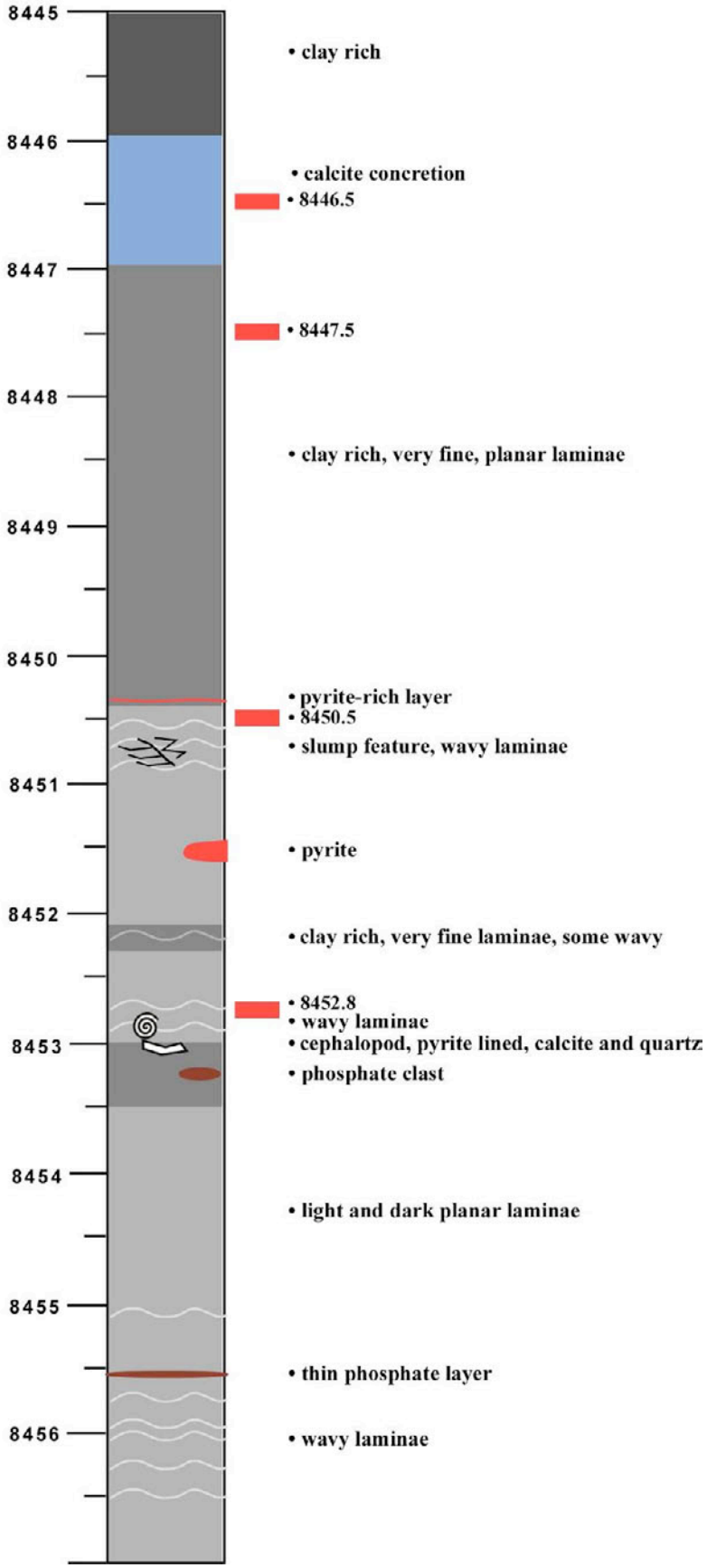
8445
8446
8447
8448
8449
8450
8451
8452
8453
8454
8455
8456
• clay rich
• calcite concretion
• 8446.5
• 8447.5
• clay rich, very fine, planar laminae
• pyrite-rich layer
• 8450.5
• slump feature, wavy laminae
• pyrite
• clay rich, very fine laminae, some wavy
• 8452.8
• wavy laminae
• cephalopod, pyrite lined, calcite and quartz
• phosphate clast
• light and dark planar laminae
• thin phosphate layer
• wavy laminae

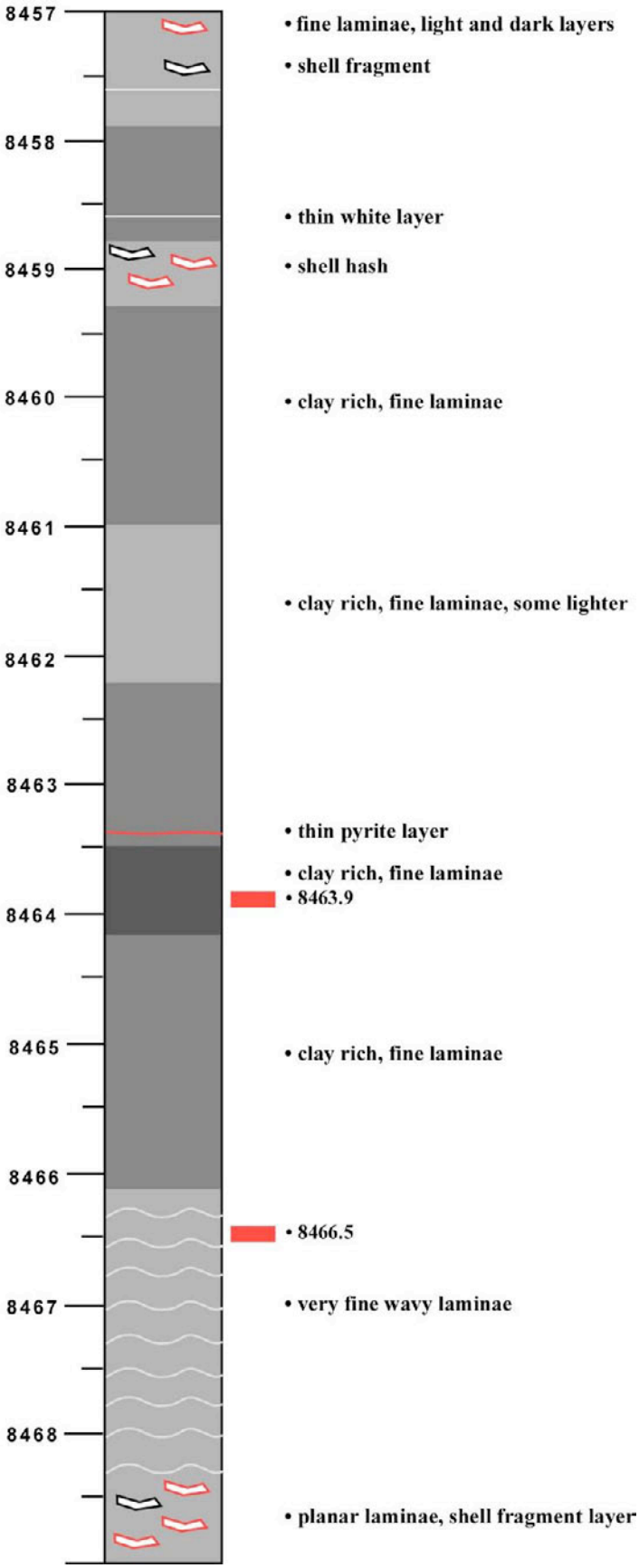
8457
8458
8459
8460
8461
8462
8463
8464
8465
8466
8467
8468
• fine laminae, light and dark layers
• shell fragment
• thin white layer
• shell hash
• clay rich, fine laminae
• clay rich, fine laminae, some lighter
• thin pyrite layer
• clay rich, fine laminae
• 8463.9
• clay rich, fine laminae
• 8466.5
• very fine wavy laminae
• planar laminae, shell fragment layer

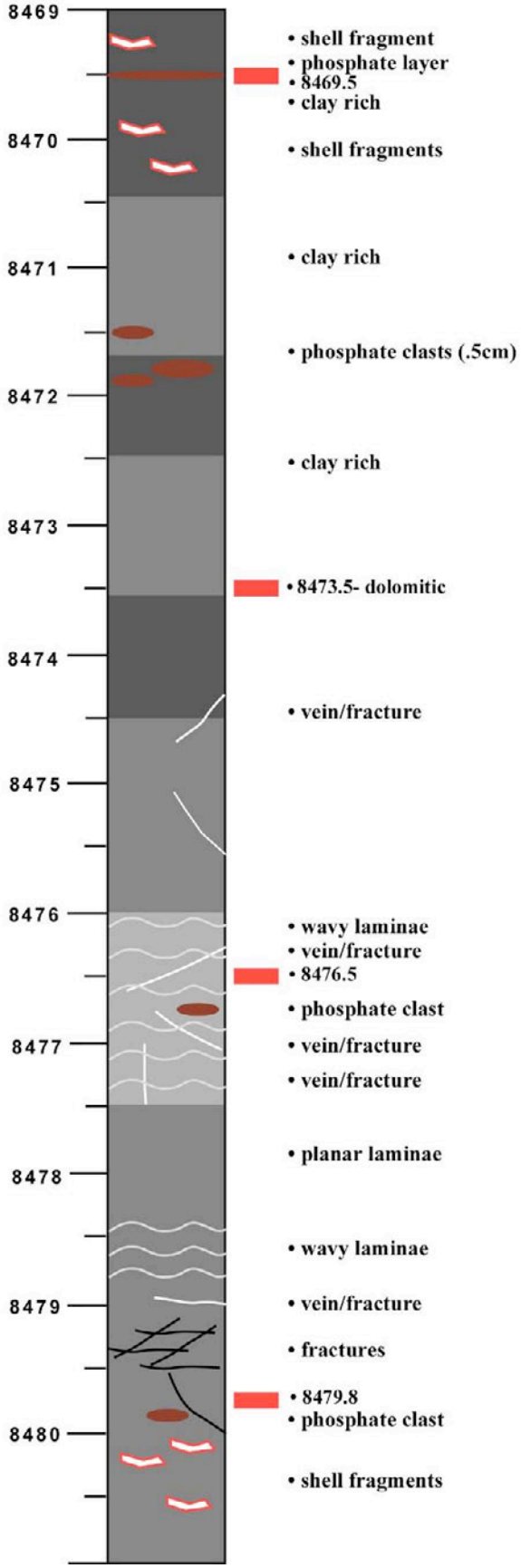
8469
8470
8471
8472
8473
8474
8475
8476
8477
8478
8479
8480
• shell fragment
• phosphate layer
• 8469.5
• clay rich
• shell fragments
• clay rich
• phosphate clasts (.5cm)
• clay rich
• 8473.5- dolomitic
• vein/fracture
• wavy laminae
• vein/fracture
• 8476.5
• phosphate clast
• vein/fracture
• vein/fracture
• planar laminae
• wavy laminae
• vein/fracture
• fractures
• 8479.8
• phosphate clast
• shell fragments

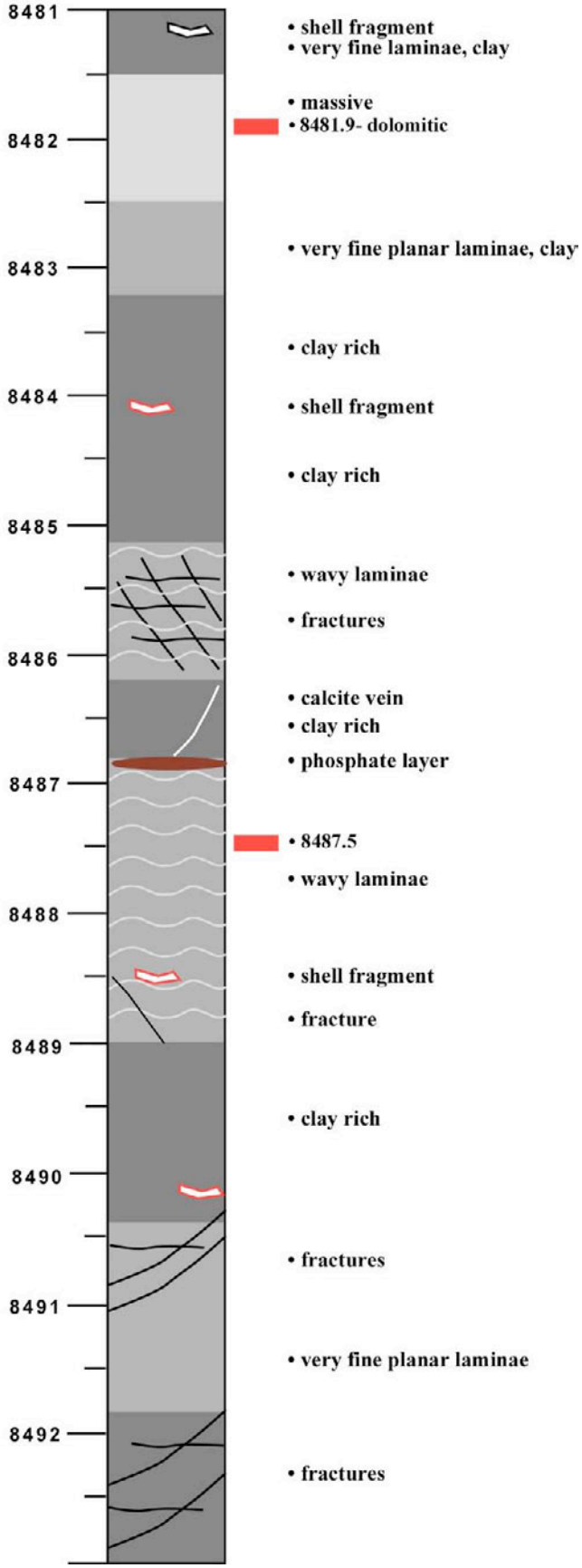
8481
8482
8483
8484
8485
8486
8487
8488
8489
8490
8491
8492
• shell fragment
• very fine laminae, clay
• massive
• 8481.9- dolomitic
• very fine planar laminae, clay
• clay rich
• shell fragment
• clay rich
• wavy laminae
• fractures
• calcite vein
• clay rich
• phosphate layer
• 8487.5
• wavy laminae
• shell fragment
• fracture
• clay rich
• fractures
• very fine planar laminae
• fractures

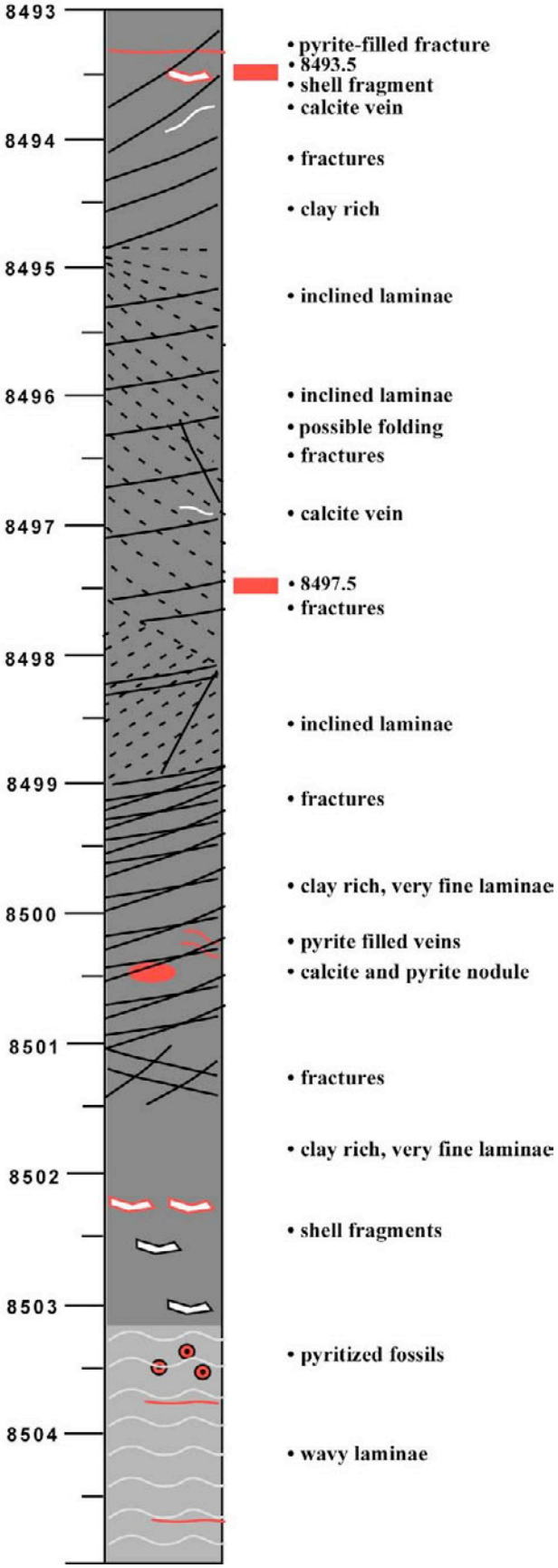
8493
8494
8495
8496
8497
8498
8499
8500
8501
8502
8503
8504
• pyrite-filled fracture
• 8493.5
• shell fragment
• calcite vein
• fractures
• clay rich
• inclined laminae
• inclined laminae
• possible folding
• fractures
• calcite vein
• 8497.5
• fractures
• inclined laminae
• fractures
• clay rich, very fine laminae
• pyrite filled veins
• calcite and pyrite nodule
• fractures
• clay rich, very fine laminae
• shell fragments
• pyritized fossils
• wavy laminae

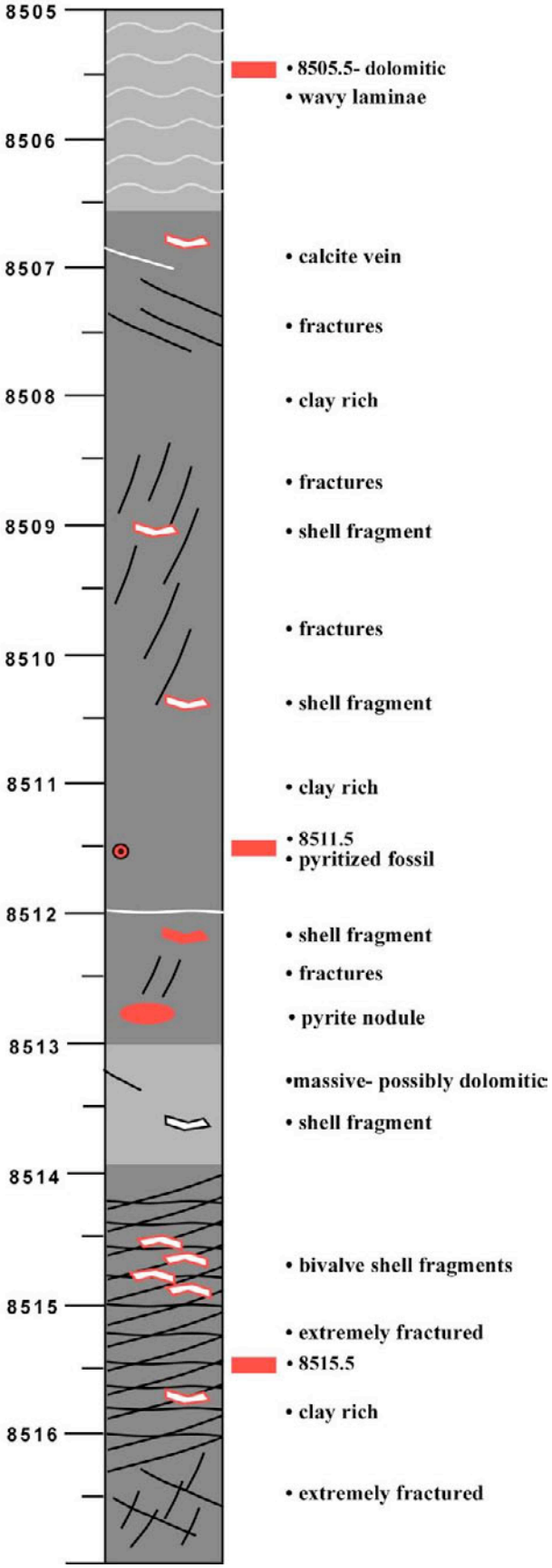
8505
8506
8507
8508
8509
8510
8511
8512
8513
8514
8515
8516
• 8505.5- dolomitic
• wavy laminae
• calcite vein
• fractures
• clay rich
• fractures
• shell fragment
• fractures
• shell fragment
• clay rich
• 8511.5
• pyritized fossil
• shell fragment
• fractures
• pyrite nodule
•massive- possibly dolomitic
• shell fragment
• bivalve shell fragments
• extremely fractured
• 8515.5
• clay rich
• extremely fractured

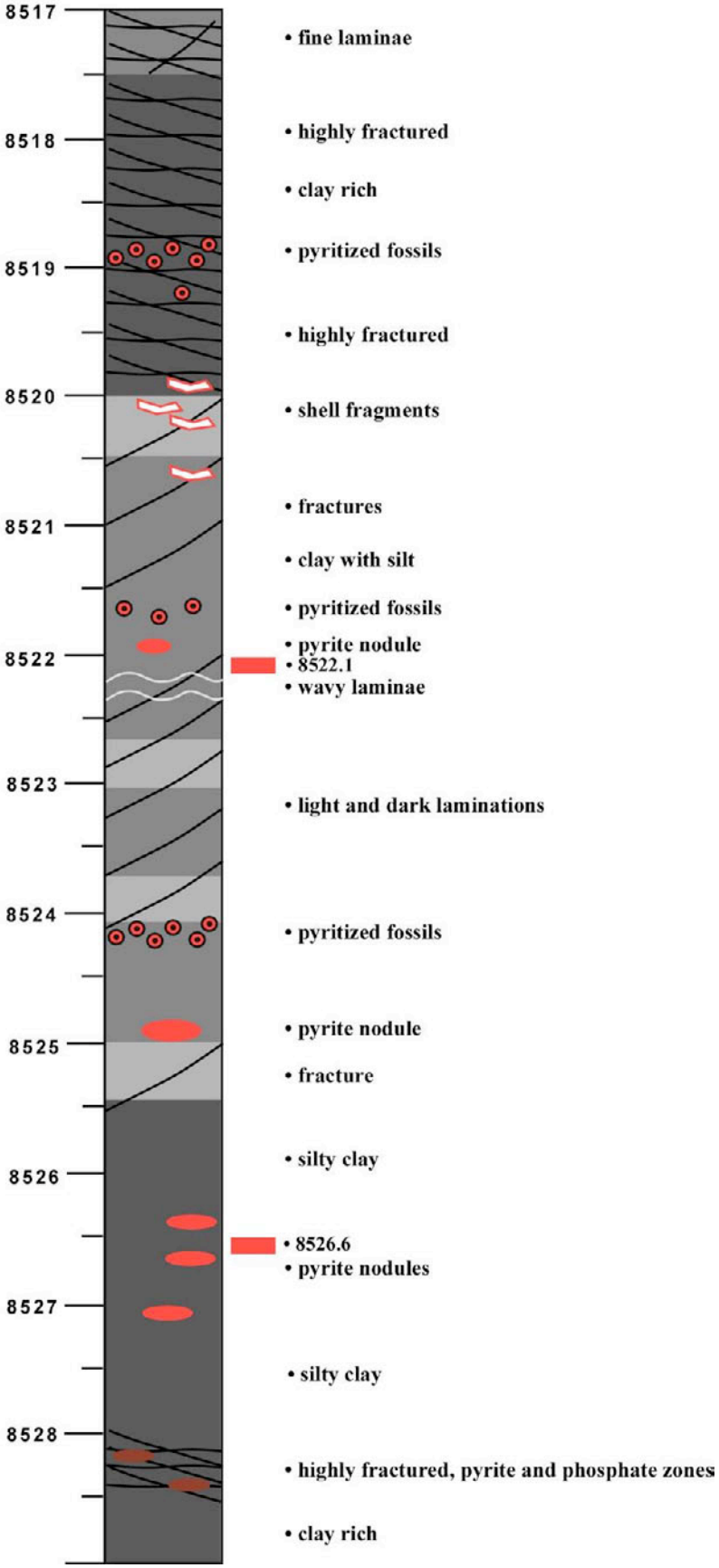
8517
8518
8519
8520
8521
8522
8523
8524
8525
8526
8527
8528
• fine laminae
• highly fractured
• clay rich
• pyritized fossils
• highly fractured
• shell fragments
• fractures
• clay with silt
• pyritized fossils
• pyrite nodule
• 8522.1
• wavy laminae
• light and dark laminations
• pyritized fossils
• pyrite nodule
• fracture
• silty clay
• 8526.6
• pyrite nodules
• silty clay
• highly fractured, pyrite and phosphate zones
• clay rich

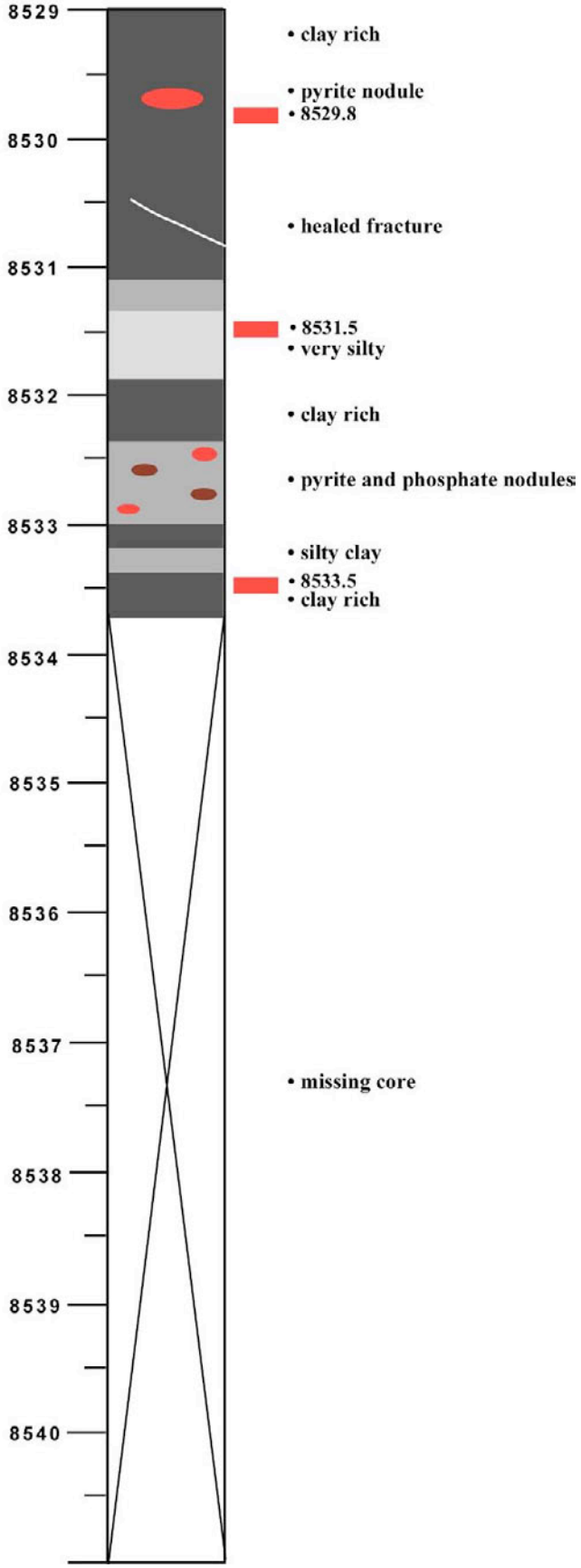
8529
8530
8531
8532
8533
8534
8535
8536
8537
8538
8539
8540
• clay rich
• pyrite nodule
• 8529.8
• healed fracture
• 8531.5
• very silty
• clay rich
• pyrite and phosphate nodules
• silty clay
• 8533.5
• clay rich
• missing core

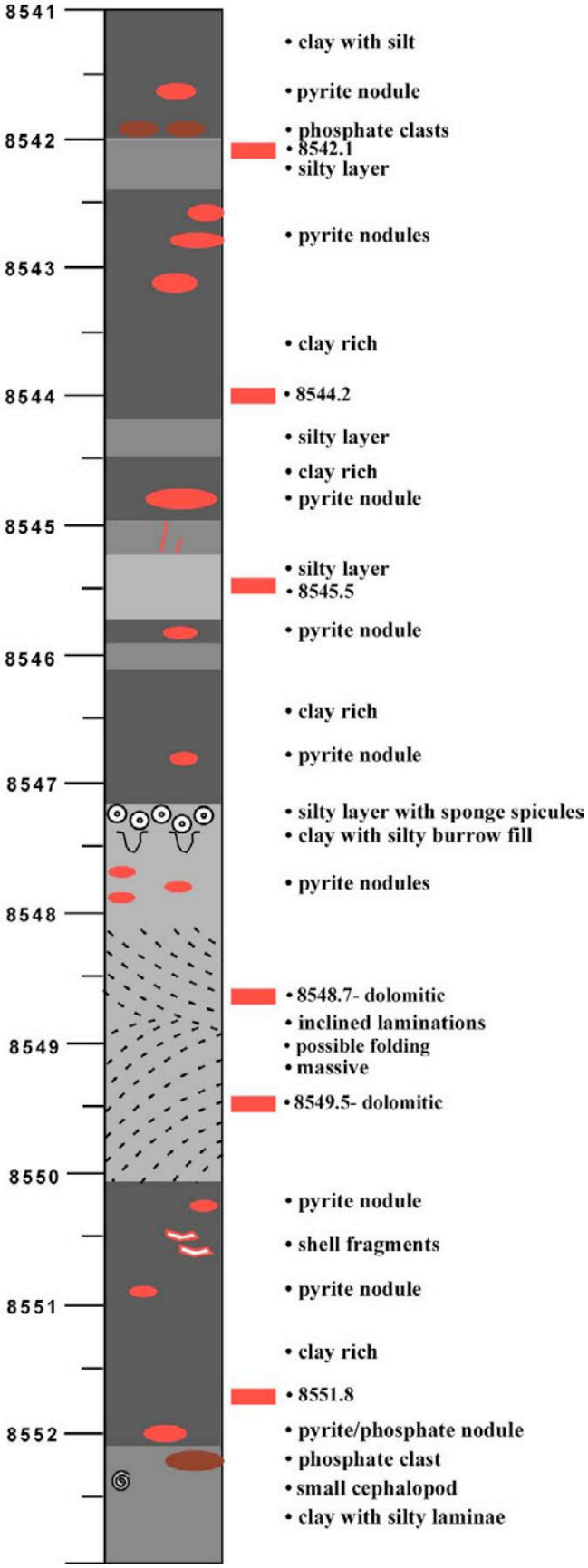
8541
8542
8543
8544
8545
8546
8547
8548
8549
8550
8551
8552
• clay with silt
• pyrite nodule
• phosphate clasts
• 8542.1
• silty layer
• pyrite nodules
• clay rich
• 8544.2
• silty layer
• clay rich
• pyrite nodule
• silty layer
• 8545.5
• pyrite nodule
• clay rich
• pyrite nodule
• silty layer with sponge spicules
• clay with silty burrow fill
• pyrite nodules
• 8548.7- dolomitic
• inclined laminations
• possible folding
• massive
• 8549.5- dolomitic
• pyrite nodule
• shell fragments
• pyrite nodule
• clay rich
• 8551.8
• pyrite/phosphate nodule
• phosphate clast
• small cephalopod
• clay with silty laminae

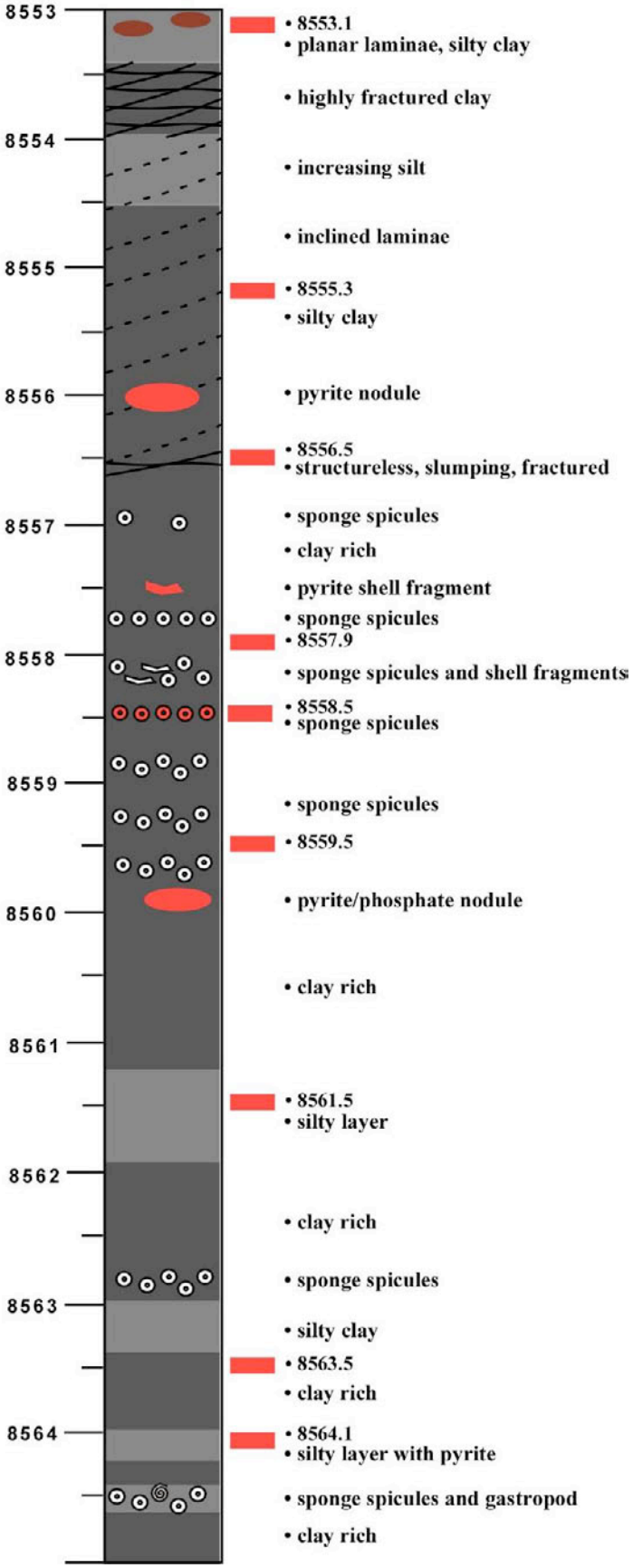
8553
8554
8555
8556
8557
8558
8559
8560
8561
8562
8563
8564
• 8553.1
• planar laminae, silty clay
• highly fractured clay
• increasing silt
• inclined laminae
• 8555.3
• silty clay
• pyrite nodule
• 8556.5
• structureless, slumping, fractured
• sponge spicules
• clay rich
• pyrite shell fragment
• sponge spicules
• 8557.9
• sponge spicules and shell fragments
• 8558.5
• sponge spicules
• sponge spicules
• 8559.5
• pyrite/phosphate nodule
• clay rich
• 8561.5
• silty layer
• clay rich
• sponge spicules
• silty clay
• 8563.5
• clay rich
• 8564.1
• silty layer with pyrite
• sponge spicules and gastropod
• clay rich

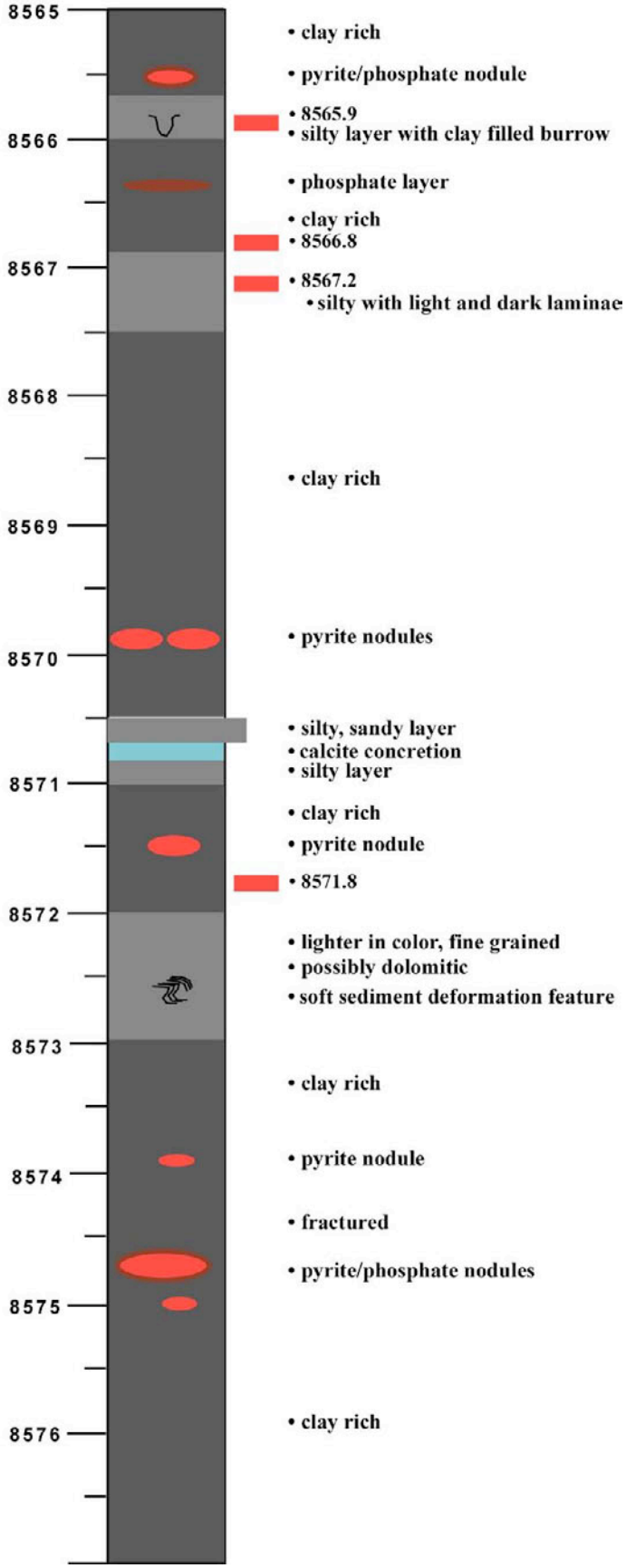
8565
8566
8567
8568
8569
8570
8571
8572
8573
8574
8575
8576
• clay rich
• pyrite/phosphate nodule
• 8565.9
• silty layer with clay filled burrow
• phosphate layer
• clay rich
• 8566.8
• 8567.2
• silty with light and dark laminae
• clay rich
• pyrite nodules
• silty, sandy layer
• calcite concretion
• silty layer
• clay rich
• pyrite nodule
• 8571.8
• lighter in color, fine grained
• possibly dolomitic
• soft sediment deformation feature
• clay rich
• pyrite nodule
• fractured
• pyrite/phosphate nodules
• clay rich

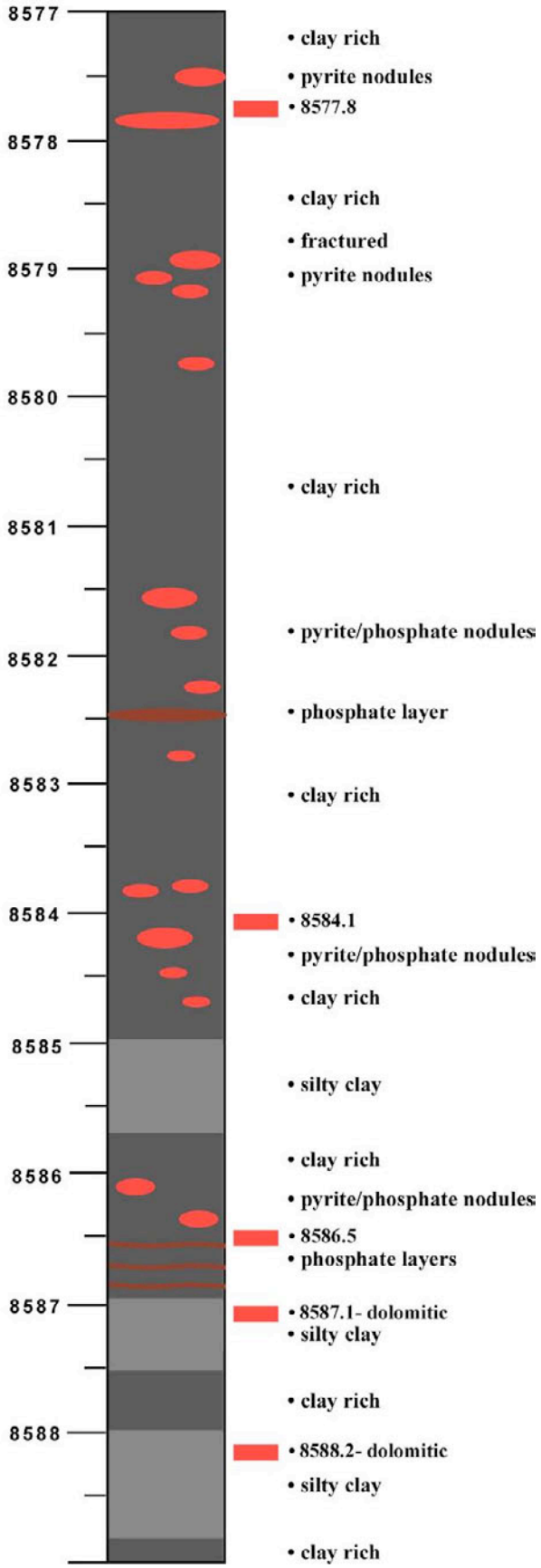
8577
8578
8579
8580
8581
8582
8583
8584
8585
8586
8587
8588
• clay rich
• pyrite nodules
• 8577.8
• clay rich
• fractured
• pyrite nodules
• clay rich
• pyrite/phosphate nodules
• phosphate layer
• clay rich
• 8584.1
• pyrite/phosphate nodules
• clay rich
• silty clay
• clay rich
• pyrite/phosphate nodules
• 8586.5
• phosphate layers
• 8587.1- dolomitic
• silty clay
• clay rich
• 8588.2- dolomitic
• silty clay
• clay rich

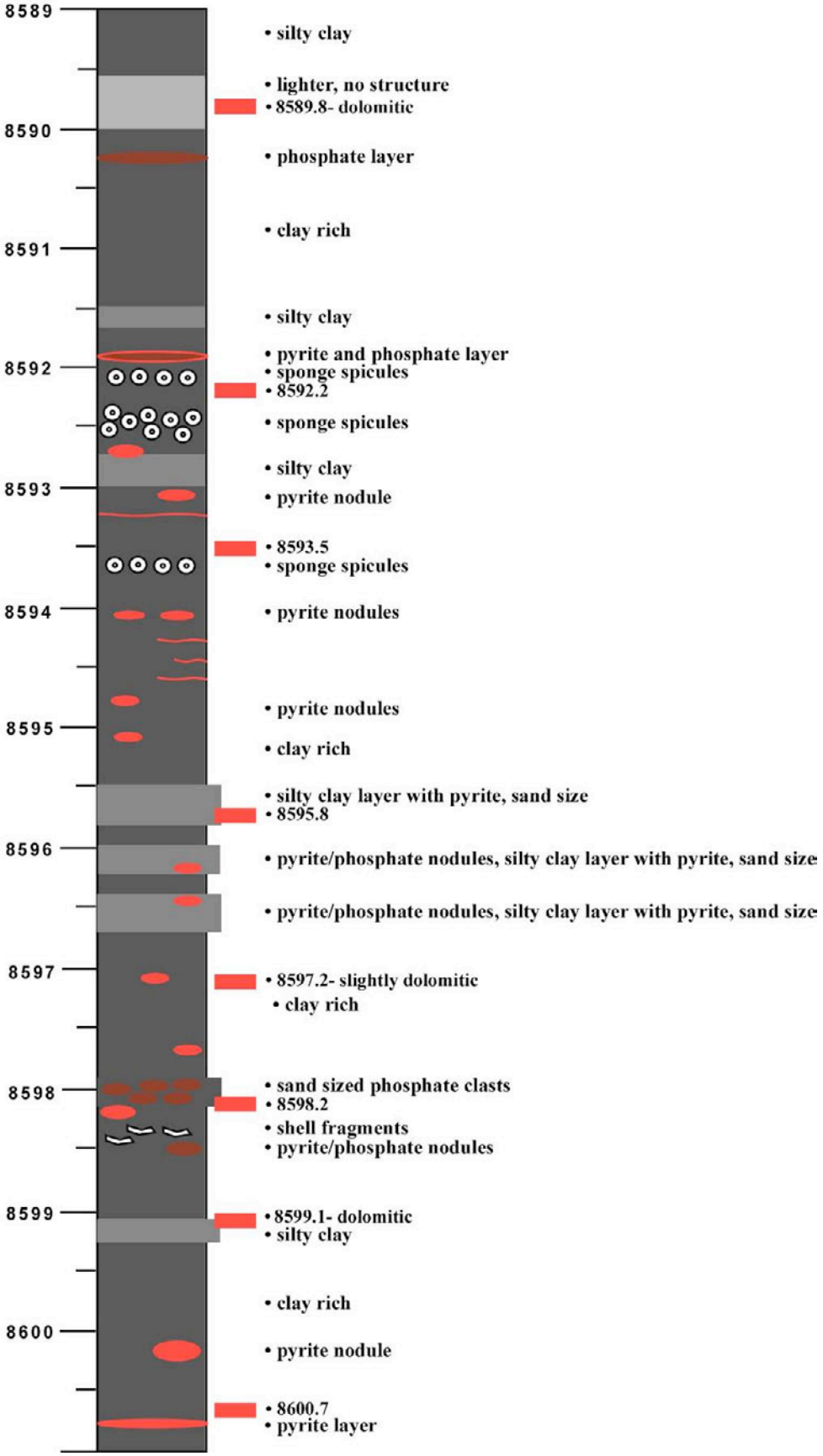
8589
8590
8591
8592
8593
8594
8595
8596
8597
8598
8599
8600
• silty clay
• lighter, no structure
• 8589.8- dolomitic
• phosphate layer
• clay rich
• silty clay
• pyrite and phosphate layer
• sponge spicules
• 8592.2
• sponge spicules
• silty clay
• pyrite nodule
• 8593.5
• sponge spicules
• pyrite nodules
• pyrite nodules
• clay rich
• silty clay layer with pyrite, sand size
• 8595.8
• pyrite/phosphate nodules, silty clay layer with pyrite, sand size
• pyrite/phosphate nodules, silty clay layer with pyrite, sand size
• 8597.2- slightly dolomitic
• clay rich
• sand sized phosphate clasts
• 8598.2
• shell fragments
• pyrite/phosphate nodules
• 8599.1- dolomitic
• silty clay
• clay rich
• pyrite nodule
• 8600.7
• pyrite layer

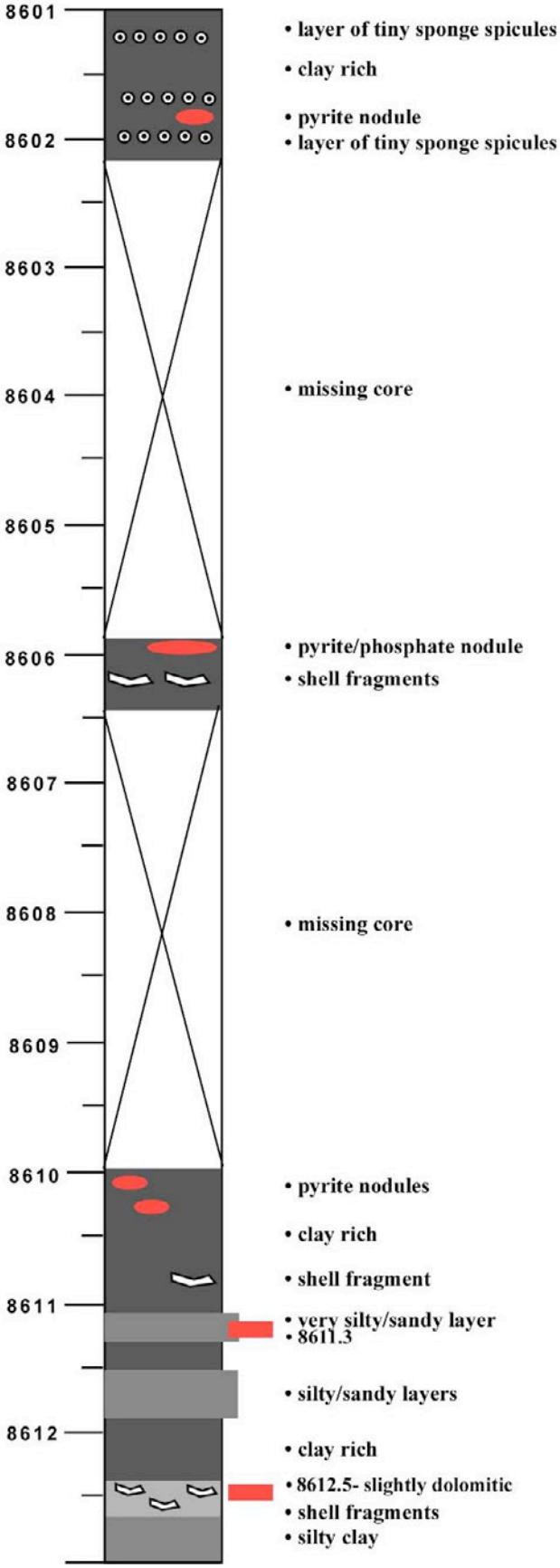
8601
8602
8603
8604
8605
8606
8607
8608
8609
8610
8611
8612
• layer of tiny sponge spicules
• clay rich
• pyrite nodule
• layer of tiny sponge spicules
• missing core
• pyrite/phosphate nodule
• shell fragments
• missing core
• pyrite nodules
• clay rich
• shell fragment
• very silty/sandy layer
• 8611.3
• silty/sandy layers
• clay rich
• 8612.5- slightly dolomitic
• shell fragments
• silty clay

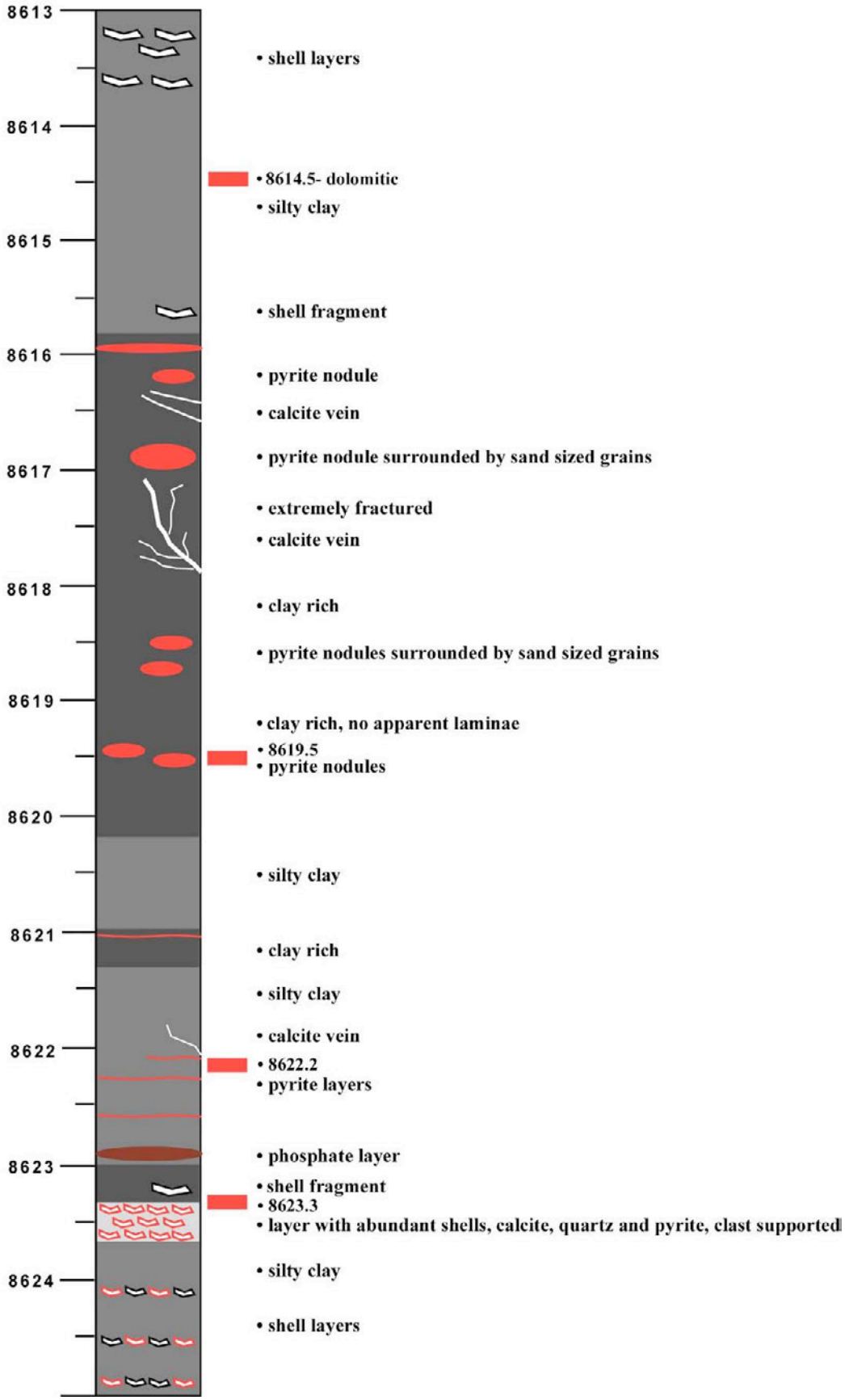
8613
8614
8615
8616
8617
8618
8619
8620
8621
8622
8623
8624
• shell layers
• 8614.5- dolomitic
• silty clay
• shell fragment
• pyrite nodule
• calcite vein
• pyrite nodule surrounded by sand sized grains
• extremely fractured
• calcite vein
• clay rich
• pyrite nodules surrounded by sand sized grains
• clay rich, no apparent laminae
• 8619.5
• pyrite nodules
• silty clay
• clay rich
• silty clay
• calcite vein
• 8622.2
• pyrite layers
• phosphate layer
• shell fragment
• 8623.3
• layer with abundant shells, calcite, quartz and pyrite, clast supported
• silty clay
• shell layers

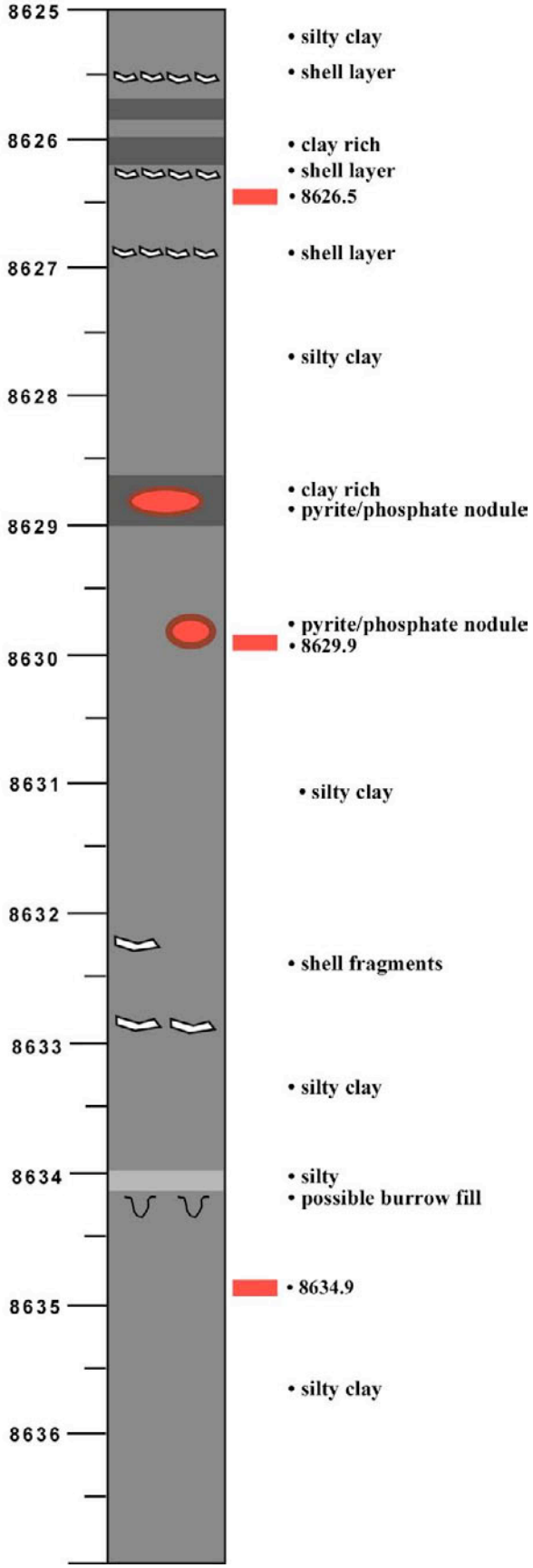
8625
8626
8627
8628
8629
8630
8631
8632
8633
8634
8635
8636
• silty clay
• shell layer
• clay rich
• shell layer
• 8626.5
• shell layer
• silty clay
• clay rich
• pyrite/phosphate nodule
• pyrite/phosphate nodule
• 8629.9
• silty clay
• shell fragments
• silty clay
• silty
• possible burrow fill
• 8634.9
• silty clay

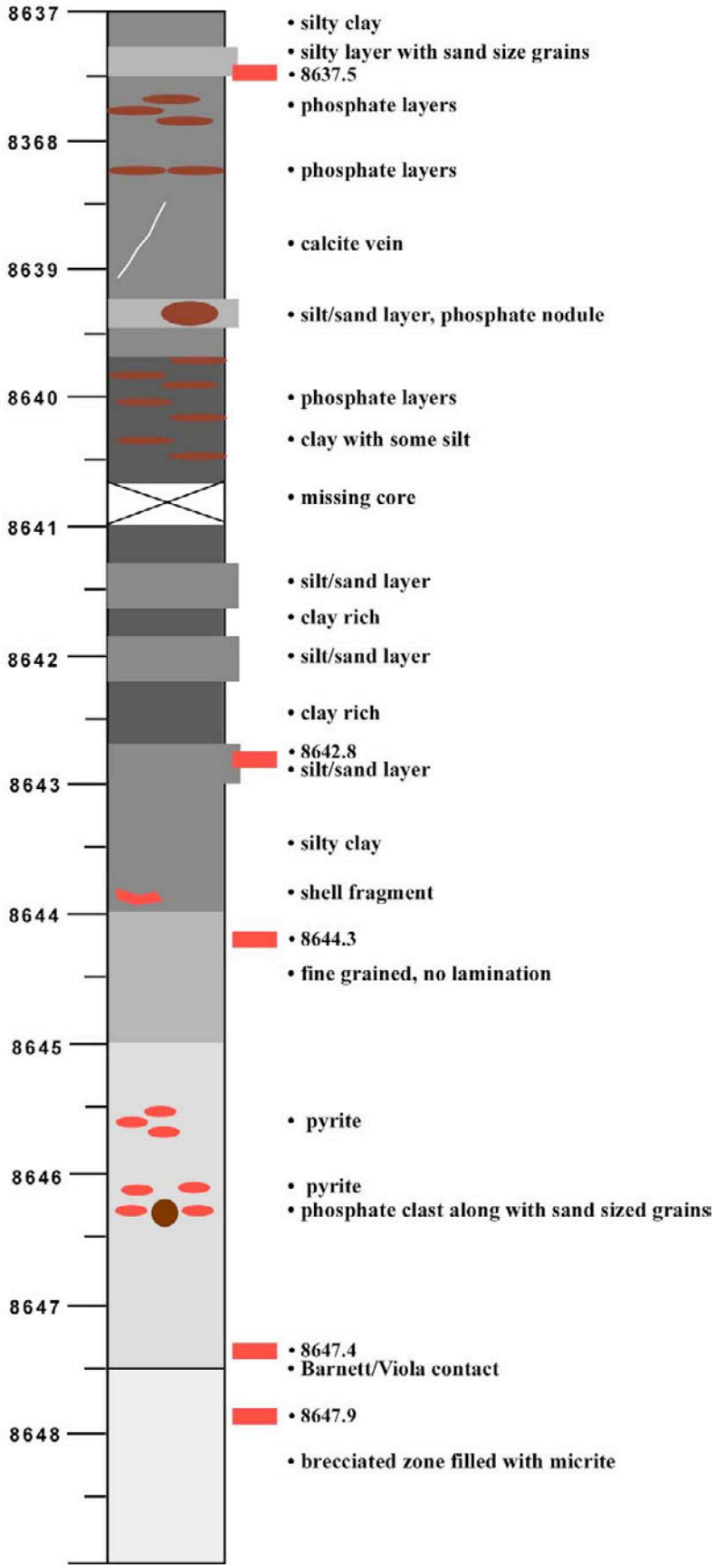
8637
8368
8639
8640
8641
8642
8643
8644
8645
8646
8647
8648
• silty clay
• silty layer with sand size grains
• 8637.5
• phosphate layers
• phosphate layers
• calcite vein
• silt/sand layer, phosphate nodule
• phosphate layers
• clay with some silt
• missing core
• silt/sand layer
• clay rich
• silt/sand layer
• clay rich
• 8642.8
• silt/sand layer
• silty clay
• shell fragment
• 8644.3
• fine grained, no lamination
• pyrite
• pyrite
• phosphate clast along with sand sized grains
• 8647.4
• Barnett/Viola contact
• 8647.9
• brecciated zone filled with micrite

Appendix 2

Core Photos

8385-8396. Upper unit. Notice the alternating parallel and nonparallel clay and silt laminae. The silt in this core consists of siliceous sponge spicules.

8409-8420. Upper unit. Notice the alternating parallel and nonparallel clay and silt laminae. The silt in this core is consists of siliceous sponge spicules.

8553-8564. Middle unit. Notice silt laminae (yellow arrows) and the pyrite and phosphate nodules (red arrow).

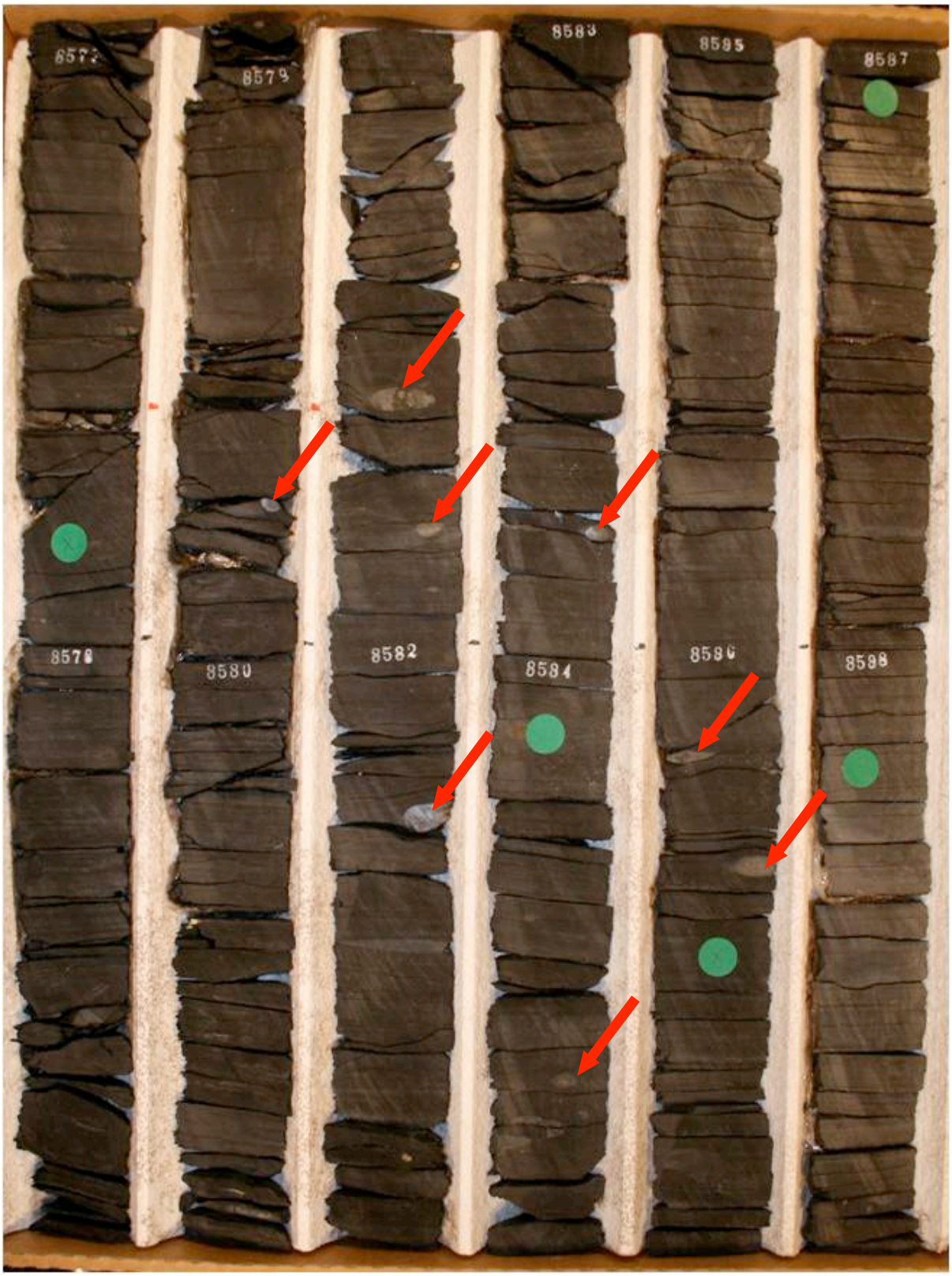

8577-8588. Middle unit. Notice the pyrite and phosphate nodules (red arrows).

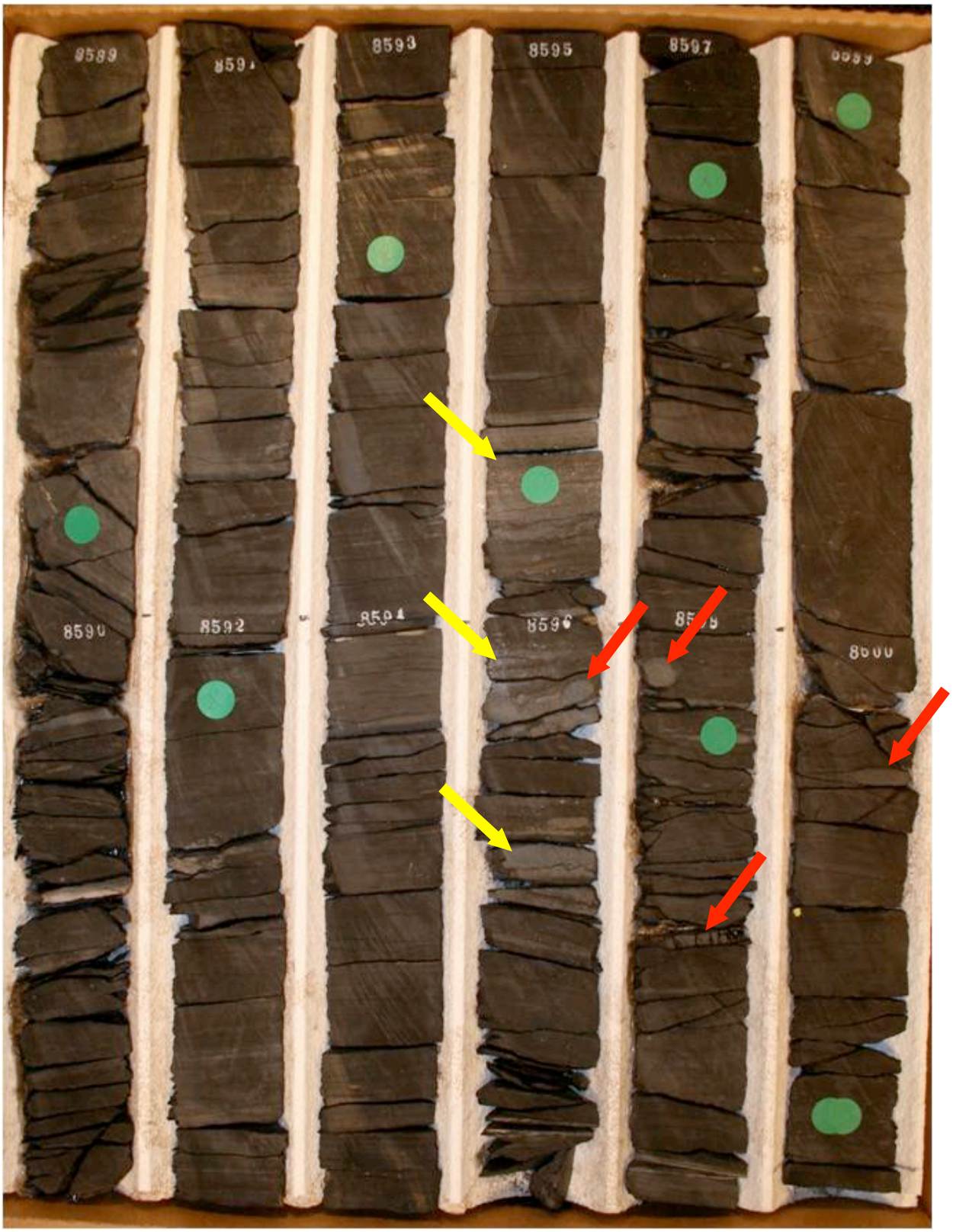

8589-8600. Contact between the middle unit and the Barnett. Notice the pyrite and phosphate nodules (red arrows) and the maximum flooding surface deposits (sandy phosphate layer-facies C_2) (yellow arrows).

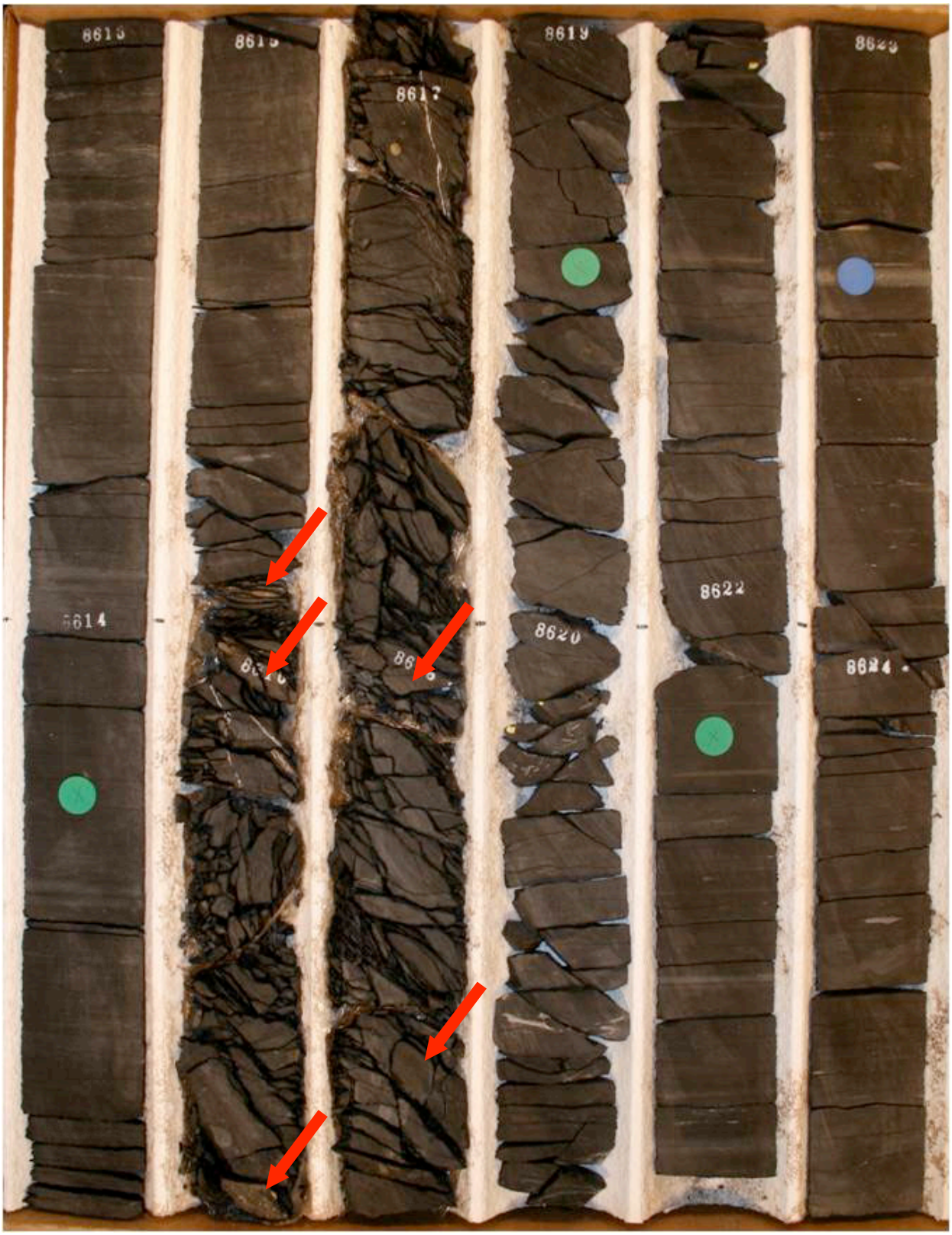

8615-8624. Barnett. Notice the pyrite and phosphate nodules (red arrows) and the extremely fractured zone. The bottom part of this core contains detrital quartz silt (facies B_3).

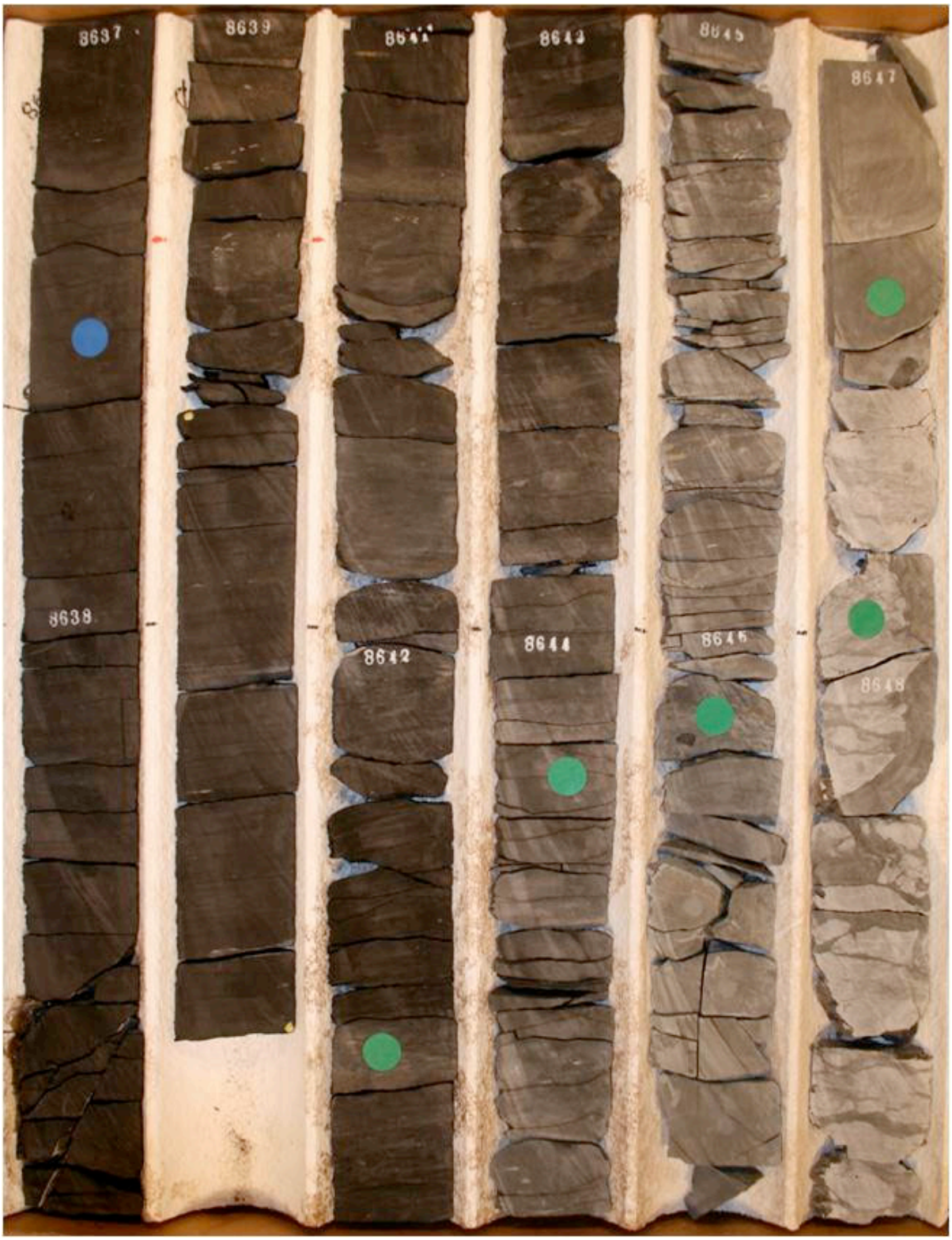

8637-8648. Barnett and Viola contact. Most of this core contains detrital quartz silt (facies B_3). Notice the gradual change between the Barnett and the Viola limestone.

Appendix 3

Geochemical Data Table

						Relative	Relative	
	Organic	Carbonate	Free	Kerogen	Organic	Hydrogen	Oxygen	Production
	Richness	Carbon	Oil	Yield	CO2	Content	Content	Index
Depth1	TOC	CC	S1	S2	S3	HI	OI	PI
(feet)	(wt.%)	(wt%)	(mg HC/g R)	mg HC/g R	mg CO2/g R	(mg HC/g TOC)	(ng HC/g TOC)	(S1(S1+S2))
8361.5	2.36	18.83	0.23	0.19	0.28	8	12	0.55
8362.5	2.04	14.94	0.18	0.12	0.23	6	11	0.60
8363.0	2.03	22.51	0.14	0.06	0.19	3	9	0.70
8364.5	3.18	15.00	0.06	0.10	0.13	3	4	0.38
8365.5	2.23	21.05	0.12	0.11	0.14	5	6	0.52
8366.5	1.80	41.22	0.18	0.10	0.11	6	6	0.64
8367.5	2.29	23.27	0.22	0.16	0.11	7	5	0.58
8368.5	2.43	20.63	0.06	0.13	0.14	5	6	0.32
8369.5	2.53	19.86	0.04	0.07	0.13	3	5	0.36
8370.5	2.61	21.01	0.07	0.16	0.17	6	7	0.30
8371.5	2.88	20.72	0.11	0.11	0.20	4	7	0.50
8372.5	2.37	21.91	0.14	0.12	0.15	5	6	0.54
8373.5	2.32	16.94	0.11	0.13	0.14	6	6	0.46
8374.5	2.16	11.25	0.11	0.11	0.11	5	5	0.50
8375.5	2.91	11.77	0.42	0.25	0.25	9	9	0.63
8376.5	3.81	8.25	0.17	0.15	0.12	4	3	0.53
8377.5	3.10	9.68	0.07	0.23	0.15	7	5	0.23
8378.5	1.90	14.50	0.12	0.07	0.09	4	5	0.63
8379.5	2.49	17.85	0.16	0.25	0.18	10	7	0.39
8381.5	2.95	17.27	0.03	0.05	0.12	2	4	0.38
8382.5	4.23	29.11	0.26	0.20	0.33	5	8	0.57
8383.5	2.66	23.18	0.07	0.07	0.17	3	6	0.50
8384.5	2.60	13.24	0.13	0.10	0.13	4	5	0.57
8385.5	2.54	21.97	0.07	0.19	0.19	7	7	0.27
8386.5	2.39	26.09	0.27	0.13	0.14	5	6	0.68
8387.5	2.15	30.23	0.09	0.13	0.32	6	15	0.41
8388.5	2.62	13.46	0.12	0.13	0.23	5	9	0.48
8389.5	2.76	10.16	0.38	0.19	0.25	7	9	0.67
8390.5	3.01	6.10	0.17	0.12	0.12	4	4	0.59
8391.5	3.03	10.81	0.08	0.17	0.15	6	5	0.32
8392.5	1.79	8.48	0.13	0.08	0.12	4	7	0.62
8393.5	2.93	3.38	0.11	0.11	0.11	4	4	0.50
8394.5	2.09	14.82	0.17	0.09	0.13	4	6	0.65
8395.5	2.52	13.61	0.08	0.06	0.18	2	7	0.57
8396.5	3.57	18.35	0.10	0.08	0.15	2	4	0.56
8397.5	3.77	15.85	0.08	0.07	0.15	2	4	0.53
8398.5	3.84	12.76	0.11	0.10	0.17	3	4	0.52
8399.5	2.98	13.68	0.07	0.06	0.34	2	11	0.54
8400.5	3.27	12.66	0.09	0.09	0.18	3	6	0.50
8402.5	3.81	8.59	0.13	0.12	0.20	3	5	0.52
8403.5	1.62	51.82	0.12	0.08	0.16	5	10	0.60

8404.5	1.22	60.65	0.13	0.08	0.15	7	12	0.62
8405.5	2.59	13.66	0.14	0.13	0.17	5	7	0.52
8406.5	2.47	24.76	0.09	0.07	0.14	3	6	0.56
8407.5	1.97	38.23	0.09	0.04	0.17	2	9	0.69
8408.5	2.55	18.43	0.16	0.10	0.18	4	7	0.62
8409.5	2.95	16.63	0.13	0.07	0.05	2	2	0.65
8410.5	3.25	12.81	0.12	0.06	0.27	2	8	0.67
8411.5	2.70	12.66	0.10	0.09	0.15	3	6	0.53
8412.5	3.08	7.29	0.05	0.09	0.35	3	11	0.36
8413.5	1.84	16.39	0.10	0.05	0.21	3	11	0.67
8414.5	2.76	8.64	0.04	0.06	0.15	2	5	0.40
8415.5	2.52	11.86	0.10	0.07	0.16	3	6	0.59
8416.5	2.96	10.01	0.04	0.05	0.14	2	5	0.44
8417.5	1.94	8.59	0.16	0.09	0.13	5	7	0.64
8418.5	1.87	7.24	0.06	0.03	0.11	2	6	0.67
8419.5	2.83	12.06	0.19	0.09	0.13	3	5	0.68
8420.5	1.96	51.20	0.09	0.06	0.19	3	10	0.60
8422.5	2.74	7.79	0.31	0.11	0.21	4	8	0.74
8423.5	4.41	5.65	0.12	0.09	0.34	2	8	0.57
8424.5	2.99	12.48	0.09	0.08	0.19	3	6	0.53
8425.5	3.39	15.34	0.13	0.09	0.19	3	6	0.59
8426.5	3.75	15.79	0.06	0.08	0.15	2	4	0.43
8427.5	4.66	14.71	0.25	0.20	0.03	4	1	0.56
8428.5	3.62	7.90	0.22	0.13	0.05	4	1	0.63
8429.5	4.04	22.55	0.16	0.11	0.02	3	0	0.59
8430.5	2.21	8.22	0.23	0.11	0.09	5	4	0.68
8431.5	4.02	15.87	0.15	0.13	0.05	3	1	0.54
8432.5	4.80	11.85	0.10	0.11	0.02	2	0	0.48
8433.5	3.07	9.18	0.29	0.13	0.02	4	1	0.69
8434.5	3.13	16.83	0.10	0.12	0.04	4	1	0.45
8435.5	2.22	18.88	0.05	0.07	0.03	3	1	0.42
8436.5	3.10	9.48	0.14	0.12	0.02	4	1	0.54
8437.5	5.13	2.87	0.25	0.21	0.05	4	1	0.54
8438.5	3.20	2.67	0.19	0.12	0.04	4	1	0.61
8439.5	3.32	13.09	0.08	0.10	0.10	3	3	0.44
8440.5	3.71	19.33	0.15	0.10	0.18	3	5	0.60
8442.5	2.93	21.23	0.19	0.11	0.11	4	4	0.63
8443.5	2.26	12.89	0.34	0.09	0.05	4	2	0.79
8444.5	4.17	15.66	1.54	0.35	0.15	8	4	0.81
8445.5	2.23	54.77	0.29	0.08	0.09	4	4	0.78
8446.5	0.80	75.39	0.04	0.01	0.02	1	3	0.80
8447.5	3.82	17.74	0.32	0.14	0.08	4	2	0.70
8448.5	3.87	18.69	0.19	0.15	0.12	4	3	0.56
8449.5	3.83	16.01	0.13	0.10	0.12	3	3	0.57
8450.5	3.58	12.43	0.07	0.11	0.26	3	7	0.39
8451.5	4.80	7.12	0.26	0.17	0.17	4	4	0.60
8452.5	3.05	22.05	0.18	0.14	0.14	5	5	0.56
8453.5	4.11	22.01	0.22	0.16	0.14	4	3	0.58
8454.5	3.83	9.73	0.19	0.12	0.10	3	3	0.61
8455.5	4.05	3.58	0.10	0.07	0.09	2	2	0.59

8456.5	4.64	22.74	0.20	0.11	0.10	2	2	0.65
8457.5	4.63	21.96	0.25	0.11	0.16	2	3	0.69
8458.5	4.96	18.77	0.25	0.12	0.18	2	4	0.68
8459.5	4.26	24.14	0.10	0.09	0.19	2	4	0.53
8460.5	5.87	23.26	0.21	0.12	0.19	2	3	0.64
8462.5	3.30	46.74	0.21	0.13	0.14	4	4	0.62
8463.5	4.11	26.67	0.15	0.11	0.30	3	7	0.58
8464.5	4.48	18.81	0.22	0.17	0.29	4	6	0.56
8465.5	4.29	17.81	0.14	0.11	0.17	3	4	0.56
8466.5	4.05	20.21	0.08	0.08	0.50	2	12	0.50
8467.5	3.92	14.96	0.06	0.06	0.08	2	2	0.50
8468.5	3.94	23.15	0.18	0.09	0.09	2	2	0.67
8469.5	4.25	11.17	0.04	0.05	0.04	1	1	0.44
8470.5	4.12	16.12	0.12	0.11	0.08	3	2	0.52
8471.5	3.87	22.46	0.13	0.09	0.12	2	3	0.59
8472.5	4.49	26.21	0.34	0.17	0.15	4	3	0.67
8473.5	2.63	59.36	0.23	0.15	0.13	6	5	0.61
8474.5	4.65	25.07	0.10	0.09	0.12	2	3	0.53
8476.5	3.33	6.53	0.13	0.09	0.06	3	2	0.59
8477.5	3.86	7.00	0.14	0.13	0.21	3	5	0.52
8478.5	2.47	8.39	0.10	0.09	0.08	4	3	0.53
8479.5	7.18	10.81	0.15	0.11	0.12	2	2	0.58
8480.5	5.33	9.30	0.17	0.15	0.11	3	2	0.53
8482.5	2.41	57.00	0.38	0.18	0.17	7	7	0.68
8483.5	4.34	11.92	0.13	0.13	0.12	3	3	0.50
8484.5	4.61	4.71	0.17	0.12	0.09	3	2	0.59
8485.5	2.91	7.03	0.47	0.25	0.37	9	13	0.65
8486.5	5.82	13.80	0.12	0.10	0.20	2	3	0.55
8487.5	3.56	20.61	0.20	0.10	0.16	3	4	0.67
8488.5	4.75	13.84	0.16	0.11	0.19	2	4	0.59
8489.5	5.49	14.38	0.17	0.13	0.14	2	3	0.57
8490.5	3.34	26.24	0.23	0.11	0.13	3	4	0.68
8491.5	3.86	27.36	0.24	0.12	0.17	3	4	0.67
8492.5	5.18	19.09	0.29	0.13	0.19	3	4	0.69
8493.5	6.59	8.07	0.13	0.14	0.14	2	2	0.48
8494.5	4.58	18.26	0.31	0.21	0.49	5	11	0.60
8495.5	5.74	18.04	0.33	0.22	0.21	4	4	0.60
8496.5	5.89	14.08	0.29	0.16	0.26	3	4	0.64
8497.5	6.38	9.94	0.08	0.11	0.16	2	3	0.42
8498.5	7.03	13.23	0.11	0.14	0.16	2	2	0.44
8499.5	5.76	6.97	0.07	0.09	0.09	2	2	0.44
8500.5	4.88	11.00	0.16	0.14	0.16	3	3	0.53
8503.5	6.00	7.96	0.12	0.12	0.13	2	2	0.50
8504.5	4.87	10.47	0.13	0.11	0.15	2	3	0.54
8505.5	3.78	28.65	0.07	0.05	0.15	1	4	0.58
8506.5	5.97	8.84	0.17	0.18	0.17	3	3	0.49
8507.5	6.52	11.76	0.12	0.12	0.17	2	3	0.50
8508.5	5.92	5.82	0.39	0.22	0.38	4	6	0.64
8509.5	7.73	6.05	0.11	0.13	0.24	2	3	0.46
8510.5	7.02	9.06	0.33	0.23	0.22	3	3	0.59

8511.5	5.93	8.90	0.17	0.15	0.13	3	2	0.53
8512.5	8.34	8.13	0.26	0.19	0.16	2	2	0.58
8513.5	3.74	46.78	0.13	0.08	0.16	2	4	0.62
8514.5	7.66	5.67	0.19	0.13	0.14	2	2	0.59
8515.5	7.17	10.63	0.17	0.15	0.14	2	2	0.53
8516.5	7.15	8.51	0.16	0.14	0.13	2	2	0.53
8517.5	6.54	5.34	0.09	0.10	0.08	2	1	0.47
8518.5	4.98	5.84	0.11	0.09	0.28	2	6	0.55
8519.5	7.84	2.64	0.24	0.18	0.21	2	3	0.57
8522.5	7.72	1.65	0.24	0.19	0.13	2	2	0.56
8523.5	4.88	3.02	0.32	0.16	0.11	3	2	0.67
8524.5	6.38	1.55	1.94	0.42	0.26	7	4	0.82
8525.5	7.30	3.38	0.32	0.22	0.21	3	3	0.59
8526.5	5.08	3.21	0.47	0.25	0.15	5	3	0.65
8527.5	4.19	11.96	0.26	0.13	0.14	3	3	0.67
8528.5	3.74	31.77	0.12	0.04	0.07	1	2	0.75
8529.5	3.80	9.06	1.01	0.20	0.11	5	3	0.83
8530.5	6.46	2.79	0.34	0.20	0.11	3	2	0.63
8531.5	6.94	1.73	0.15	0.14	0.13	2	2	0.52
8532.5	4.53	22.54	0.23	0.14	0.13	3	3	0.62
8533.5	6.39	3.07	0.23	0.17	0.17	3	3	0.58
8541.5	4.62	1.38	0.10	0.10	0.10	2	2	0.50
8542.5	4.91	23.70	0.43	0.21	0.02	4	0	0.67
8543.5	5.09	0.30	0.16	0.16	0.17	3	3	0.50
8544.5	7.76		0.17	0.16	0.16	2	2	0.52
8545.5	2.81	33.40	0.05	0.06	0.19	2	7	0.45
8546.5	5.15	1.65	0.14	0.17	0.12	3	2	0.45
8547.5	7.07	1.99	0.22	0.18	0.15	3	2	0.55
8548.5	4.52	43.35	0.16	0.11	0.21	2	5	0.59
8549.5	5.21	33.65	0.11	0.13	0.05	2	1	0.46
8550.5	8.89	2.38	0.14	0.15	0.15	2	2	0.48
8551.5	6.82	0.78	0.21	0.19	0.13	3	2	0.53
8552.5	2.92	12.58	0.10	0.06	0.10	2	3	0.63
8553.5	6.15	0.48	0.09	0.16	0.28	3	5	0.36
8554.5	5.44	1.23	0.20	0.21	0.18	4	3	0.49
8555.5	6.43	2.91	0.11	0.16	0.14	2	2	0.41
8556.5	5.04	2.45	0.05	0.12	0.07	2	1	0.29
8557.5	4.16	5.97	0.17	0.12	0.09	3	2	0.59
8558.5	3.90	1.58	0.18	0.19	0.13	5	3	0.49
8559.5	2.82	1.80	0.02	0.07	0.07	2	2	0.22
8561.5	2.17	22.59	0.16	0.11	0.13	5	6	0.59
8562.5	3.26	4.13	0.13	0.10	0.12	3	4	0.57
8563.5	4.72	3.16	0.07	0.12	0.05	3	1	0.37
8564.5	4.29	2.03	0.08	0.14	0.06	3	1	0.36
8565.5	3.17	2.07	0.14	0.11	0.12	3	4	0.56
8566.5	3.25	2.34	0.13	0.10	0.00	3	0	0.57
8567.5	3.87	7.60	0.17	0.13	0.04	3	1	0.57
8568.5	4.89	3.54	0.09	0.14	0.38	3	8	0.39
8569.5	3.89	44.98	0.21	0.10	0.17	3	4	0.68
8570.5	3.97	14.06	0.10	0.12	0.12	3	3	0.45

8571.5	5.12	7.68	0.05	0.09	0.15	2	3	0.36
8572.5	5.06	6.17	0.21	0.13	0.22	3	4	0.62
8573.5	2.82	0.30	0.04	0.10	0.14	4	5	0.29
8574.5	5.27	2.55	0.07	0.37	0.09	7	2	0.16
8575.5	4.95	18.47	0.16	0.10	0.07	2	1	0.62
8575.5	3.95	3.16	0.11	0.11	0.11	3	3	0.50
8576.5	3.64	3.89	0.13	0.08	0.12	2	3	0.62
8577.5	5.21	4.35	0.21	0.14	0.19	3	4	0.60
8578.5	5.38	4.17	0.11	0.16	0.49	3	9	0.41
8579.5	4.84	2.13	0.16	0.18	0.35	4	7	0.47
8580.5	4.24	2.47	0.29	0.34	0.08	8	2	0.46
8582.5	3.31	1.97	0.07	0.09	0.10	3	3	0.44
8583.5	5.27	0.70	0.09	0.24	0.08	5	2	0.27
8584.5	3.68	1.08	0.05	0.08	0.01	2	0	0.38
8585.5	4.16	1.88	0.06	0.10	0.01	2	0	0.38
8585.5	2.52	3.46	0.15	0.08	0.01	3	0	0.65
8586.5	3.10	3.88	0.05	0.08	0.03	3	1	0.38
8587.5	2.41	2.85	0.05	0.09	0.23	4	10	0.36
8588.5	1.54	49.20	0.16	0.08	0.03	5	2	0.67
8589.5	4.54	14.74	0.03	0.07	0.14	2	3	0.30
8590.5	0.77	2.25	0.03	0.04	0.07	5	9	0.43
8591.5	1.68	11.66	0.14	0.05	0.07	3	4	0.74
8592.5	2.85	1.27	0.10	0.19	0.15	7	5	0.34
8593.5	5.57	1.48	0.10	0.18	0.11	3	2	0.36
8594.5	5.61	1.67	0.11	0.17	0.10	3	2	0.39
8595.5	4.14	2.63	0.36	0.19	0.13	5	3	0.65
8596.5	4.29	0.68	0.05	0.16	0.09	4	2	0.24
8597.5	4.07	2.39	0.07	0.20	0.13	5	3	0.26
8598.5	1.97	69.62	0.11	0.07	0.19	4	10	0.61
8599.5	3.70	8.47	1.50	0.30	0.23	8	6	0.83
8610.5	3.55	4.66	0.17	0.19	0.10	5	3	0.47
8611.5	3.17	35.00	0.17	0.11	0.15	3	5	0.61
8612.5	3.87	23.28	0.06	0.10	0.26	3	7	0.38
8613.5	3.80	27.04	0.20	0.12	0.16	3	4	0.63
8614.5	3.29	31.97	0.15	0.15	0.14	5	4	0.50
8615.5	3.66	22.08	0.09	0.14	0.15	4	4	0.39
8616.5	3.52	10.18	0.04	0.08	0.07	2	2	0.33
8617.5	5.51	3.35	0.05	0.18	0.16	3	3	0.22
8618.5	4.36	3.80	0.07	0.17	0.08	4	2	0.29
8619.5	4.24	0.59	0.04	0.15	0.00	4	0	0.21
8621.5	5.42	1.78	0.04	0.18	0.02	3	0	0.18
8622.5	7.29	10.11	0.11	0.21	0.13	3	2	0.34
8623.5	6.58	22.81	0.14	0.25	0.15	4	2	0.36
8624.5	3.61	7.44	0.15	0.13	0.10	4	3	0.54
8625.5	6.12	28.81	0.11	0.18	0.13	3	2	0.38
8626.5	2.57	8.49	0.07	0.08	0.11	3	4	0.47
8627.5	2.97	1.58	0.08	0.19	0.06	6	2	0.30
8628.5	5.97	1.97	0.13	0.23	0.13	4	2	0.36
8629.5	1.49	1.38	0.21	0.11	0.05	7	3	0.66
8630.5	3.51	13.06	0.14	0.11	0.10	3	3	0.56

8631.5	2.03	8.97	0.09	0.13	0.06	6	3	0.41
8632.5	1.97	7.46	0.14	0.10	0.07	5	4	0.58
8633.5	3.90	8.65	0.20	0.12	0.08	3	2	0.63
8634.5	4.66	16.58	0.20	0.13	0.12	3	3	0.61
8635.5	3.89	17.32	0.24	0.15	0.13	4	3	0.62
8636.5	3.89	11.05	0.09	0.10	0.11	3	3	0.47
8637.5	3.44	26.13	0.06	0.07	0.09	2	3	0.46
8638.5	3.02	16.76	0.10	0.06	0.17	2	6	0.63
8639.5	3.06	17.62	0.10	0.10	0.08	3	3	0.50
8641.5	5.60	6.18	0.06	0.18	0.03	3	1	0.25
8642.5	1.69	8.27	0.08	0.07	0.11	4	7	0.53
8643.5	5.07	11.82	0.15	0.15	0.09	3	2	0.50
8644.5	0.26	4.00	0.09	0.04	0.04	15	15	0.69
8645.5	0.17	4.51	0.05	0.04	0.05	24	29	0.56
8646.5	0.12	34.52	0.06	0.01	0.09	8	75	0.86
8647.5	0.13	16.26	0.05	0.06	0.14	46	108	0.45

VITA

Personal Background	Rachael Marie Monroe Born October 27, 1984, Corpus Christi, TX Daughter of Michael and Clarissa Creel Married to Justin G. Monroe, April 5, 2008
Education	Bachelor of Science in Geology, 2007 The University of Texas at Dallas, Richardson, TX Master of Science in Geology, 2009 Texas Christian University, Fort Worth, TX
Experience	Intern Geologist, 2004-2007 Matador Resources, Dallas, TX Intern Geologist, 2007-2009 EOG Resources, Fort Worth, TX Teaching Assistant, 2007-2009 Geology Department, TCU, Fort Worth, TX

ABSTRACT

PETROGRAPHIC AND STRATIGRAPHIC ANALYSIS OF THE BARNETT SHALE (MISSISSIPPIAN) IN HILL COUNTY, TEXAS: EVIDENCE FOR EUSTACY AND TECTONISM

By Rachael Monroe, M.S., 2009
Department of Geology
Texas Christian University

Dr. John Breyer- Professor of Geology

The major facies in the EOG Gordon SWD core are mudstone, siltstone, phosphatic layers, shell layers, and a carbonate concretion. Facies C_2 is a sandy phosphate layer, which concentrated organic matter. Facies C_2 is traceable and can be interpreted as a condensed section associated with a maximum flooding surface. The uranium in phosphate and organic matter cause a high gamma-ray reading in this interval. High TOC and high gamma-ray response occur in the same intervals of the core, but their magnitudes are not directly related. The Barnett deposition was sourced from the north and was a function of eustacy. The middle and upper unit were sourced from the Ouachita fold-thrust belt. The siltstone facies, common in these intervals, is rich in sponge spicules and is sourced from a reef growing on the thrust belt. A change in relative sea level in these two intervals is due to both eustacy and tectonics.